Part (A)

CHAPTER III

RESULTS AND DISCUSSION

3.1 Electrochemical Characterization of Microemulsion Systems

This section presents some results from the electrochemical experiments to provide some information on the structure of microemulsions containing cetyltrimethylammonium bromide (CTAB), sodium dodecyl sulphate (SDS), and octylphenoxypoly(oxyethylene) (Triton X-100) surfactants. These three microemulsion types will be used as media for electrochemical reactions in the next sections. Before the degression into the details of the electrochemical experiments, there are some requirements that should be fulfilled for a suitable probe which should be used in characterizing microemulsion. The requirements for a suitable probe are summarized as following:

1- Electroactive.

2- Reversible behaviour.

3- Hydrophobic in nature, i.e, very low solubility in O/W microemulsions

4- The half-wave potential of the probe not too positive or too negative, preferably between 400 mV to -200 mV.

5- Negligible or no adsorption on the electrode surface.

6- No effect on the chemical properties of the surfactant solution.

The probe that was found to be most suitable for this research is ferrocene (Fc). Other probes which were tested include methylviologen, vinylferrocene and tetrathiafulvalen (TTF). But ferrocene was found most efficient.

The voltammograms of 1mM ferrocene (Fc) were recorded in CTAB, SDS and Triton X-100 microemulsions containing 0.10 M NaBr supporting electrolyte. The voltammograms were recorded in the potential window from 0.0 to +500 mV (versus SCE) and at potential sweep rates between 20 and 200 mV/sec. Well defined voltammograms were obtained in all microemulsion

media as represented in Fig.(1). The voltammograms show one anodic and one cathodic peak on the anodic and cathodic sweeps. The anodic peak current, $I_{p,a}$, and cathodic peak current, $I_{p,c}$, are almost of equal heights as shown from Tables (2-4). The anodic to cathodic peak current ratios ($I_{p,a}/I_{p,c}$) does not exceed 1.074, which indicate the reversibility of the electrode process and confirmed that, there is no adsorption on the electrode surface. The peak potential separation ΔE_p = ($E_{p,a}$ - $E_{p,c}$) is almost around the theoritical value for one-electron transfer ~ 60 mV in CTAB, SDS and Triton X-100 microemulsions. These results indicate that the electrochemical oxidation of ferrocene (Fc) is a one-electron process forming ferrocenium ion (Fc^+) as following:

$$Fc \quad \Leftrightarrow \quad Fc^+ + e$$

The voltammograms recorded at different sweep rates varying from 20 to 200 mV/sec are essentially similar and show one anodic and one cathodic peak. The constancy of the cathodic and anodic peak potentials, $E_{p,a}$ and $E_{p,c}$, respectively, confirms the reversible nature of the electrode reaction. Also, the peak potenial separation ΔE_p values fall within the range from 58-63 mV for CTAB, 56-61 mV in SDS and 50-58 mV in Triton X-100 microemulsions within the experimental error of ~5 mV as given in Tables (2-4).

On using Randless-Sevcik equation [168] which is given as:

$$\mathbf{I_p = 0.4463(n^{3/2}F^{3/2})/(R^{1/2}T^{1/2})D^{1/2}AC\upsilon^{1/2}} \qquad \textbf{(III.1)}$$

the plots of anodic peak current ($I_{p,a}$) versus square root of sweep rate ($\upsilon^{1/2}$), straight lines intersecting the origin were obtained and shown in Fig. (2). These results indicate that the

electrode process is diffusion controlled [148]. Also, the plots of cathodic peak current, $I_{p,c}$, versus $\upsilon^{1/2}$ show linear correlations passing through the origin. The slopes of $I_{p,a}$ vs. $\upsilon^{1/2}$ were used to estimate the apparent diffusion coefficient of the reductant (D_O). The apparent diffusion coefficient values for ferrocene in CTAB, SDS and Triton X-100 microemulsions were determined and found to be $2x10^{-7}$, $5.6x10^{-7}$ and $3.40x10^{-7}$ cm^2/sec, respectively.

Therefore, cyclic voltammograms of ferrocene in the different microemulsion systems are well-behaved in the sense that they yielded linear $I_{p,a}$ versus $\upsilon^{1/2}$ plots, nearly unity of $I_{p,a}/I_{p,c}$ ratios and constant values for $(E_{p,a} + E_{p,c})/2$ at sweep rates of 20 to 200 mV/sec. Since ferrocene (Fc) is hydrophobic in nature, its solubility in water is $5x10^{-5}$ M [97] and of solubility 0.15 M in dodecane [183]. Singly charged Fc^+ cation is water soluble. Thus $Fc^{0/+}$ couple represents the limiting case where one form of the probe is oil soluble (Fc^0) and the other (Fc^+) is water soluble.

By using Stokes-Einstein equation [184] which states that:

$$D = KT/6\pi\eta R_h \qquad \textbf{(III.2)}$$

where D is the diffusion coefficient of microemulsion droplet in cm^2/sec, K is the Boltzman constant in erg/K, η is the viscosity coefficient of the continuous medium in centipoise (cp), and R_h is the radius of microemulsion droplet in cm. The radius of microemulsion droplets of CTAB, SDS and Triton X-100 were determined by using the values of the apparent diffusion coefficients and was found to be 123, 44 and 72 A°, respectively.

3.1.1 Effect of hydrocarbon

The effect of oil content on the diffusion coefficient and the radius of microemulsion systems of SDS and Triton X-100 was studied in the range from 0.50 to 3.20% (wt./wt.) of n-

octane, by using ferrocene as electroactive probe. Voltammograms obtained at different percentages of oil content indicate the slight decrease in peak current on increasing the oil content in microemulsion systems, as shown in Figs.(3&4). Results shown in Tables (5&6) indicate that as the oil content increased the heterogeneity of microemulsions is increased, this reflects the increased size of the droplets, sizes indicate the microstructure of microemulsion. The plots of the half-wave potential ($E_{1/2}$) versus the weight percent of n-octane (oil) showed a positive shift of $E_{1/2}$ as the oil content is increased, as represented by Fig.(5). As it is shown from Tables (5&6), the half-wave potential of the electroactive probe is dependent on the composition of microemulsion.

3.1.2 Temperature effect

The effect of temperature on the voltammetric behaviour of ferrocene in CTAB, SDS and Triton X-100 microemulsions was recorded at 288, 298 and 303° K and represented in Figs.(6-8). The microemulsion composition is represented by Table (1). Results obtained from cyclic voltammetry given in Tables (7-12), showed a slight increase of peak current as the temperature is increased. The diffusion coefficient in different microemulsion systems shows a slight increase ranging from 1.3-1.5% per degree. This rate is very low compared with the values reported in pure aqueous solutions 2-3% per degree [185]. The slow rate of increasing of diffusion coefficient with the temperature reveals the solubility of ferrocene in the oil droplet or in the hydrophobic core.

3.1.3 Rotating disk voltammetry (RDV)

The rotating disk voltammetry experiments were carried out successfully in CTAB, SDS and Triton X-100 microemulsion systems using 1 mM ferrocene electroactive probe. The effect of

rotation speed of the glassy carbon electrode was carried out using linear sweep voltammetry. The voltammograms were recorded at small sweep rate, 5 mV/sec, to obtain a steady state plateau and avoiding peaked shape. The voltammograms recorded in different microemulsion systems are essentially similar showing the one step oxidation-plateau. The effect of rotation speed on the voltammograms was recorded at angular velocities varying from 250 to 2000 RPM. As shown from Figs. (9-11), on increasing the angular velocity the limiting current is increased, whereas the half-wave potential is constant and not affected by the electrode rotation.

On employing the Levich equation [159]:

$$i_l = 0.62nFACD^{2/3}\nu^{-1/6}\omega^{1/2} \qquad \textbf{(III.3)}$$

where i_l is the limiting current in amp., ω is the angular velocity in rad/sec, ν is the kinematic viscosity in cm^2/sec and other terms have their usual meanings, the plots of the limiting current (i_l) versus square root of the angular velocity ($\omega^{1/2}$) for ferrocene in cationic, anionic and nonionic systems showed linear correlations intersecting the origin, as shown from Fig. (12), where the limiting current was measured at the steady state at 400 mV. These typical results indicating that the electrode process under mass transfer control. The slopes of these linear plots were used to estimate the apparent diffusion coefficients of microemulsion droplets. Generally a good agreement for the diffusion coefficient values obtained from rotating disk voltammetry with those obtained from cyclic voltammetry.

The half-wave potential and the number of electrons consumed in the oxidation process were determined from the logarithmic analysis of the oxidation waves of ferrocene in CTAB, SDS and Triton X-100 microemulsion systems at 1000 RPM. On using the following relationship:

$$E = E_{1/2} - 2.303RT/nF.\log[i/(i_l - i)] \quad \text{(III.4)}$$

and on plotting $\log[i/(i_l - i)]$ versus E straight lines in all media are obtained as shown in Fig. (13). The half-wave potential ($E_{1/2}$) of the system was determined from the potential axis at $\log[i/(i_l - i)]$ value equal to zero, where $i = i_l/2$ at the $E_{1/2}$ value. The half-wave potentials were determined and found to be 258, 218 and 236 mV for ferrocene in CTAB, SDS and Triton X-100, respectively. These values indicate the electrostatic repulsion effect of CTAB on the anodic branch; therefore the redox potential of the system appears at more positive value. The slopes of these plots was found to be 15.83, 17.12 and 16.72 V^{-1} for CTAB, SDS and Triton X-100, respectively which is consistent with a one electron transfer process.

3.1.4 Chronocoulometry

An important phenomena to be considered in electrochemical investigations in surfactant solutions is the surfactant adsorption on the electrode surface and its effect on the electrochemical reactions. A quantitative information about the adsorption in the electrochemical system could be obtained by using double-potential step chronocoulometry. From the advantages of the double-potential step chronocoulometric experiments is that the net potential change is zero. The chronocoulometric responses of 1mM ferrocene in CTAB, SDS and Triton X-100 microemulsion systems were recorded by plotting the charge versus time. The stepping potential was from 0.0 to 500 mV, this potential window was preselected from cyclic voltammetric behaviour of ferrocene in these microemulsion systems. Typical chronocoulograms of the forward step in these microemulsion systems were obtained by plotting the total amount of diffusional charge (Q_{tot}) versus time (t), as represented in Figs. (14a-16a). The plots were also tested by plotting the

amount of collecting charge versus $t^{1/2}$ and versus [θ] for the forward and reverse steps by using the following two equations [172-173], respectively:

$$Q_{tot} = [2nFAD_O^{1/2}C_O t^{1/2}]/\pi^{1/2} + Q_c + Q_{ads} \quad \textbf{(III.5)}$$

where, $Q_{ads} = nF\Gamma_O$

$$Q_r = [2nFAD_O^{1/2}C_O(\theta)]/\pi^{1/2} + Q_c + nF\Gamma_R \quad \textbf{(III.6)}$$

Such typical plots of Q_{tot} versus $t^{1/2}$ and Q_r versus θ is called Anson-plots and have shown in Figs. (14b-16b) for ferrocene in CTAB, SDS and Triton X-100 microemulsions. From the difference of intercepts of the forward and reverse steps of the Anson plots, the capacitive component in Q_{tot} is cancelled out. The amount of adsorbed reactant species (Γ_O) thus can be obtained quantitatively in the general form as following:

$$\textbf{Intercept 1 - Intercept 2} = nF(\Gamma_O - \Gamma_R) \quad \textbf{(III.7)}$$

Typical values of Γ_O of ferrocene in CTAB, SDS and Triton X-100 microemulsions is in the range of 10^{-12} to 10^{-13} moles indicating a negligible adsorption on the electrode surface compared to the bulk concentration of the reactant molecules (1 mM).

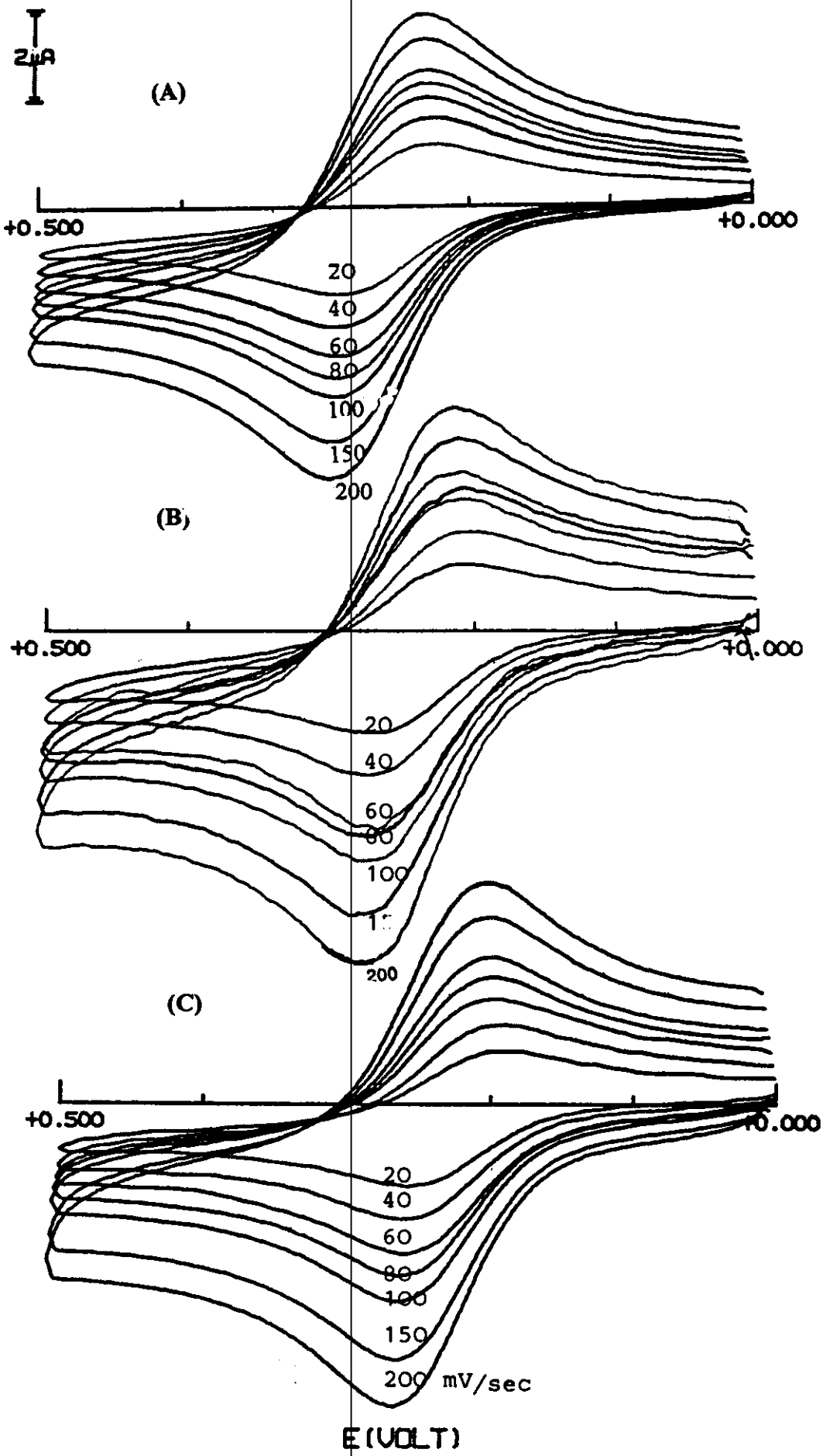

Figure 1: Cyclic voltammograms of 1 mM ferrocene in (a) CTAB microemulsion, (b) Triton X-100 microemulsion and (c) SDS microemulsion, the sweep rates are 20, 40, 60, 80, 100, 150 and 200 mV/sec.

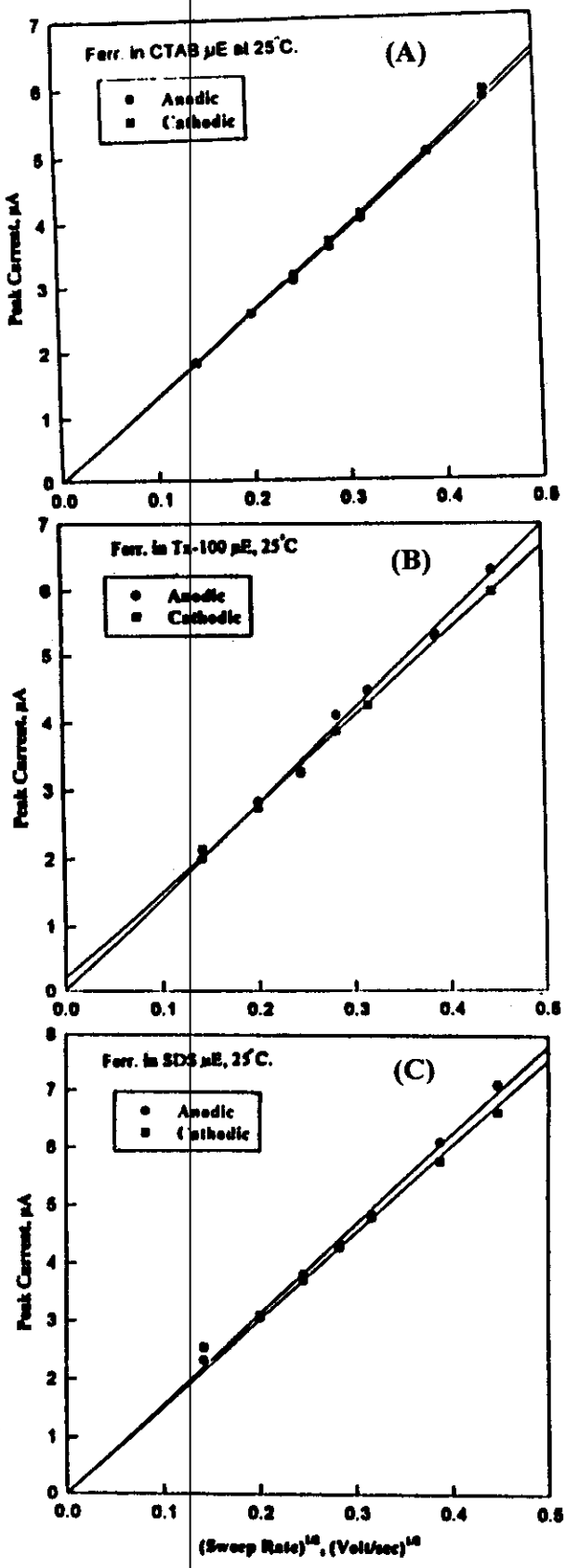

Figure 2: The plots of anodic and cathodic peak currents versus ($\upsilon^{1/2}$) in (a) CTAB microemulsion, (b) Triton X-100 microemulsion and (c) SDS microemulsion at 25°C.

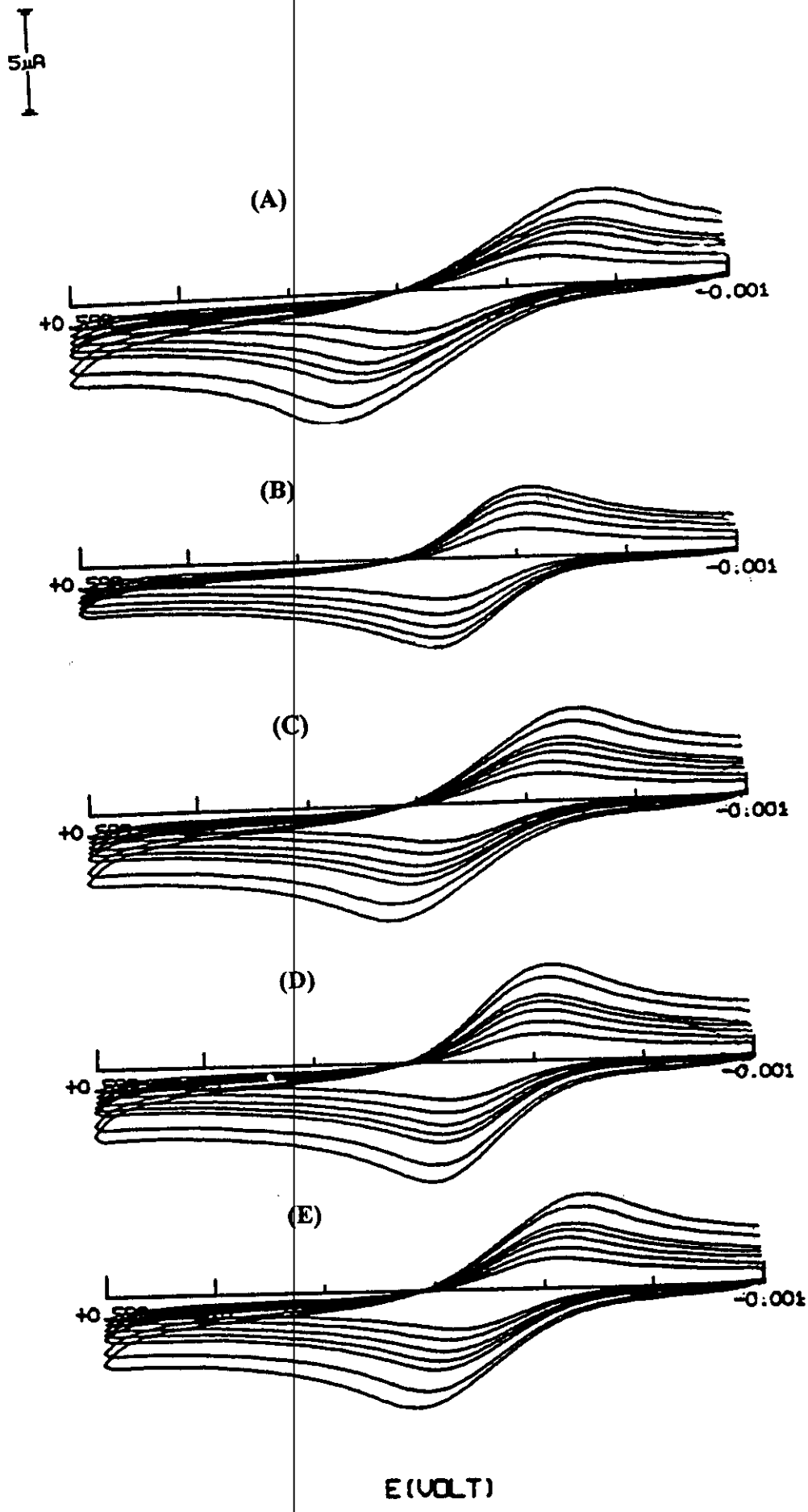

Figure 3: Cyclic voltammograms of 1 mM ferrocene recorded in Triton X-100 microemulsion systems containing (a) 0.5% n-octane, (b) 1.0% n-octane, (c) 1.5% n-octane, (d) 2.0% n-octane and (e) 2.5% n-octane, at 25°C. The sweep rates are 20, 40, 60, 80, 100, 150 and 200 mV/sec.

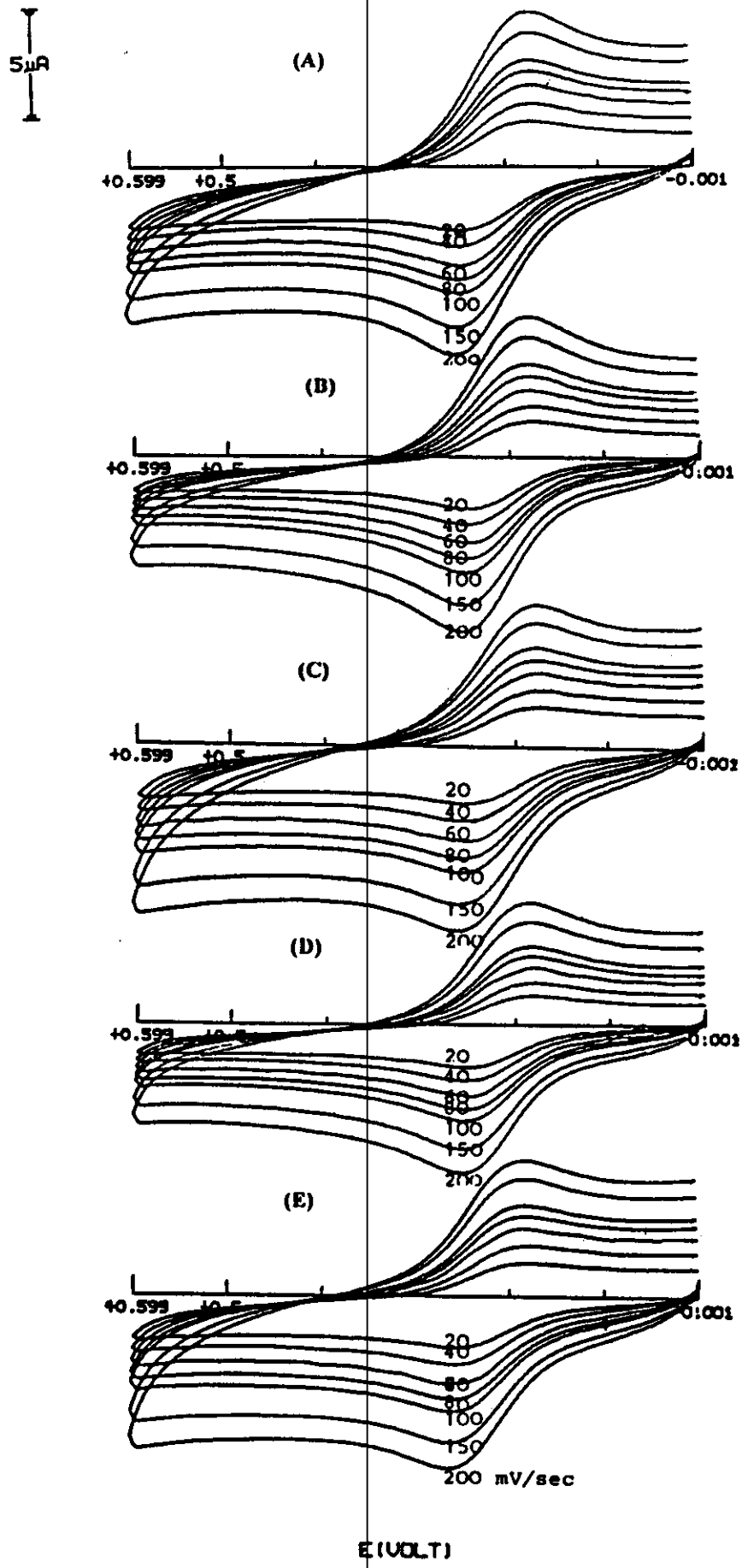

Figure 4: Cyclic voltammograms of 1 mM ferrocene recorded in SDS microemulsion systems containing (a) 0.5% n-octane, (b) 1.0% n-octane, (c) 1.5% n-octane, (d) 2.0% n-octane and (e) 2.5% n-octane, at 25°C. The sweep rates are 20, 40, 60, 80, 100, 150 and 200 mV/sec.

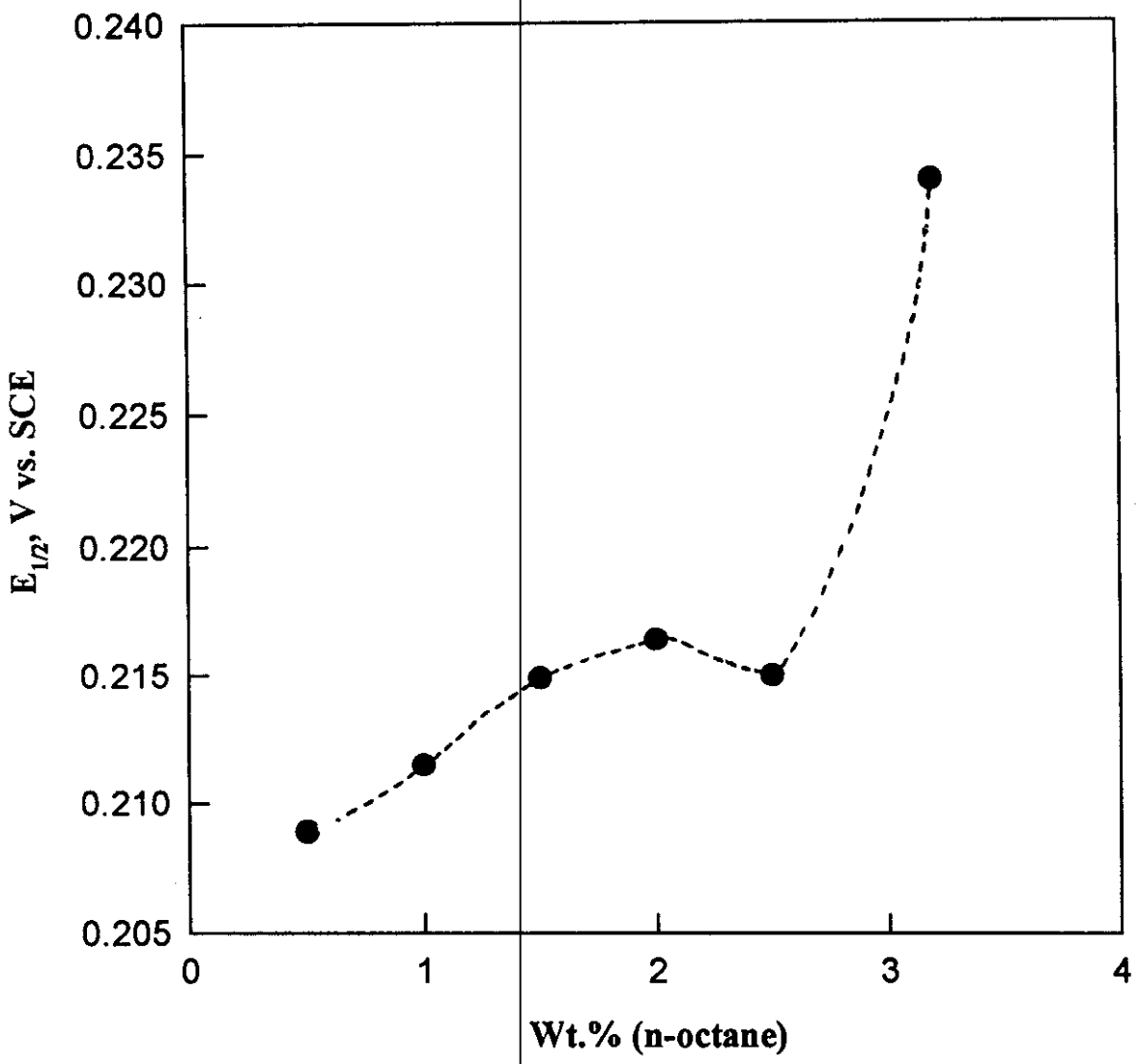

Figure 5: The dependence of half-wave potential ($E_{1/2}$) of 1 mM ferrocene in SDS microemulsion on the hydrocarbon contents.

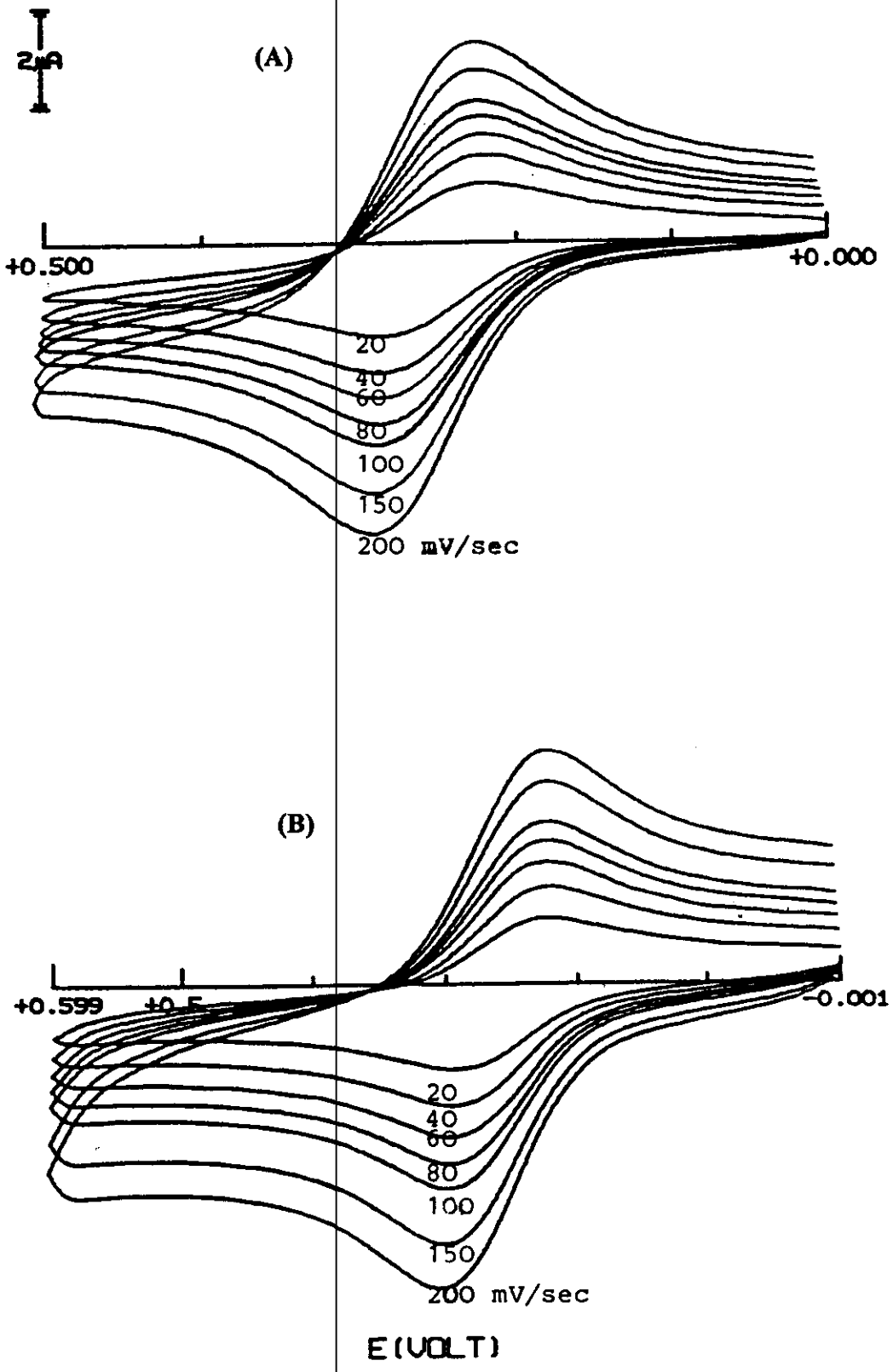

Figure 6: Cyclic voltammograms of 1 mM ferrocene in CTAB microemulsion system at (a) 15°C and (b) 30°C.

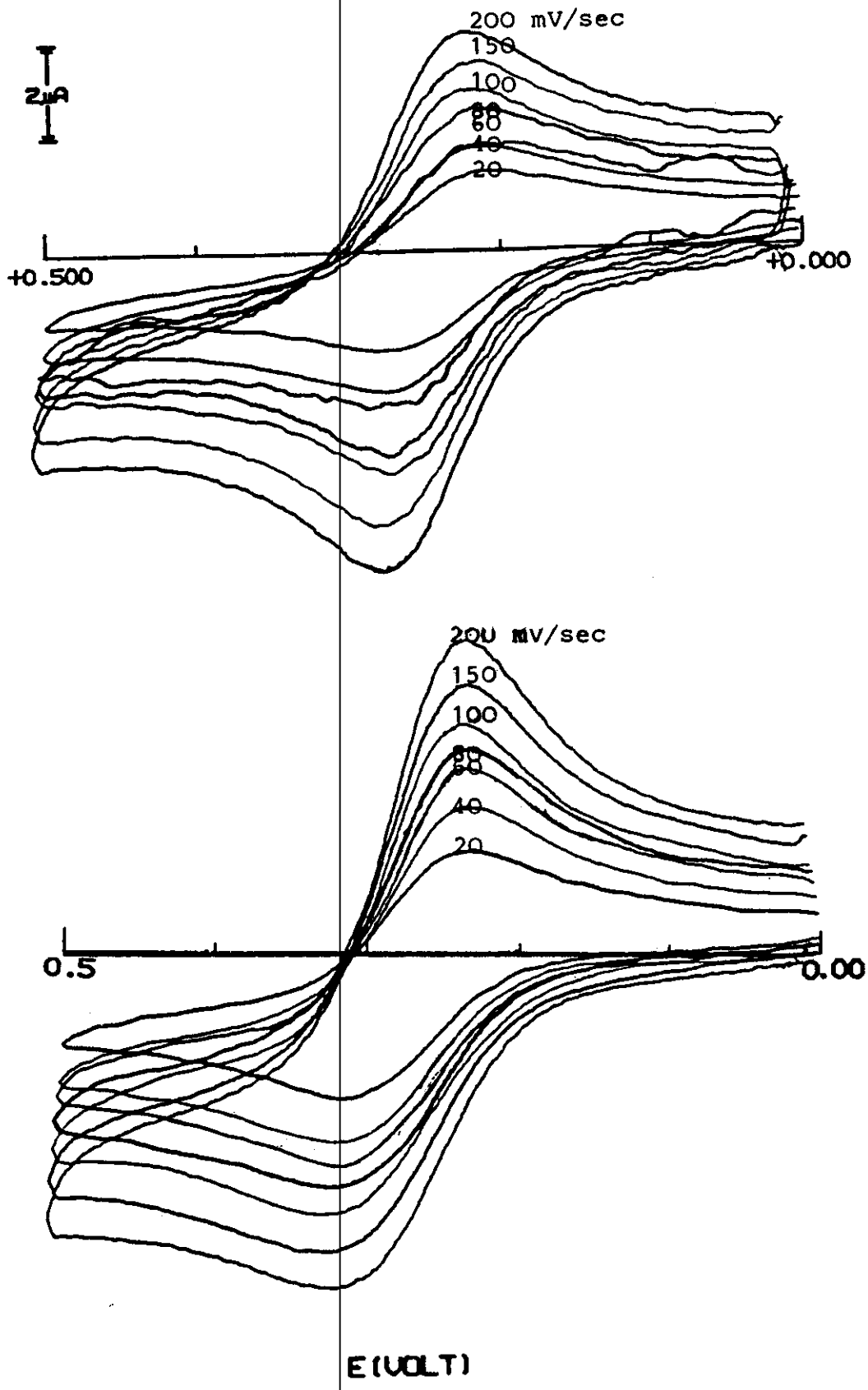

Figure 7: Cyclic voltammograms of 1 mM ferrocene in Triton X-100 microemulsion system at (a) 15°C and (b) 30°C.

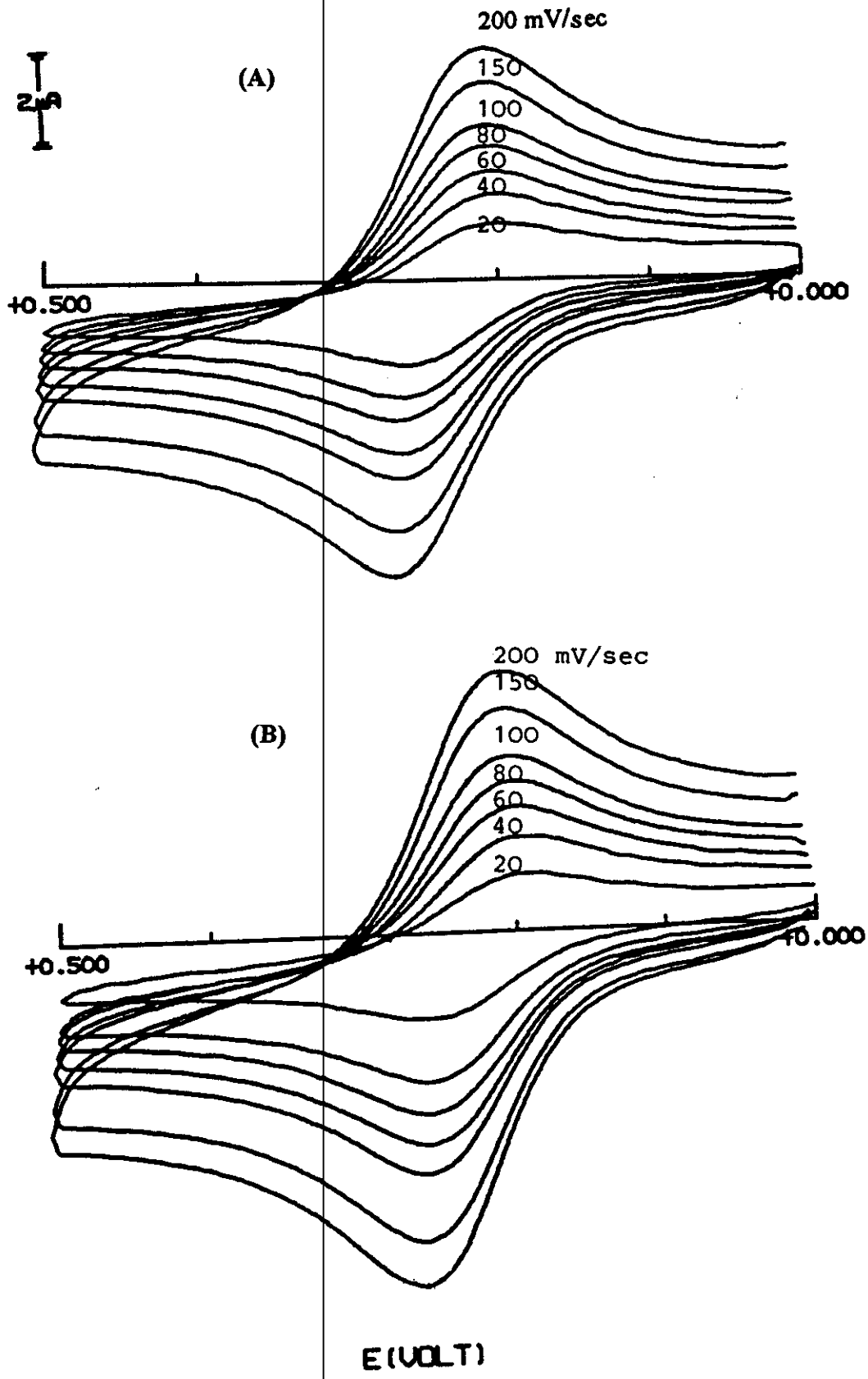

Figure 8: Cyclic voltammograms of 1 mM ferrocene in SDS microemulsion system at (a) 15°C and (b) 30°C.

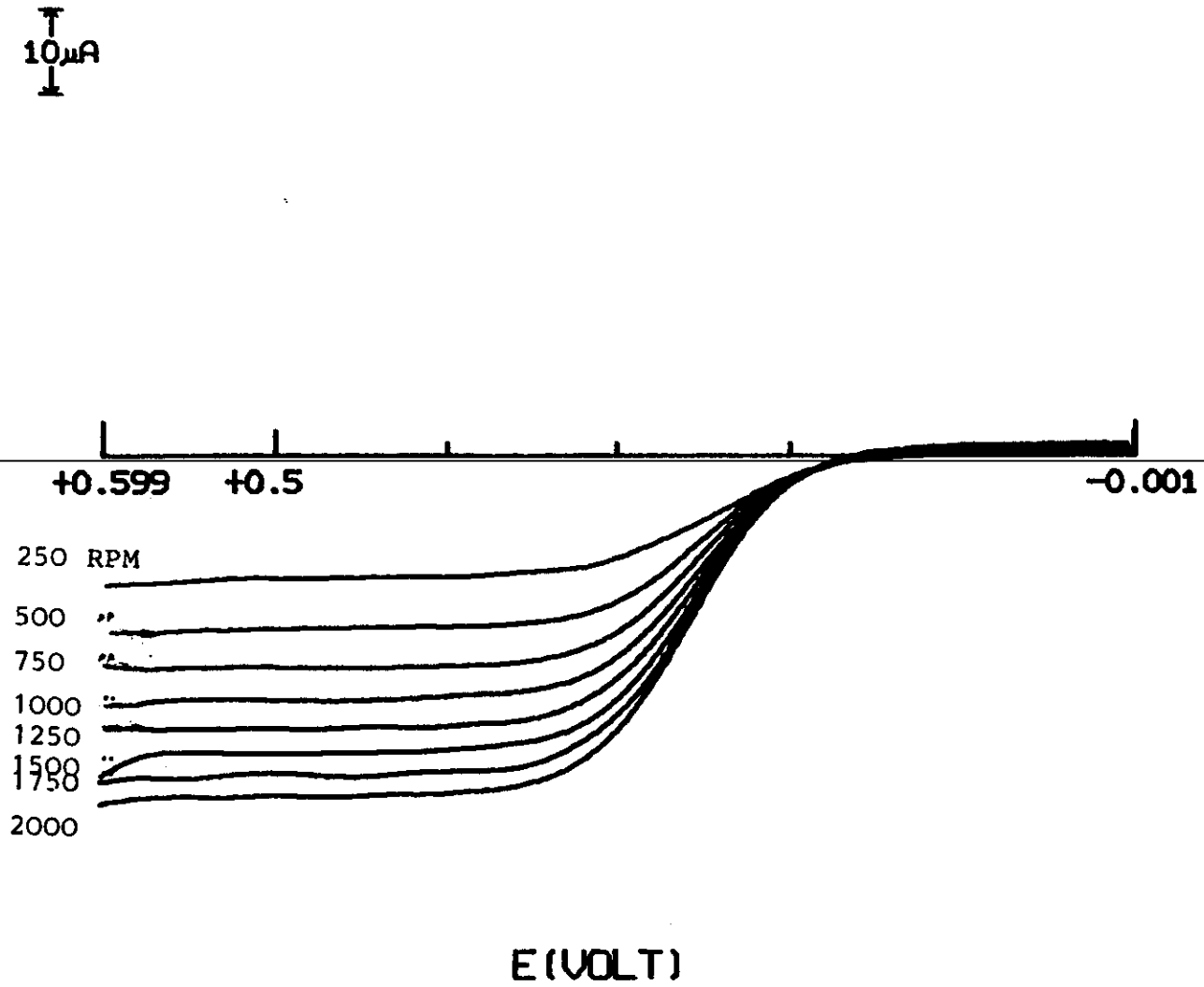

Figure 9: The effect of rotation speed of glassy carbon electrode on the linear sweep voltammograms obtained for 1 mM ferrocene in CTAB microemulsion. The rotation speeds are 250, 500, 750, 1000, 1250, 1500, 1750 and 2000 RPM.

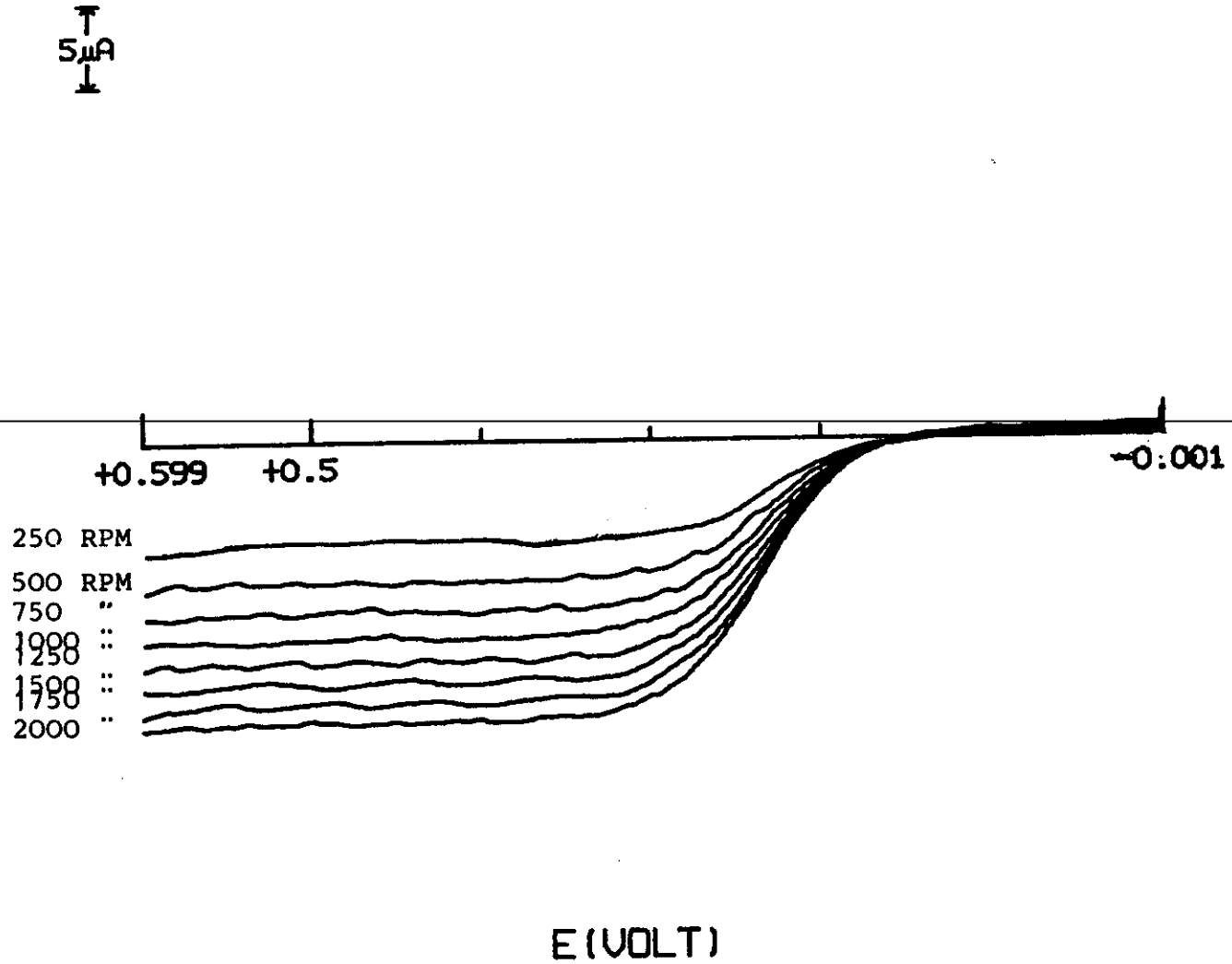

Figure 10: The effect of rotation speed of glassy carbon electrode on the linear sweep voltammograms obtained for 1 mM ferrocene in Triton X-100 microemulsion. The rotation speeds are 250, 500, 750, 1000, 1250, 1500, 1750 and 2000 RPM.

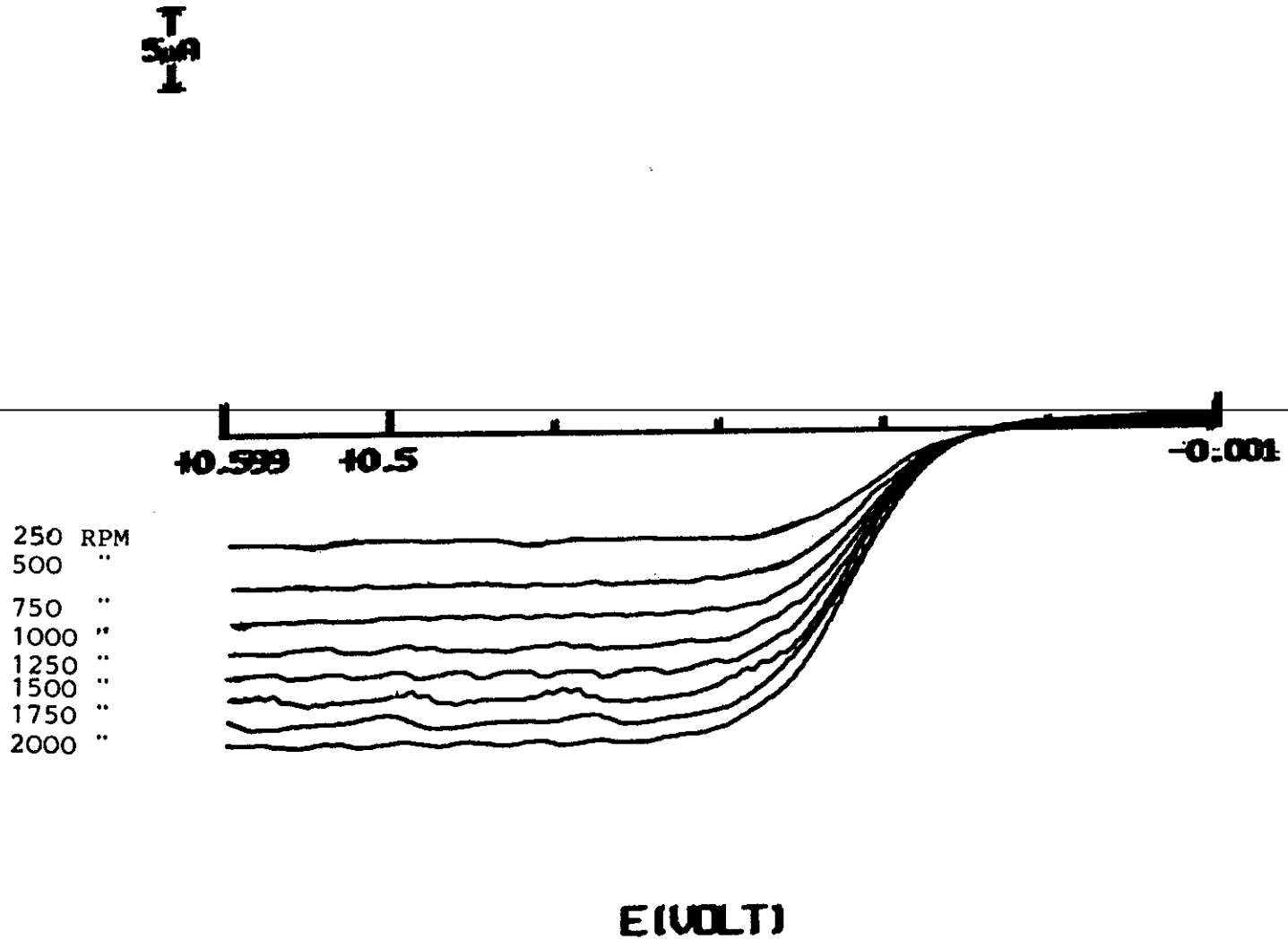

Figure 11: The effect of rotation speed of glassy carbon electrode on the linear sweep voltammograms obtained for 1 mM ferrocene in SDS microemulsion. The rotation speeds are 250, 500, 750, 1000, 1250, 1500, 1750 and 2000 RPM.

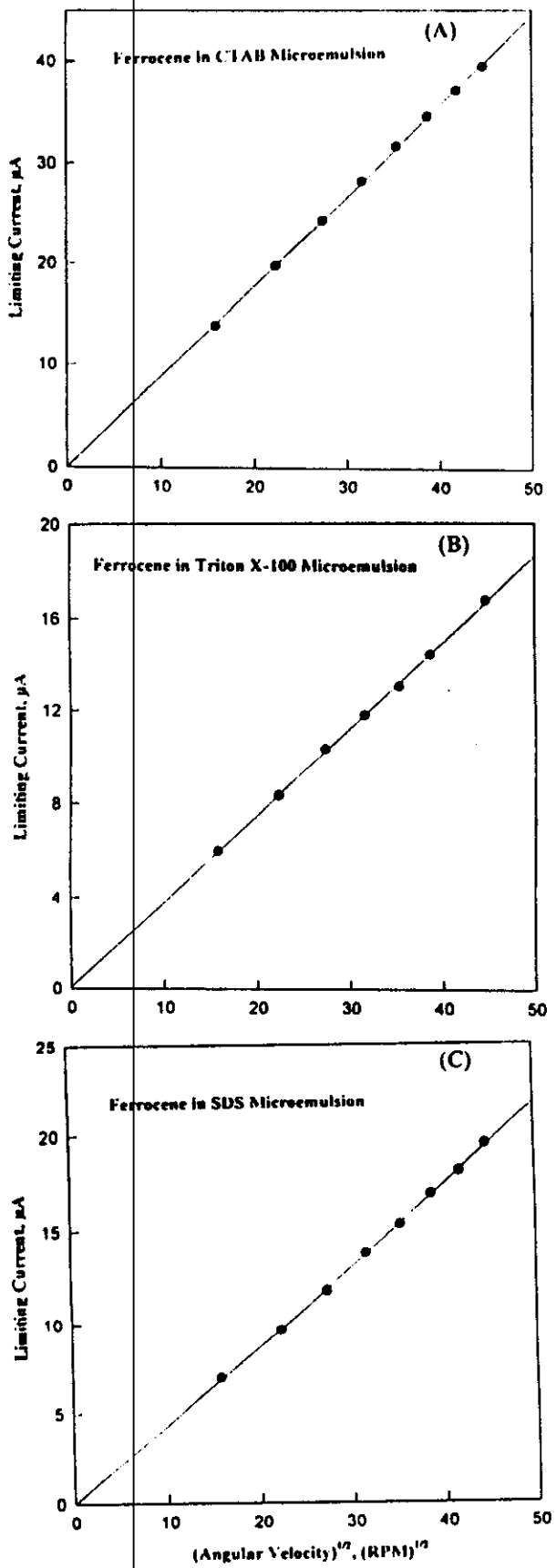

Figure 12: The plots of the limiting current (i_l) versus the square root of angular velocity ($\omega^{1/2}$) for 1mM ferrocene in (a) CTAB microemulsion, (b) Triton X-100 microemulsion and (c) SDS microemulsion.

RDV-Logarithmic Analysis of Ferrocene in Microemulsion Systems

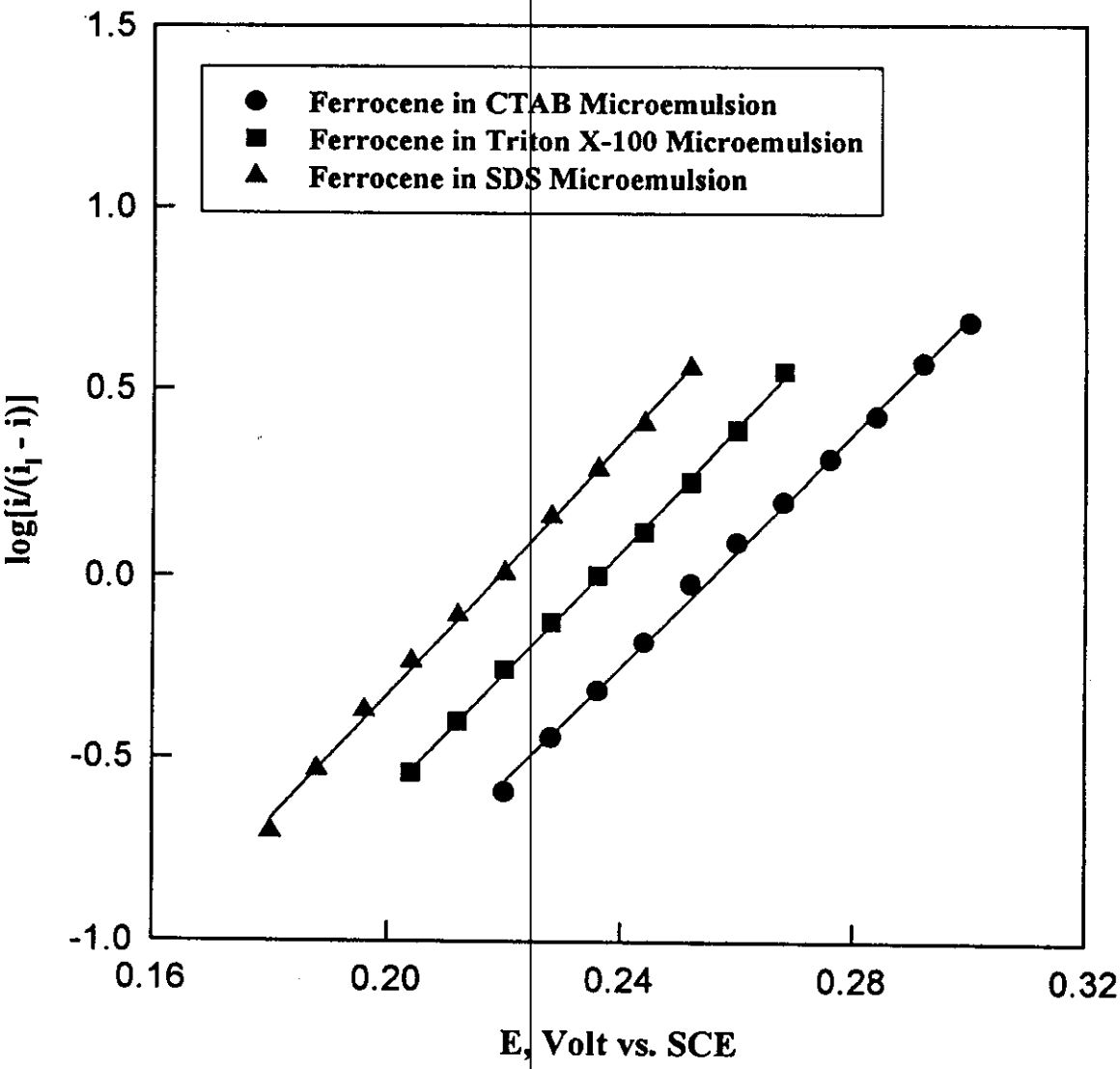

Figure 13:

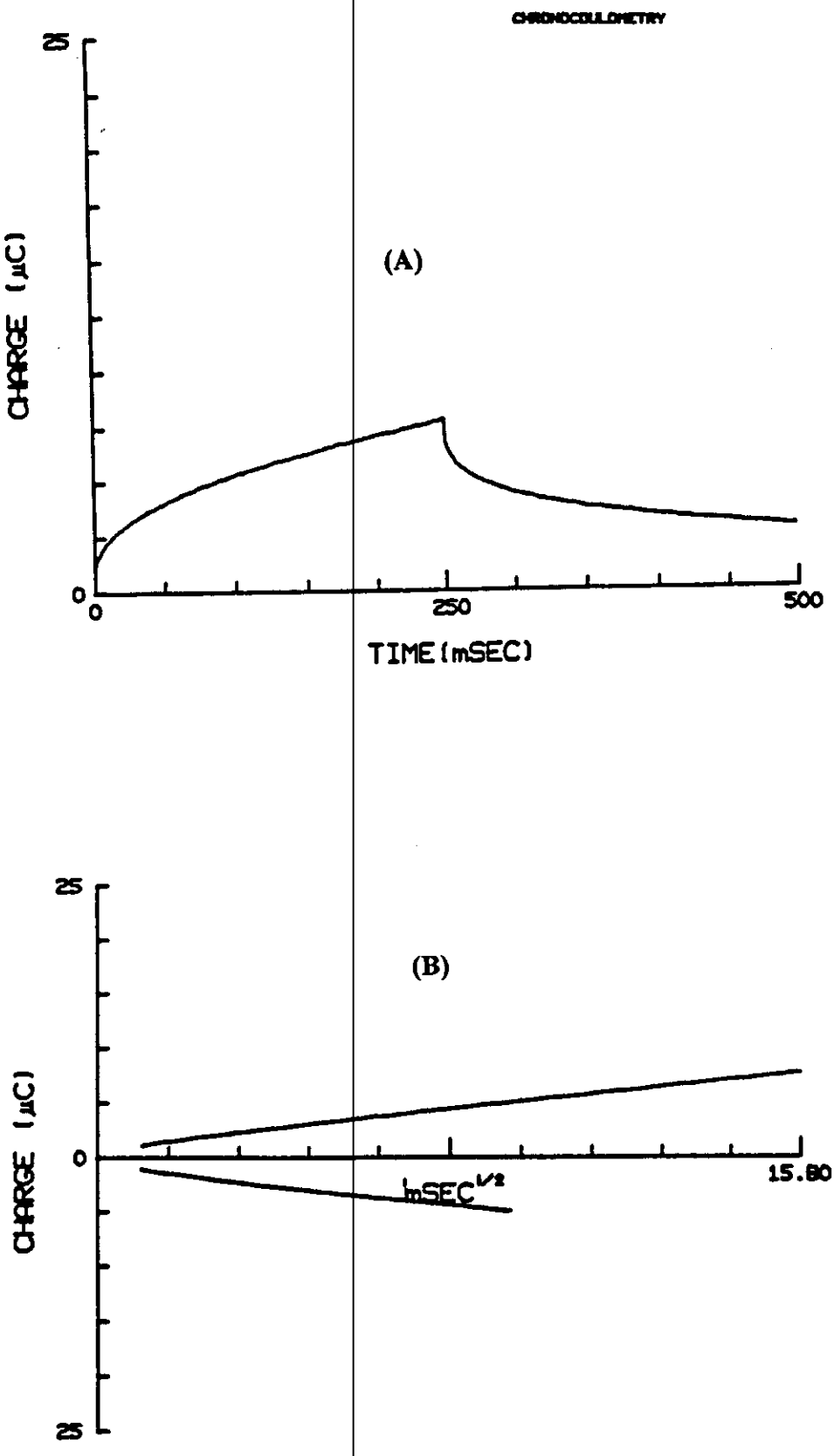

Figure 14: Chronocoulometric responses of 1 mM ferrocene in CTAB microemulsion system at 25°C, (a) Charge versus time and (b) Anson plots.

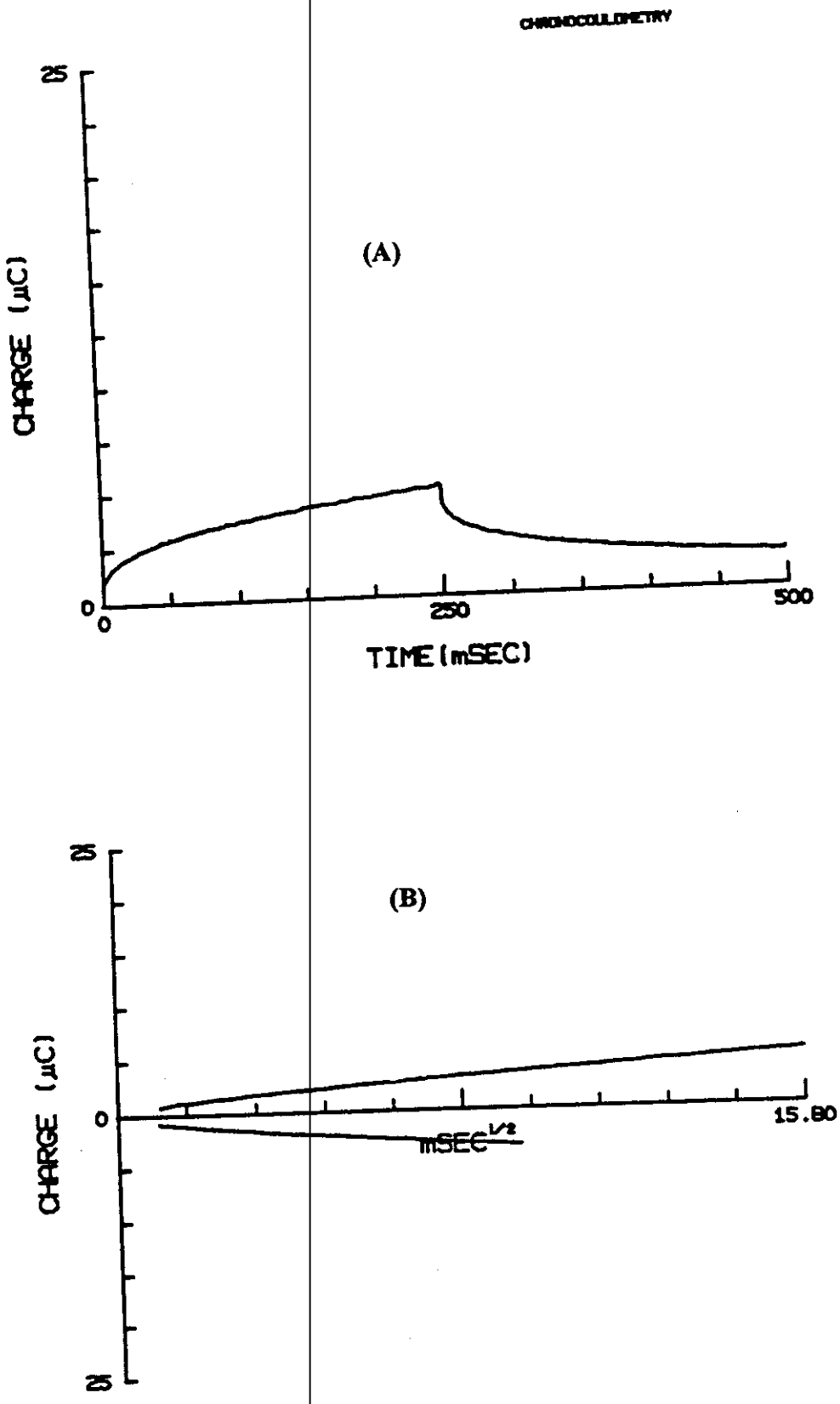

Figure 15: Chronocoulometric responses of 1 mM ferrocene in Triton X-100 microemulsion system at 25°C. (a) Charge versus time and (b) Anson plots.

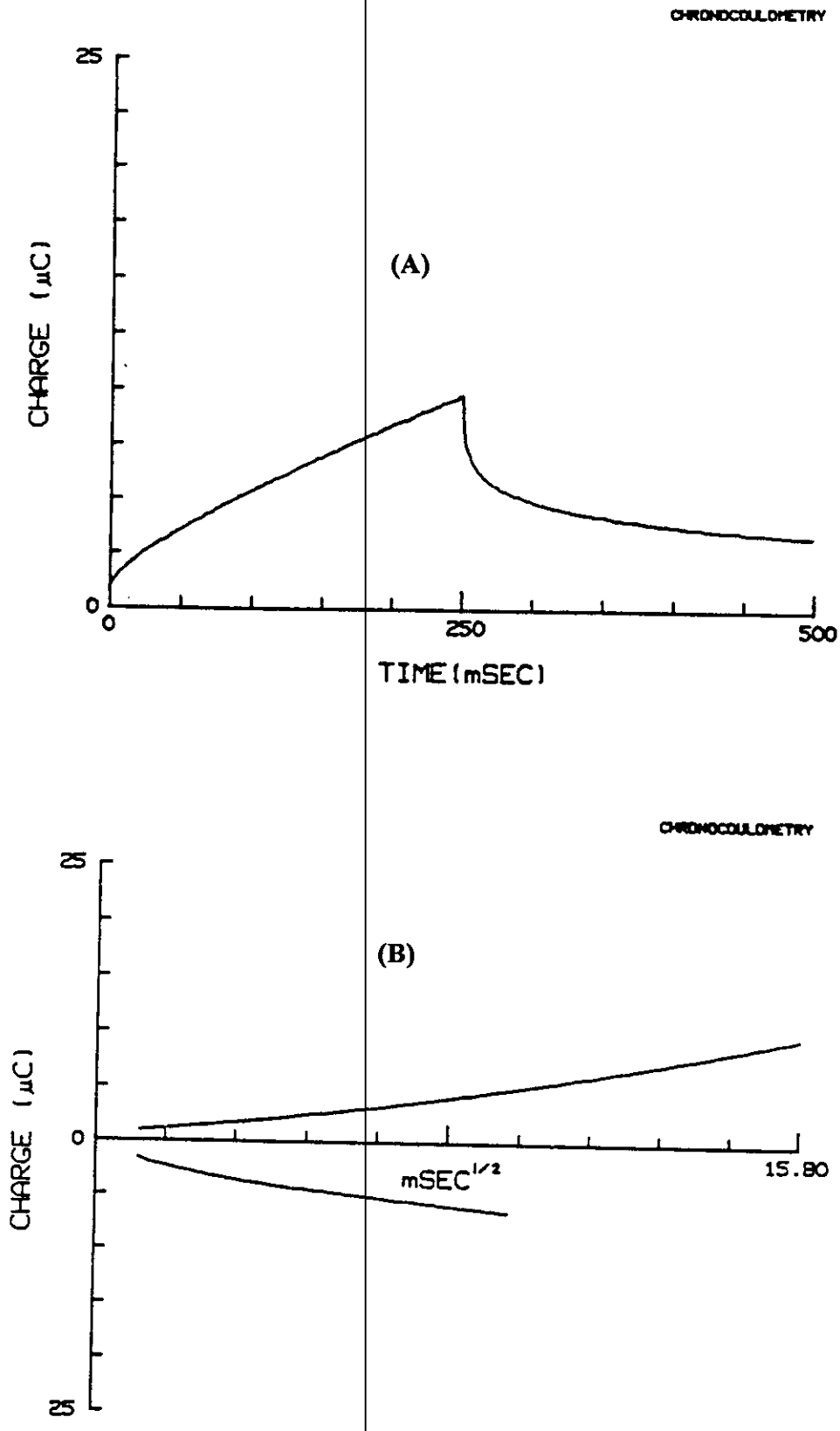

Figure 16: Chronocoulometric responses of 1 mM ferrocene in SDS microemulsion system at 25°C, (a) Charge versus time and (b) Anson plots.

Table 2 : Cyclic Voltammetric Data Obtained for 1 mM Ferrocene in CTAB Microemulsion system at 25°C.

Sweep Rate mV/sec	$E_{p,a}$ mV	$E_{p,c}$ mV	$I_{p,a}$ μA	$I_{p,c}$ μA	$I_{p,a}/I_{p,c}$ -	ΔE_p mV	$E_{1/2}$ mV
20	283	223	1.83	1.83	1.004	60	253
40	283	224	2.56	2.57	0.998	59	253
60	285	226	3.07	3.16	0.972	59	255
80	287	228	3.59	3.69	0.973	59	257
100	288	228	4.02	4.10	0.980	60	258
150	288	227	5.01	5.01	1.000	61	257
200	289	228	5.79	5.90	0.982	61	258
							$E_{1/2}$(average) = 256

Table 4 : Cyclic Voltammetric Data Obtained for 1 mM Ferrocene in SDS Microemulsion system at 25°C.

Sweep Rate mV/sec	$E_{p,a}$ mV	$E_{p,c}$ mV	$I_{p,a}$ μA	$I_{p,c}$ μA	$I_{p,a}/I_{p,c}$ -	ΔE_p mV	$E_{1/2}$ mV
20	245	1.95	2.33	2.55	0.914	50	220
40	249	198	3.05	3.10	0.984	51	223
60	257	205	3.80	3.70	1.027	52	231
80	259	209	4.27	4.32	0.988	50	234
100	268	212	4.85	4.80	1.010	56	240
150	269	219	6.10	5.77	1.057	50	244
200	270	220	7.12	6.63	1.074	50	245
						$E_{1/2}$(average) =	234

Table 5 : Cyclic Voltammetric Data Obtained for 1 mM Ferrocene in SDS Microemulsion Systems Containing Different Amounts of n-Octane at 25°C.

Sweep Rate mV/sec	$E_{p,a}$ mV	$E_{p,c}$ mV	$I_{p,a}$ μA	$I_{p,c}$ μA	$I_{p,a}/I_{p,c}$ -	ΔE_p mV
(A) 0.5% n-Octane						
20	244	178	3.69	3.54	1.041	66
40	244	179	4.57	4.52	1.009	65
60	246	179	5.69	5.61	1.013	67
80	246	178	6.52	6.54	0.997	68
100	248	177	7.29	7.35	0.992	71
150	250	176	9.31	9.31	1.000	74
200	251	177	10.83	10.67	1.015	74
(B) 1.0% n-Octane						
20	240	178	2.98	3.02	0.986	62
40	240	180	3.96	3.96	1.000	60
60	241	182	5.00	5.00	1.000	59
80	242	183	5.96	5.94	1.003	59
100	242	184	6.73	6.69	1.006	58
150	243	186	8.67	8.46	1.025	57
200	244	188	10.21	9.81	1.040	56
(C) 1.5% n-Octane						
20	242	180	3.17	3.37	0.938	62
40	244	182	4.17	4.44	0.940	62
60	245	183	5.31	5.61	0.946	62
80	245	183	6.27	6.50	0.965	62
100	245	183	7.10	7.46	0.953	62
150	248	185	8.95	9.17	0.976	63
200	250	185	10.41	10.48	0.994	65

Follow:

Sweep Rate mV/sec	$E_{p,a}$ mV	$E_{p,c}$ mV	$I_{p,a}$ μA	$I_{p,c}$ μA	$I_{p,a}/I_{p,c}$ -	ΔE_p mV
(D) 2.0% n-Octane						
20	254	192	2.90	2.81	1.030	62
40	254	194	3.90	3.92	0.995	60
60	253	193	4.96	5.00	0.992	60
80	255	193	5.82	5.82	1.000	62
100	256	194	6.60	6.50	1.016	62
150	257	194	8.42	8.38	1.005	63
200	258	195	9.95	9.95	1.000	63
(E) 2.5% n-Octane						
20	245	189	2.90	2.49	1.165	56
40	246	191	3.31	3.33	0.994	55
60	248	191	4.00	4.37	0.915	57
80	248	192	5.00	5.13	0.975	56
100	249	192	5.67	5.83	0.973	57
150	250	194	7.00	7.49	0.935	56
200	251	194	8.50	8.89	0.956	57

Table 6: Cyclic Voltammetric Data Obtained for 1 mM Ferrocene in Triton X-100 Microemulsion Systems Containing Different Amounts of n-Octane at 25°C.

Sweep Rate mV/sec	$E_{p,a}$ mV	$E_{p,c}$ mV	$I_{p,a}$ μA	$I_{p,c}$ μA	$I_{p,a}/I_{p,c}$ -	ΔE_p mV
(A) 0.50% n-Octane						
20	288	166	1.98	1.88	1.055	122
40	306	160	2.69	2.50	1.075	146
60	326	144	3.33	3.13	1.067	182
80	332	138	3.75	3.65	1.028	194
100	340	135	4.17	4.10	1.015	205
150	354	121	5.25	5.00	1.050	233
200	364	116	6.04	5.92	1.021	248
(B) 1.0% n-Octane						
20	270	195	1.92	1.92	1.000	75
40	273	195	2.71	2.79	0.970	78
60	273	193	3.31	3.35	0.987	80
80	274	191	3.85	3.88	0.995	83
100	274	190	4.35	4.48	0.972	84
(C) 1.5% n-Octane						
20	282	185	1.75	1.73	1.012	97
40	288	181	2.33	2.40	0.974	107
60	296	178	2.92	2.92	1.000	118
80	302	171	3.35	3.40	0.988	131
100	308	169	3.81	3.85	0.989	139
150	320	164	4.77	4.79	0.996	156
200	326	160	5.60	5.63	0.996	166

Follow:

Sweep Rate mV/sec	$E_{p,a}$ mV	$E_{p,c}$ mV	$I_{p,a}$ μA	$I_{p,c}$ μA	$I_{p,a}/I_{p,c}$ -	ΔE_p mV
(D) 2.0% n-Octane						
20	270	198	1.83	1.88	0.978	72
40	270	199	2.45	2.50	0.992	71
60	275	195	3.10	3.13	0.993	80
80	274	195	3.54	3.54	1.000	79
100	274	194	3.96	3.98	0.995	80
150	283	192	5.02	4.92	1.021	91
200	287	191	5.88	5.73	1.018	96
(E) 2.5% n-Octane						
20	278	187	1.84	1.83	1.006	91
40	280	184	2.31	2.29	1.009	96
60	285	183	2.92	2.91	1.002	102
80	290	179	3.33	3.35	0.994	111
100	292	178	3.79	3.75	1.011	114
150	302	173	4.79	4.79	1.000	129
200	311	168	5.65	5.63	1.004	143

Table 7: Cyclic Voltammetric Data Obtained for 1 mM Ferrocene in CTAB Microemulsion system at 15°C.

Sweep Rate mV/sec	$E_{p,a}$ mV	$E_{p,c}$ mV	$I_{p,a}$ μA	$I_{p,c}$ μA	$I_{p,a}/I_{p,c}$ -	ΔE_p mV	$E_{1/2}$ mV
20	298	235	1.44	1.54	0.938	63	266
40	298	235	1.94	2.27	0.853	63	266
60	300	236	2.33	2.78	0.893	64	268
80	301	235	2.66	3.12	0.855	66	268
100	301	236	2.98	3.42	0.870	65	268
150	302	237	3.70	4.10	0.902	65	269
200	302	238	4.31	4.57	0.944	64	270
							$E_{1/2(average)} = 268$

Table 8: Cyclic Voltammetric Data Obtained for 1 mM Ferrocene in CTAB Microemulsion system at 30°C.

Sweep Rate mV/sec	$E_{p,a}$ mV	$E_{p,c}$ mV	$I_{p,a}$ μA	$I_{p,c}$ μA	$I_{p,a}/I_{p,c}$ -	ΔE_p mV	$E_{1/2}$ mV
20	285	225	1.91	2.11	0.903	60	255
40	284	226	2.61	2.79	0.934	58	255
60	286	228	3.26	3.33	0.979	58	257
80	290	230	3.73	38.83	0.976	60	260
100	291	229	4.12	4.19	0.983	61	260
150	291	229	5.13	5.05	1.016	61	260
200	292	229	5.95	5.73	1.038	63	260
							$E_{1/2}$(average) = 258

Table 9: Cyclic Voltammetric Data Obtained for 1 mM Ferrocene in Triton X-100 Microemulsion system at 30°C.

Sweep Rate mV/sec	$E_{p,a}$ mV	$E_{p,c}$ mV	$I_{p,a}$ μA	$I_{p,c}$ μA	$I_{p,a}/I_{p,c}$ -	ΔE_p mV	$E_{1/2}$ mV
20	264	206	2.24	2.25	0.996	58	235
40	266	206	3.17	3.10	1.023	60	236
60	268	208	4.27	4.20	1.017	60	238
80	268	210	4.49	4.51	0.995	58	239
100	269	211	5.02	5.01	1.001	58	240
150	269	211	6.15	6.05	1.017	58	240
200	269	212	7.28	7.15	1.019	57	240
						Average =	238

Table 10: Cyclic Voltammetric Data Obtained for 1 mM Ferrocene in Triton X-100 Microemulsion system at 30°C.

Sweep Rate mV/sec	$E_{p,a}$ mV	$E_{p,c}$ mV	$I_{p,a}$ μA	$I_{p,c}$ μA	$I_{p,a}/I_{p,c}$ -	ΔE_p mV	$E_{1/2}$ mV
20	264	206	2.24	2.25	0.996	58	235
40	266	206	3.17	3.10	1.023	60	236
60	268	208	4.27	4.20	1.017	60	238
80	268	210	4.49	4.51	0.995	58	239
100	269	211	5.02	5.01	1.001	58	240
150	269	211	6.15	6.05	1.017	58	240
200	269	212	7.28	7.15	1.019	57	240
						$E_{1/2}$(average) =	238

Table 11: Cyclic Voltammetric Data Obtained for 1 mM Ferrocene in SDS Microemulsion system at 15°C.

Sweep Rate mV/sec	$E_{p,a}$ mV	$E_{p,c}$ mV	$I_{p,a}$ μA	$I_{p,c}$ μA	$I_{p,a}/I_{p,c}$ -	ΔE_p mV	$E_{1/2}$ mV
20	259	200	1.92	1.94	0.989	59	229
40	258	201	2.47	2.56	0.968	57	229
60	260	202	2.86	3.16	0.906	58	231
80	261	203	3.48	3.78	0.921	58	232
100	262	205	3.95	4.27	0.926	57	233
150	263	207	4.92	5.22	0.941	56	235
200	263	207	5.61	6.21	0.904	56	235
							$E_{1/2}$(average) = 232

Table 12: Cyclic Voltammetric Data Obtained for 1 mM Ferrocene in SDS Microemulsion system at 30°C.

Sweep Rate mV/sec	$E_{p,a}$ mV	$E_{p,c}$ mV	$I_{p,a}$ μA	$I_{p,c}$ μA	$I_{p,a}/I_{p,c}$ -	ΔE_p mV	$E_{1/2}$ mV
20	258	197	2.25	2.18	1.033	61	227
40	257	198	3.44	3.31	1.040	59	227
60	259	200	3.99	4.04	0.987	59	229
80	260	202	4.55	4.74	0.961	58	231
100	262	204	5.08	5.34	0.950	58	233
150	264	205	6.40	6.49	0.986	59	234
200	266	206	7.32	7.41	0.987	60	236
						Average =	231

3.2 Voltammetric Detection of Micelles

The electrochemical techniques were used successfully for the determination of the critical micelle concentration (CMC) of the prepared polymeric surfactant, sodium 11-acrylamidoundecanoate (Na 11-AAU). Such techniques used are rotating disk voltammetry (RDV) and cyclic voltammetry. On using the RDV method, a known concentration of the electroactive probe was added to a series of the monomeric surfactant solution, Na 11-AAU, containing indifferent supporting electrolyte, NaBr 0.1 M. The surfactant concentration was varied in the range from $1x10^{-4}$ to $2x10^{-3}$ M. The effect of rotation speed on the voltammograms of $7x10^{-5}$ M electroactive ferrocene was recorded at rotation speeds 250, 500, 750, 1000, 1250, 1500, 1750 and 2000 RPM in such surfactant solutions. The scan rate used was 5 mV/sec in these experiments at all rotation speeds. The limiting current (i_l) measured from the current-potential response at the steady state was found to linearly increase on increasining the rotation speed. Fig. (17), showed that on increasing the surfactant concentration as the limiting current is slightly decreased up to a concentration $4x10^{-4}$ M a significant decrease was observed on the limiting current values. At concentrations beyond that point (i_l) is slightly decreased again producing an S-shapped behaviour for the current respose to the surfactant concentration. The voltammetric behaviour of ferrocene is reversible in such cases as indicated from the analysis of the rotating disk voltammogram at rotation speed 1000 RPM. On plotting $\ln[i/(i_l - i)]$ vs. E a straight line of slope equal to 0.059 is obtained which corresponds to a one electron transfer. Also, the cyclic voltammograms showed a reversible behaviour of ferrocene in such media as indicated from the peak separations, ΔE_p, which have values in the range from 57 to 63 mV corresponding to the one electron transfer. Furthermore, this

behaviour of decreasing the limiting diffusion current in rotating disk experiments on increasing surfactant concentration is not attributed to surfactant adsorption, because chronocoulometry showed that there is a negligible adsorption at all surfactant concentrations. Therefore, this can be only attributed to structural changes of surfactant and a transition from monomer surfactant molecule to aggregates.

On using Levich equation [159]:

$$i_l = 0.62\ nFACD_1^{2/3}\nu^{-1/6}\omega^{1/2} \qquad \textbf{(III.3)}$$

where, i_l is the limiting diffusion current (amp), n is the number of electrons transferred, F is the Faraday's constant, A is the area of the electrode, C is the concentration of the electroactive probe, ν is the kinematic viscosity of the solution and ω is the angular velocity (rad s^{-1}). The plots of i_l versus $\omega^{1/2}$ for the electrochemical oxidation of ferrocene at different Na 11-AAU concentrations give linear correlations passing through the origin Fig. (17), confirming the diffusion nature of the electrochemical reactions. The slope values were used to estimate the apparent diffusion coefficient.

The corresponding micelle sizes were often calculated from the diffusion coefficient values using the Stokes-Einstein equation (III.2), and since the electroactive probe is distibuted between the continuous aqueous phase and the micelles, the Levich equation (III.3) may be written in the pseudophase approximation as:

$$i_l = 0.62nFA\{D_1^{2/3}(C_1 - C_2) + D_2^{2/3}C_2\}\nu^{-1/6}\omega^{1/2} \qquad \textbf{(III.8)}$$

where C_1 and D_1 are the total concentration of the probe and aqueous phase diffusion coefficient, respectively; C_2 is the concentration (relative to the total volume) of the probe in the micelles and D_2 is the micelle diffusion coefficient.

At kinematic viscosities common to moderately dilute aqueous solutions, the root-angular velocity dependence of the Levich equation allows to extract a slope

$$S_o = \partial i_l/\partial \omega^{1/2} = i_l/\omega^{1/2} \qquad \textbf{(III.9)}$$

The analogous quantity derived from equation (III.8) when divided by equation (III.9), gives

$$S/S_o = [(C_1 - C_2)/C_1 + (D_2/D_1)^{2/3}(C_2/C_1)]x(\nu/\nu_o)^{-1/6} \qquad \textbf{(III.10)}$$

The slope of the i_l versus $\omega^{1/2}$ of ferrocene in a very dilute surfactant solution is considered as the slope in pure aqueous media (S_o). On plotting the ratio of slopes (S/S_o) against the logarithm of surfactant concentration, an S-shapped curve was obtained as given in Fig. (18). The use of the ratio of slope in rotating disk method provides an exact method of determining the critical micelle concentration by avoiding the fluctuation in the probe concentration, the inflection point on the curve indicate the critical micelle concentration (CMC) and it was found to equal $4x10^{-4}$ M.

Limiting Current of Ferrocene in Polymeric Surfactant [Na 11-AAU] of Different Concentration

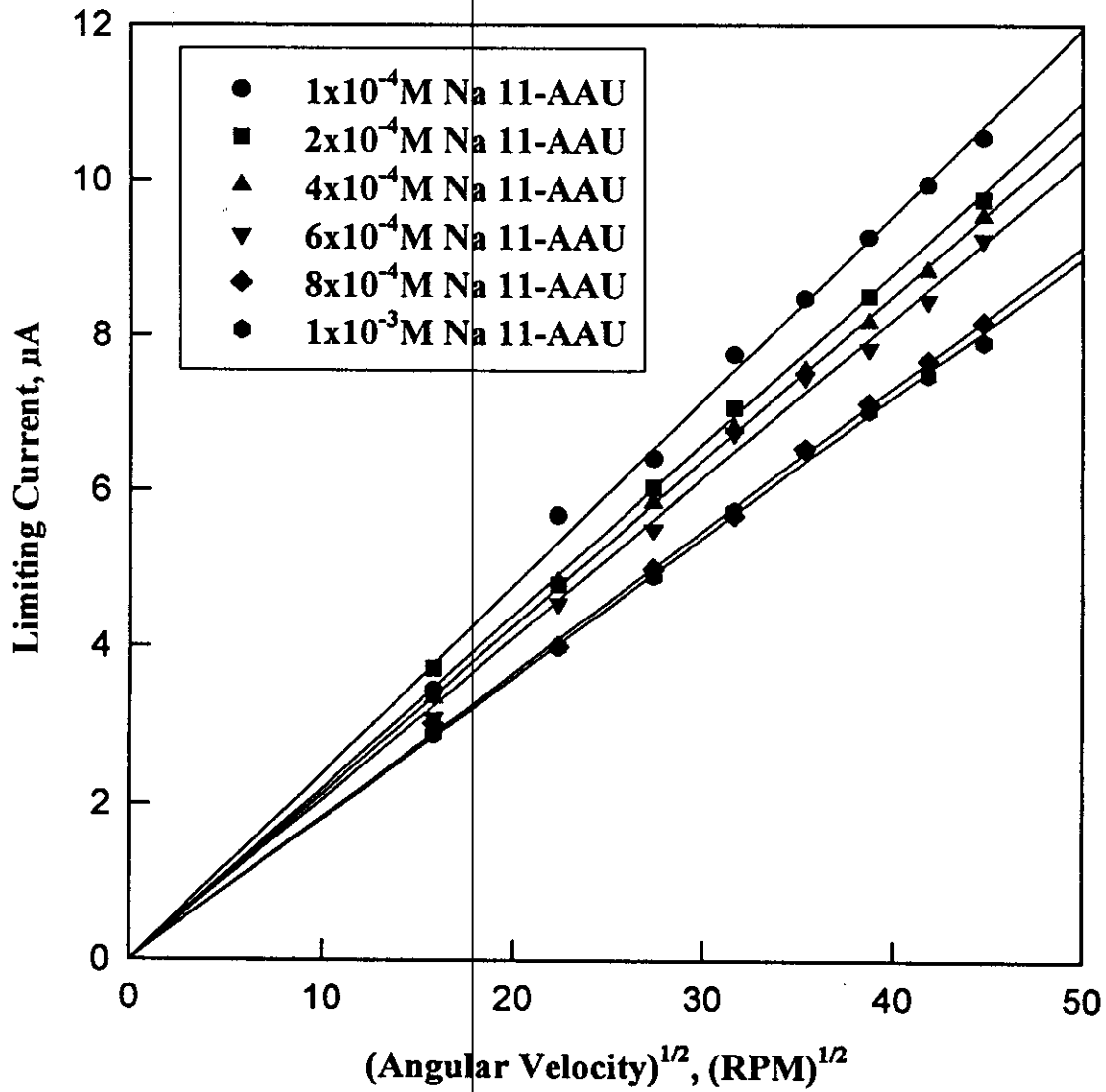

Figure 17:

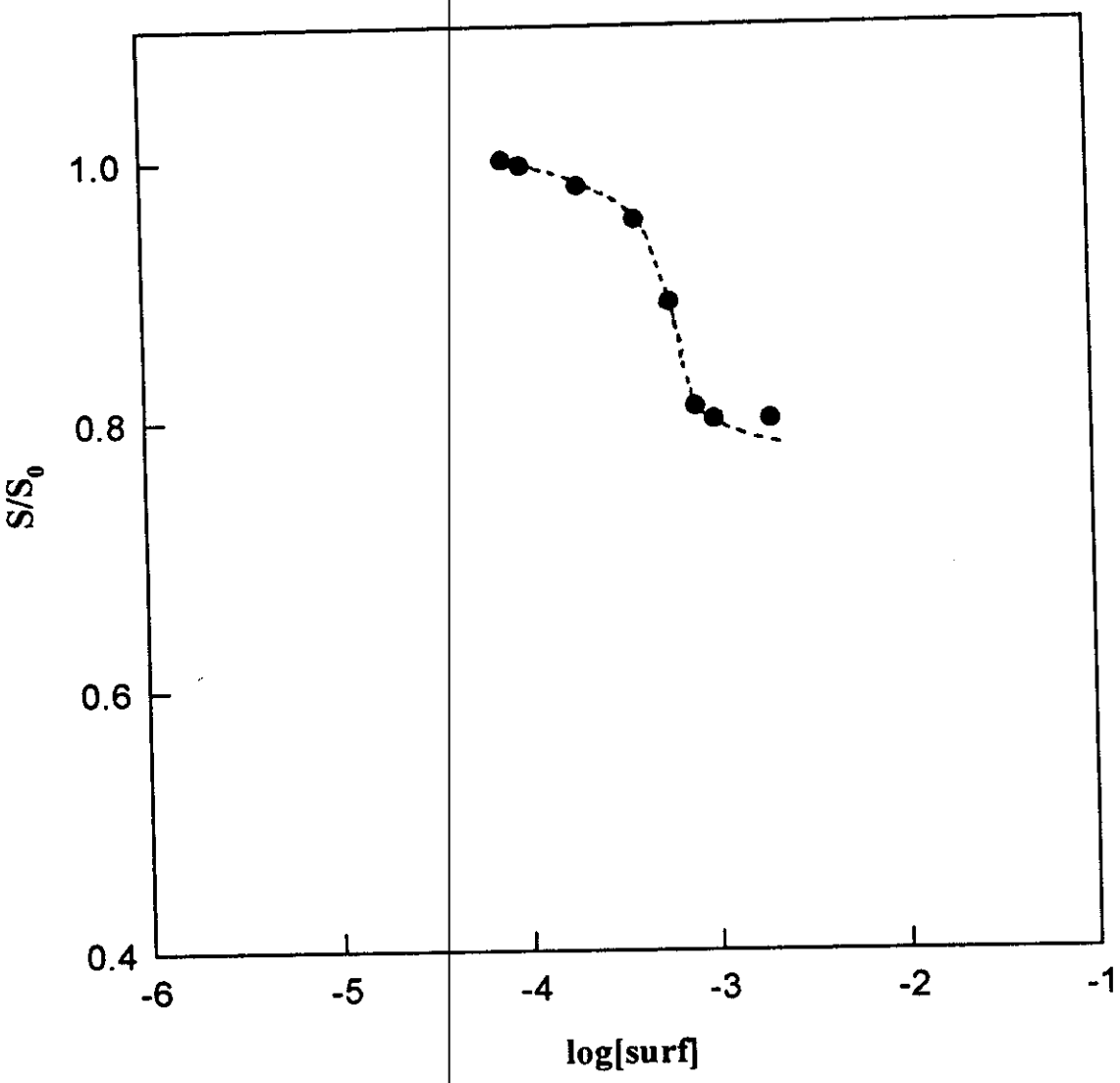

Figure 18: The plots of the ratio of slopes of i_l versus $\omega^{1/2}$ obtained from aqueous and in surfactant solutions (S/S_0) against the logarithm of surfactant concentration.

3.3 Electrochemical Investigations in Microemulsion and in Pure Aqueous Media

3.3.1 1-Amino-9,10-anthraquinone

The voltammograms of 0.30 mM 1-amino-9,10-anthraquinone (1AAQ) were recorded in micellar solutions and microemulsion systems of three different surfactant types as well as pure aqueous solution at 25 °C. Cationic (cetyltrimethylammonium bromide, CTAB), anionic (sodium dodecyl sulphate, SDS), and nonionic {octylphenoxypoly(oxyethylene), Triton X-100} model surfactants were used in this investigation with a composition given in Table (1). Well defined voltammograms were obtained for 1AAQ reduction in CTAB, SDS and Triton X-100 microemulsions. The voltammograms showed only one cathodic peak on the cathodic scan and one anodic peak on the reverse scan in all microemulsion media as represented by Figs. (19a-21a). Also, the voltammograms of $9x10^{-5}$ M 1AAQ in the corresponding pure aqueous solution containing only 0.1 M NaBr supporting electrolyte showed a similar voltammetric response as shown in Fig. (22a). Except in CTAB micelles a shoulder appears in addition to the main reduction peak, and one oxidation peak was observed as represented by Fig.(19b). The voltammograms recorded at different sweep rates varying from 20 to 200 mV/sec are similar and showed one cathodic and one anodic peak. The cathodic and anodic peak potential values ($E_{p,c}$ and $E_{p,a}$) remain nearly constant on increasing sweep rate. The voltammograms recorded in the corresponding micellar solutions are essentially similar; Figs. (19b-21b). The voltammetric data of 1AAQ in various surfactant systems are summarized in Tables (13-15). The peak potential separation ΔE_p ($\Delta E_p = E_{p,c} - E_{p,a}$) is very close to 30 mV at very small sweep rates. These data suggested that the reduction of 1AAQ is chemically reversible with a net transfer of two electrons, since $\Delta E_p = 0.059/n$. On increasing the sweep rate, the peak separation ΔE_p is slightly increased from 28 to 53 mV, Tables (13-15). These facts lead generally to the electrochemical-chemical-

electrochemical (ECE) reaction nature. Protonation of the anion radical generally leads to a disproportionation reaction [186,187]. The disproportionation reaction of anionic free radical of $1AAQ^{-\cdot}$ is favored by the decrease of the energy difference between $1AAQ^{-\cdot}$ and $1AAQ^{--}$ due to hydrogen bond solvation of the carbonyl group by water molecules [188,189]. Therefore, our results were interpreted in terms of disproportionation of the anion free radical ($1AAQ^{-\cdot}$) to the original quinone and hydroquinone in the presence of water. The disproportionation reaction that takes place under the present experimental conditions can be represented as following:

$$1AAQ + e^{-} \Leftrightarrow 1AAQ^{-\cdot} \qquad \text{(i)}$$

$$2(1AAQ^{-\cdot}) + 2H^{+} \Leftrightarrow 1AAQ + 1AAQH_2 \qquad \text{(ii)}$$

The peak currents on the cathodic and anodic branches of sweep are not equal, and the ratio $I_{p,a}/I_{p,c}$ is less than unity for 1AAQ in microemulsion systems and much less in micellar solutions (Tables 13-15). On employing the Randles-Sevcik equation (III.1), the plots of cathodic and anodic peak currents ($I_{p,c}$ & $I_{p,a}$) versus $\upsilon^{1/2}$ for 1AAQ in micellar and microemulsion media showed linear correlations passing almost through the origin confirming that the electrode process is mainly diffusion controlled [168], Fig.(23). On the other hand, the plots of $I_{p,c}$ versus $\upsilon^{1/2}$ for the reduction of 1AAQ in pure aqueous solution is deviated from linearity at high sweep rates, as shown from Fig. (22b). This behaviour may be attributed to adsorption on the electrode surface and/or dimerization of the free anionic radical ($1AAQ^{-\cdot}$). The diffusion coefficients of the oxidized and reduced forms (D_O and D_R) were determined from the slopes of these linear plots. The values which obtained at different temperatures and given in Table (16), indicate the partitioning of 1AAQ between oil droplet, surfactant film and aqueous domain.

There is a considerable increase in the solubility of 1AAQ in micellar solutions and microemulsions compared to the aqueous solutions (<<0.1 mM). The increase in solubility of a substance in the presence of surfactants can be due to a variety of interactions [91]. Electrostatic attraction of the oppositely charged ends of the dipoles by ionic micelles, association with micelles via surface adsorption on the surfactant film, and solubilization in the hydrophobic core of the micelles are a few appropriate examples. The non-polar domain size is larger in microemulsions compared to micelles due to the additional oil component. The exact location of the substrate in micellar solutions and microemulsions thus depends on a variety of factors like the nature of the substrate, the type of surfactant, the nature of the counter ions in ionic surfactants, the solubility of substrate in oil, the type of added electrolyte, etc. The location is not usually known and can be controversial. Regardless of the specifics of the interaction, the attachment of an electroactive substance to the micelle or microemulsion droplet generally leads to a diffusion current which is very much less than that observed in pure aqueous or non-aqueous solutions at the same concentration.

An important aspect to be considered in electrochemical investigation in surfactant solutions is the adsorption of the surfactant on the electrode surface and its effect on the electrochemical reactions. Our previous electrochemical investigation of ferrocene in CTAB, SDS, and Triton X-100 microemulsions did not show any significant effect that could be ascribed to surfactant adsorption on the electrode surface. All the results observed in these studies could be explained based on electrostatic and hydrophobic interactions of the surfactant with the various species (reactant, intermediates and products) of the electrochemical reaction. In the absence of such interactions the electrochemical behaviour is not significantly affected [95]. In the present investigation, the decreased ratio of $I_{p,a}/I_{p,c}$ from unity suggests the presence of adsorption. Only in cationic CTAB systems (micelles and microemulsion) adsorption is more probable at the 1AAQ

reduction potential (negatively charged electrode). But this is not the case since the peak current ratio ($I_{p,a}/I_{p,c}$) is higher in CTAB than other systems (SDS and Triton X-100), Tables (13-15).

Since cationic surfactants are known to stabilize anion radicals [190], the stabilization of $1AA\overline{Q}^{\cdot}$ by CTAB seems to hinder the disproportionation reaction (ii) to a large extent. The slightly smaller ΔE_p (30 mV) in micellar solutions compared to about 53 mV in microemulsions shows that the stabilization in microemulsions is less than in micellar solutions. This is because the electrostatic effects are generally less in microemulsions than in micellar solutions due to the decreased charge density on the surface of the microemulsion droplets compared to the micelles. Also, ΔE_p values are close to 30 mV at very slow sweep rates and increase with increasing sweep rates. These characteristics are typical of a reversible charge transfer reaction followed by a slow chemical reaction [142]. The chemical reaction following the first electron transfer, is the disproportionation of $1AA\overline{Q}^{\cdot}$ to the corresponding hydroquinone and the reactant (reaction ii). Since 1AAQ is slightly soluble in aqueous media, stabilization of reactant and intermediate ($1AA\overline{Q}^{\cdot}$) takes place hydrophobic as well as electrostatic effects and diffusion coefficient values indicate the partitioning effect of 1AAQ.

Values of $I_{p,a}/I_{p,c}$ for the depolarizer species (1AAQ) in SDS or Triton X-100 micelles and microemulsion media are not much different (Tables 14&15). SDS anionic, is known to kinetically stabilizes anion radicals of nitrobenzene [91], stabilization is also possible in the presence of non-ionic surfactant molecules where the anion radical will be present at the interface between the hydrocarbon core and the polar poly(oxyethylene) sheath. The partial stabilization of $1AA\overline{Q}^{\cdot}$ by SDS and Triton X-100 surfactants thus slows down the disproportionation reaction (2), while in CTAB systems the stabilization is more pronounced and tend to inhibit reaction (ii).

Differences are observed in the values of E_p, ΔE_p and $I_{p,a}/I_{p,c}$ between micellar solutions or microemulsions (Tables 13-15). The constancy of cathodic peak potential $E_{p,c}$ and slightly less

negative shift of anodic peak potential $E_{p,a}$ on increasing sweep rate give a voltammetric response similar to that of a slow chemical reaction following a reversible charge transfer reaction. Also changes in half-wave potential ($E_{1/2}$) are expected due to the different effects of the surfactant as local environment on the relative stabilities of the reactant and product of the electron transfer reaction.

Generally the hydrophobic effect which stabilizes 1AAQ in all the surfactant systems is also expected to stabilize $1AA\overline{Q}^{\cdot}$ to a similar extent. $1AA\overline{Q}^{\cdot}$ is further stabilized by a strong electrostatic interaction in CTAB systems. Therefore, in CTAB systems the stabilization of the product is stronger than the stabilization of the reactant. This decreases the free energy of the product which leads to a decrease in the energy of activation of the reaction and thus, the reduction process takes place at a less negative potential.

Based on the above results, $E_{1/2}$ should be shifted to a less negative value in the CTAB micellar solution and microemulsion. $E_{1/2}$ values in SDS and Triton X-100 micellar solutions and microemulsions are expected to be the same. The average of the $E_{p,c}$ and $E_{p,a}$ values is taken as the $E_{1/2}$ for CTAB micellar solution and microemulsion. The average of $E_{p,c}$ and $E_{p,a}$ values obtained at very low sweep rates where the reaction is nearly reversible is taken as the $E_{1/2}$ for the SDS and Triton X-100 systems. $E_{1/2}$ values shown in Table (17) for CTAB and SDS systems follow the expected trend. It appears that hydrophobic interaction is predominant in the SDS systems in which the reactant and product are stabilized to the same extent. $E_{1/2}$ values in Triton X-100 systems suggest that the stabilization of the product is stronger than reactant stabilization. Additional stabilization is thus imparted to the product other than by hydrophobic effect. It is not clear at the present what type of interaction is responsible for this. It is postulated that $1AA\overline{Q}^{\cdot}$ is buried into the hydrophilic domains of ethylene oxide groups of the surfactant and thereby stabilized.

3.3.1.1 Chronocoulometry of 1AAQ

The chronocoulometric response of 1-amino-9,10-anthraquinone (1AAQ) was recorded in micellar solutions and microemulsion media of three different types of surfactants. CTAB, SDS and Triton X-100 model surfactants were used in this investigation. The chronocoulograms of 1AAQ in different microemulsion systems were recorded by stepping the potential from 0.0 to -1200 mV and switched back to the original value by applyng pulse width of 250 millisecond, Figs. (24a-26a). In order to quantify the electrode process; Anson plots were used to estimate the amount of adsorbed reactant species. The plots of the total amount of charge (Q_{tot}) versus $t^{1/2}$ and Q_{tot} versus θ for the forward and reverse reactions respectively, showed linear correlations in different media. Typical Anson plots of 1AAQ in different microemulsion systems are represented by Figs. (24b-26b). A similar chronocoulograms were also observed in micellar solutions. Values of the intercepts of both forward and reverse steps were used to estimate the amount of adsorbed reactant species, Table (18). This is by considering that there is no alteration or negligible contribution by adsorption on the Helmoholtz diffusion layer structure. Therefore, the capacitive term of charge (Q_c) for both forward and reverse reactions should be the same.

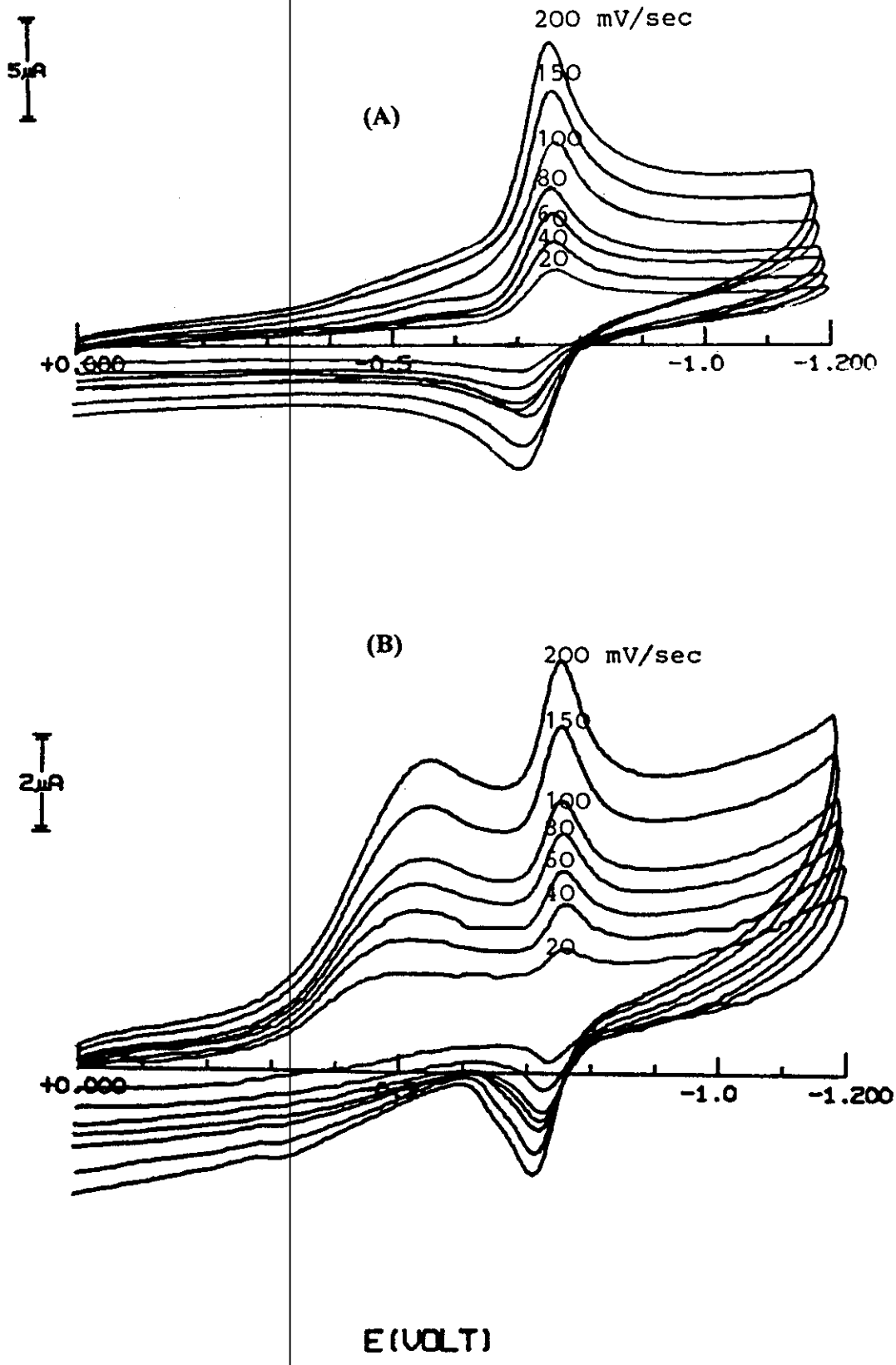

Figure 19: Cyclic voltammograms of 0.30 mM of 1AAQ in CTAB systems (a) microemulsion and (b) micelles. The sweep rates are 20, 40, 60, 80, 100, 150, and 200 mV/sec.

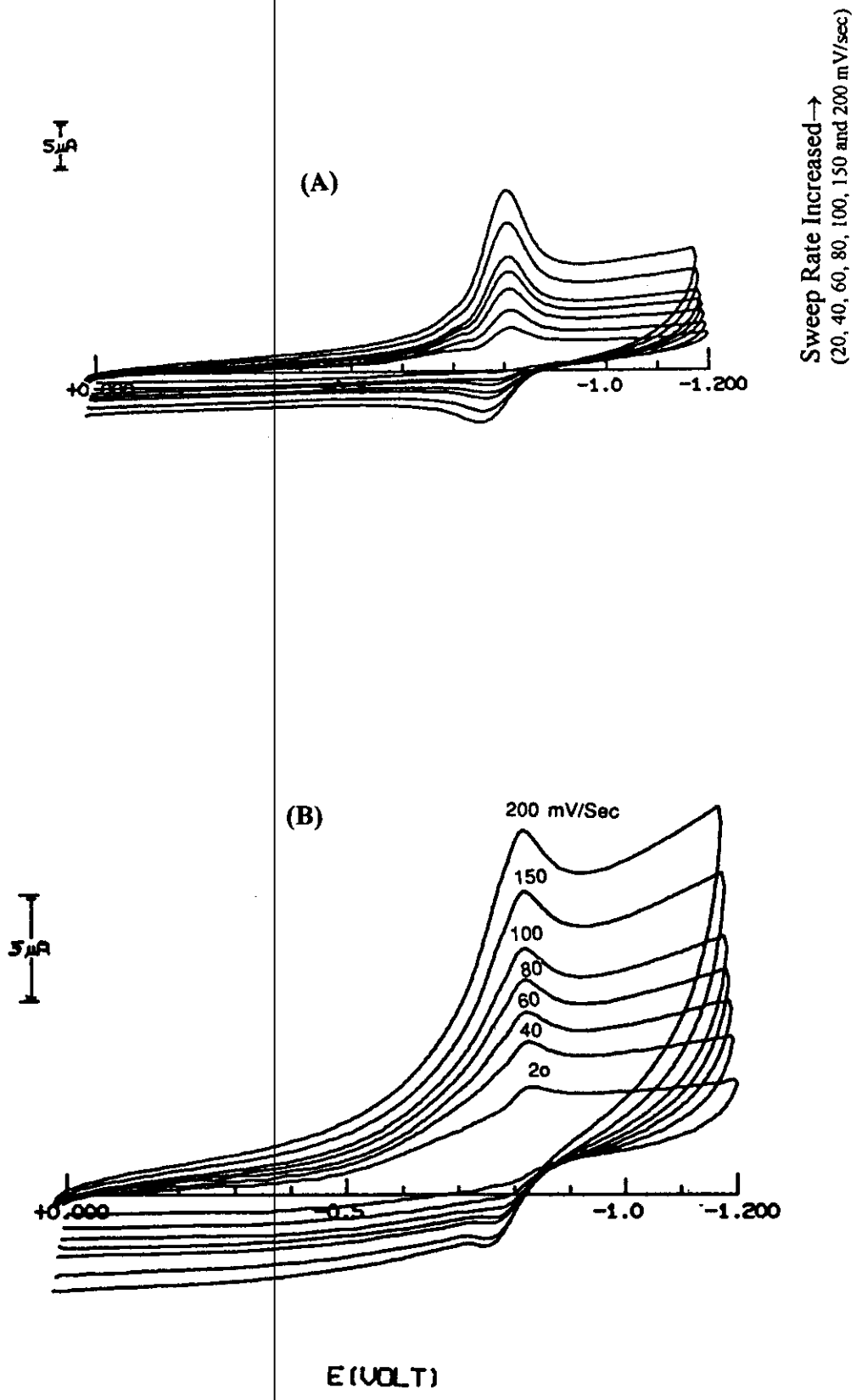

Figure 20: Cyclic voltammograms of 0.30 mM of 1AAQ in SDS systems (a) microemulsion and (b) micelles. The sweep rates are 20, 40, 60, 80, 100, 150, and 200 mV/sec.

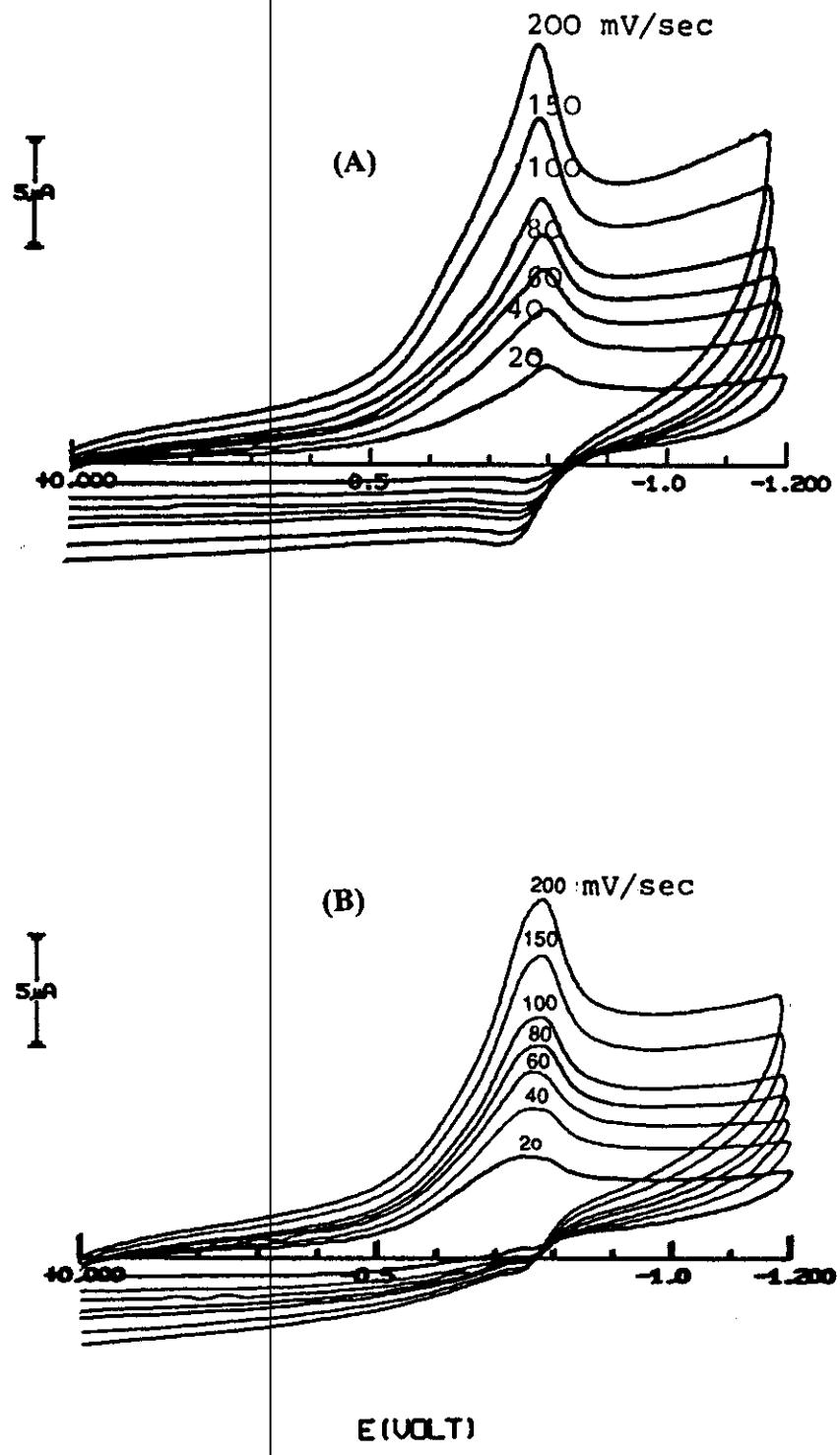

Figure 21: Cyclic voltammograms of 0.30 mM of 1AAQ in Triton X-100 systems (a) microemulsion and (b) micelles. The sweep rates are 20, 40, 60, 80, 100, 150, and 200 mV/sec.

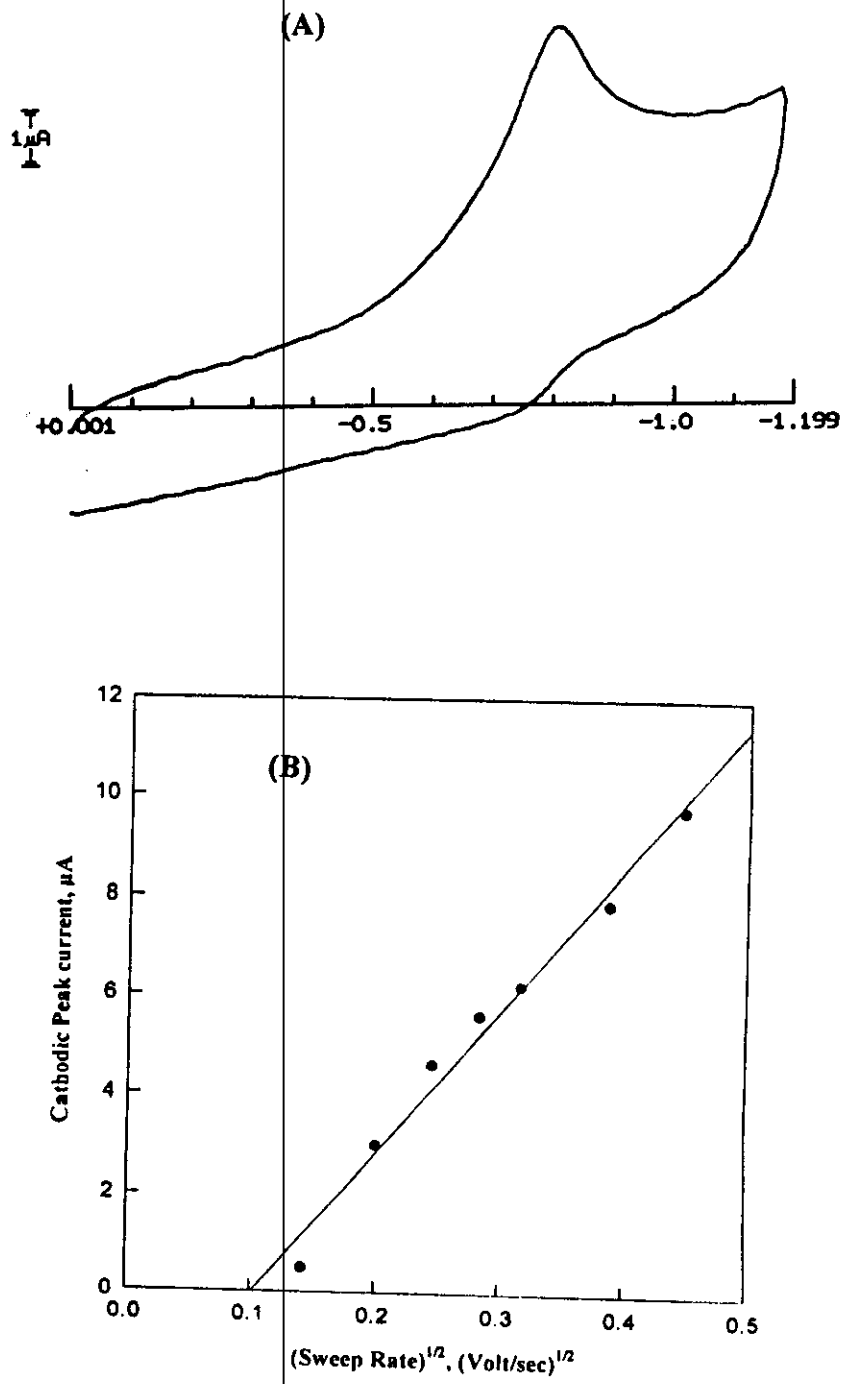

Figure. 22: The cathodic peak current of 1AAQ obtained from cyclic voltammetry, (a) and its plot versus $\upsilon^{1/2}$, (b).

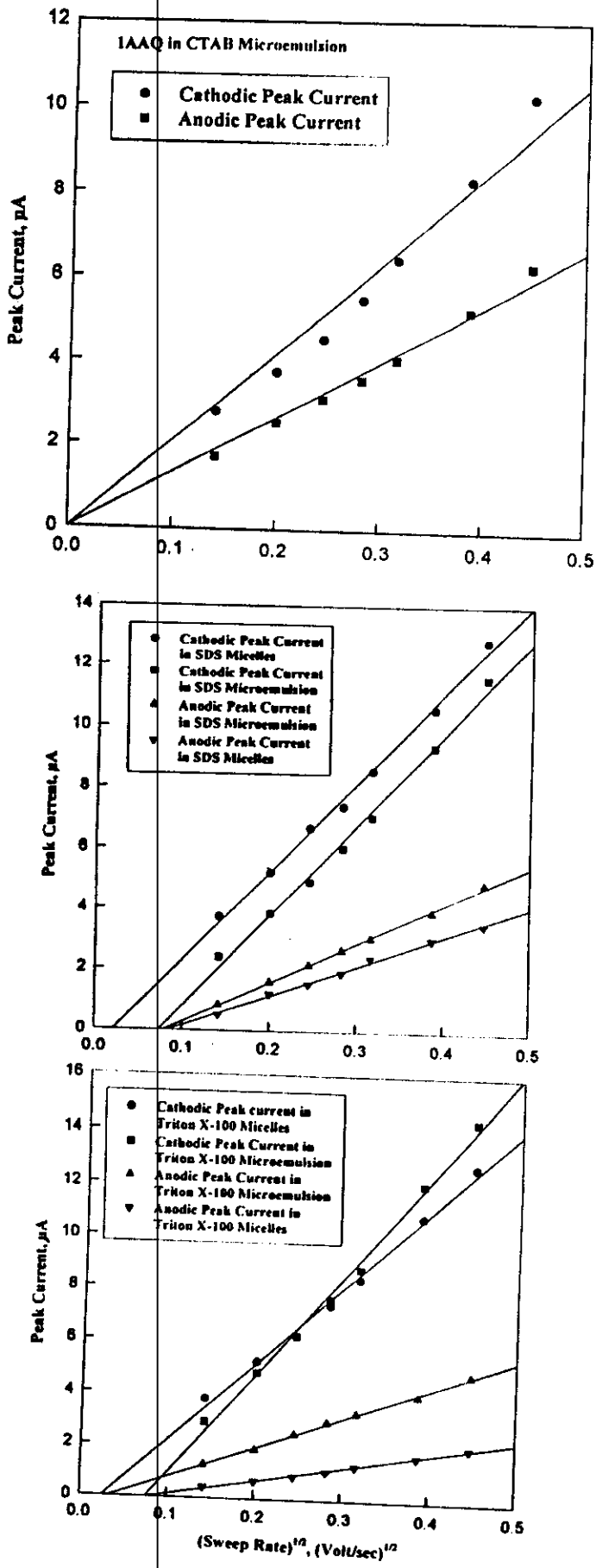
IAAQ in CTAB Microemulsion
Cathodic Peak Current
Anodic Peak Current
Peak Current, μA
Cathodic Peak Current in SDS Micelles
Cathodic Peak Current in SDS Microemulsion
Anodic Peak Current in SDS Microemulsion
Anodic Peak Current in SDS Micelles
Peak Current, μA
Cathodic Peak current in Triton X-100 Micelles
Cathodic Peak Current in Triton X-100 Microemulsion
Anodic Peak Current in Triton X-100 Microemulsion
Anodic Peak Current in Triton X-100 Micelles
Peak Current, μA
(Sweep Rate)^1/2, (Volt/sec)^1/2

Figure 23:

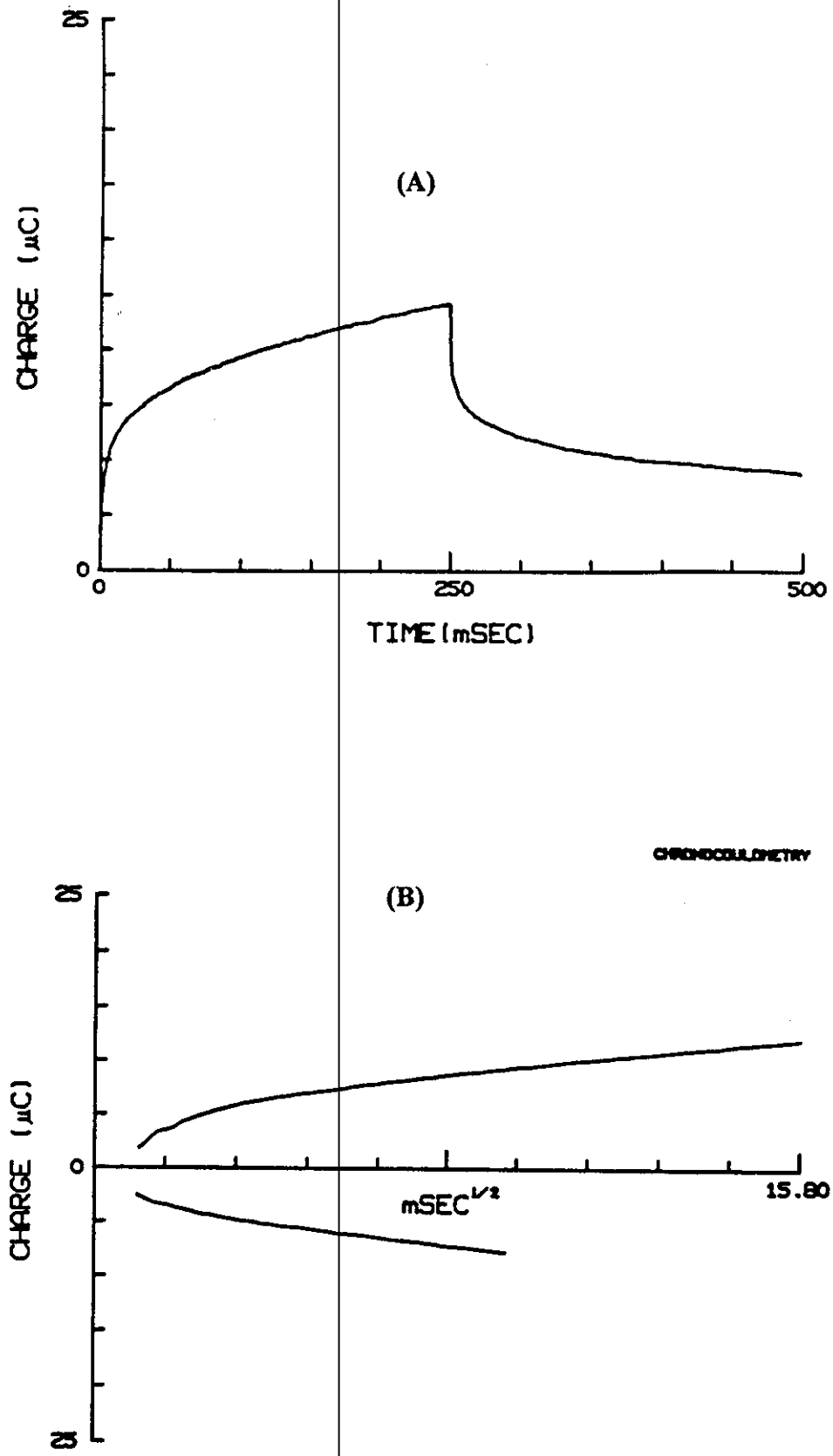

Figure 24: Chronocoulometric responses of 0.30 mM 1AAQ in CTAB microemulsion system at 25°C, (a) Charge versus time and (b) Anson plots.

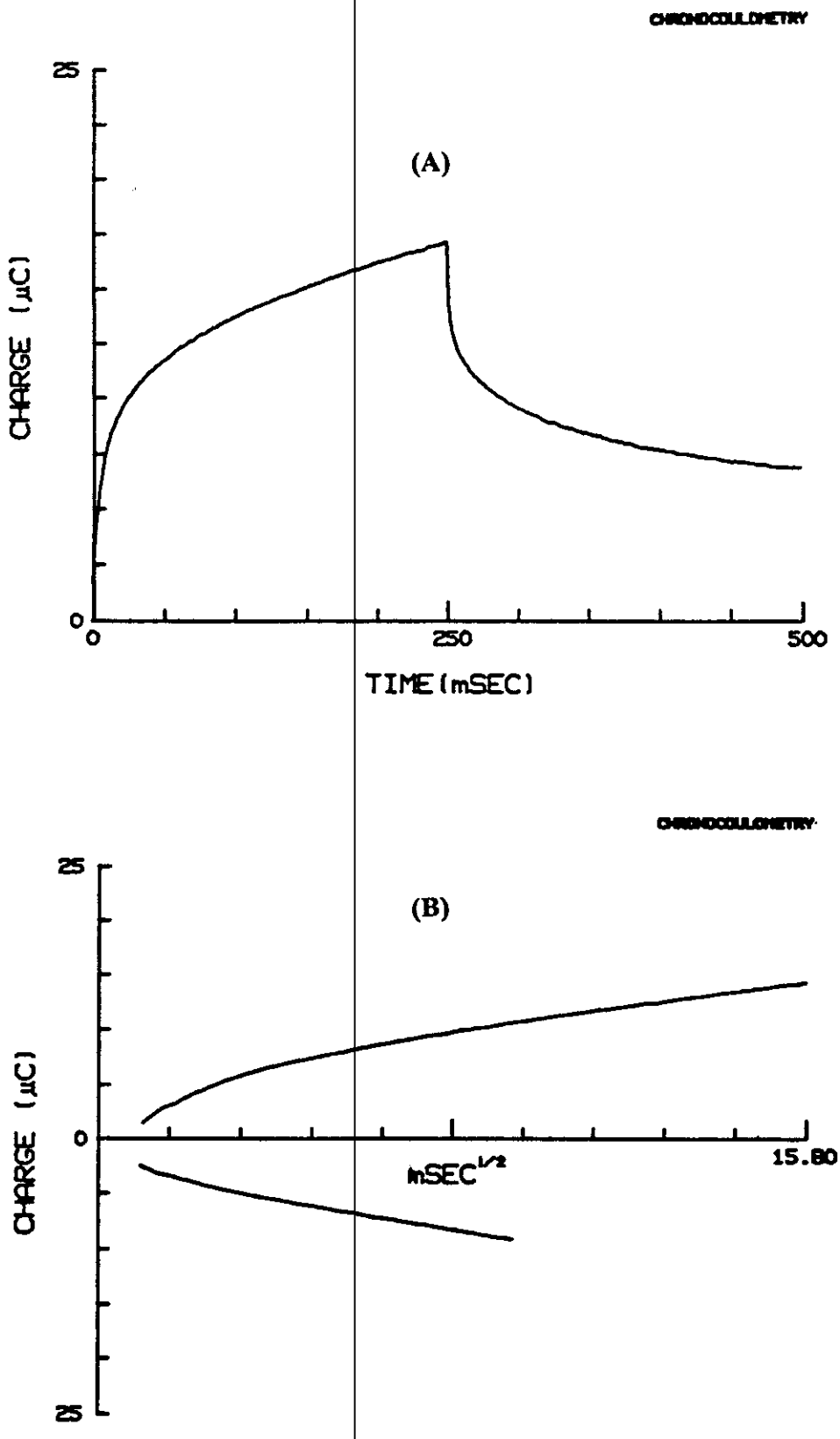

Figure 25: Chronocoulometric responses of 0.30 mM 1AAQ in SDS microemulsion system at 25°C, (a) Charge versus time and (b) Anson plots.

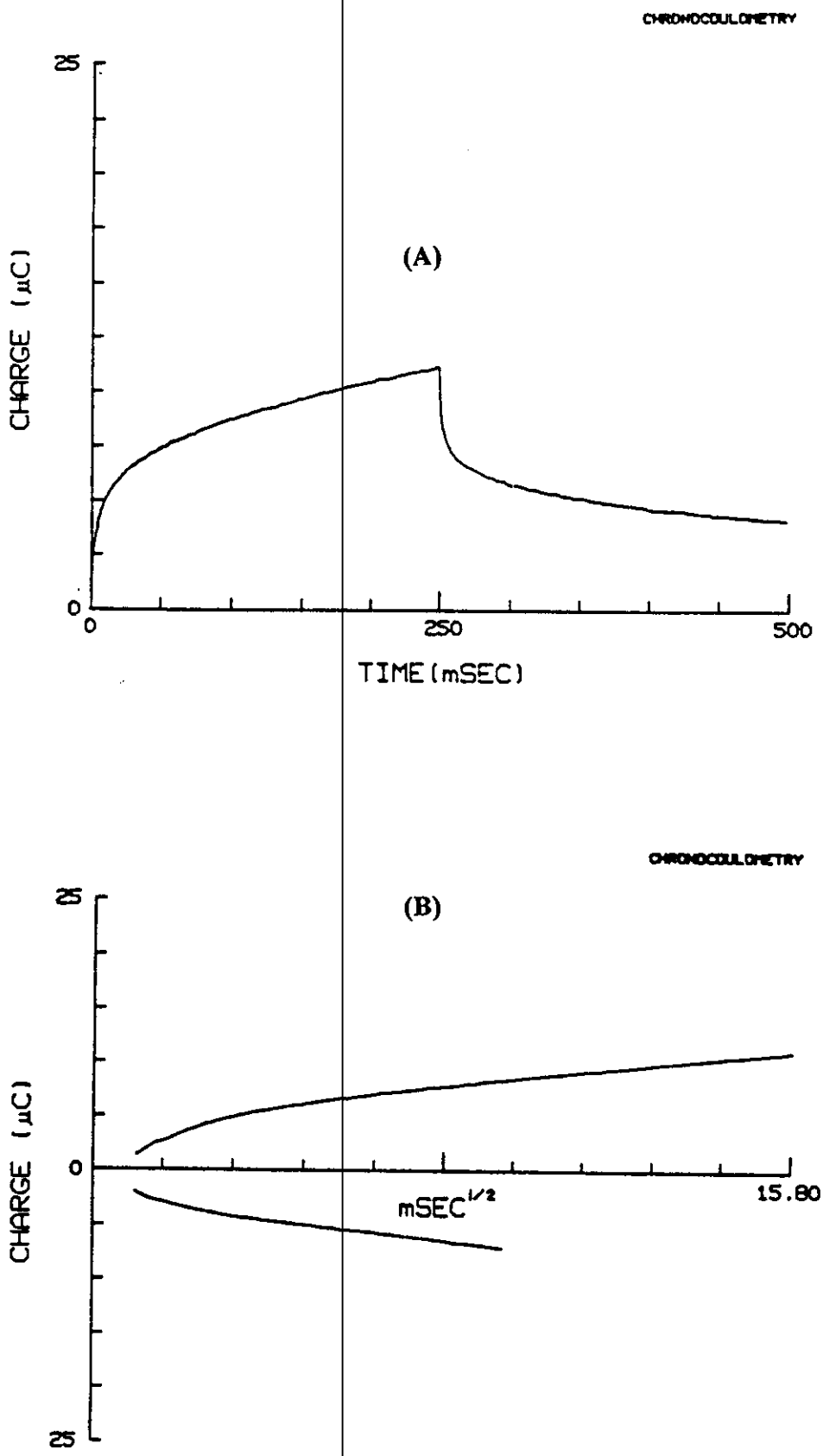

Figure 26: Chronocoulometric responses of 0.30 mM 1AAQ in Triton X-100 microemulsion system at 25°C, (a) Charge versus time and (b) Anson plots.

Table 13: Cyclic Voltammetric Data Obtained for 0.3 mM 1AAQ in CTAB Systems at 25°C.

System	Sweep Rate mV/Sec	$-E_{p,c}$ mV	$-E_{p,a}$ mV	$I_{p,c}$ µA	$I_{p,a}$ µA	$I_{p,a}/I_{p,c}$ -	ΔE_p mV
(A) CTAB MicellarSolution							
	20	750	722	0.56	0.60	1.20	28
	40	751	722	1.18	1.01	0.86	29
	60	753	720	1.79	1.46	0.82	33
	80	757	718	2.15	2.02	0.94	39
	100	758	716	2.42	2.32	0.96	42
	150	759	714	2.91	2.42	0.83	45
	200	760	715	3.36	2.92	0.87	45
(B) CTAB Microemulsion							
	20	756	724	2.34	1.70	0.73	32
	40	756	720	3.40	2.54	0.75	36
	60	757	718	4.54	3.12	0.69	39
	80	755	716	5.50	3.58	0.65	39
	100	757	718	6.44	4.08	0.63	39
	150	758	718	8.30	5.24	0.63	40
	200	760	721	10.24	6.30	0.62	39

Table 15: Cyclic Voltammetric Data Obtained for 0.3 mM 1AAQ in SDS Systems at 25°C.

System	Sweep Rate mV/Sec	$-E_{p,c}$ mV	$-E_{p,a}$ mV	$I_{p,c}$ μA	$I_{p,a}$ μA	$I_{p,a}/I_{p,c}$ -	ΔE_p mV
(A) SDS Micellar Solution							
	20	824	792	3.73	0.51	0.14	32
	40	818	784	5.22	1.22	0.23	34
	60	816	783	6.67	1.55	0.23	33
	80	816	783	7.37	1.92	0.26	33
	100	814	782	8.57	2.41	0.28	32
	150	810	782	10.57	3.02	0.29	28
	200	813	780	12.82	3.51	0.27	33
(B) SDS Microemulsion							
	20	800	771	2.40	0.84	0.35	29
	40	803	770	3.84	1.60	0.42	33
	60	803	766	4.92	2.16	0.44	37
	80	804	765	6.04	2.64	0.44	39
	100	802	760	7.04	3.04	0.43	43
	150	801	758	9.36	3.92	0.42	43
	200	803	750	11.56	4.88	0.42	53

Table 16: Diffusion Coefficient Values of Reductant and Oxidant Species for 1AAQ in Different Systems.

System	15°C		25°C		30°C	
	$D_R x10^7$ cm2/sec	$D_O x10^7$ cm2/sec	$D_R x10^7$ cm2/sec	$D_O x10^7$ cm2/sec	$D_R x10^7$ cm2/sec	$D_O x10^7$ cm2/sec
A- 1AAQ in Triton X-100 Microemulsion:						
	49.90	3.65	61.50	5.71	85.90	6.54
B- 1AAQ in Triton X-100 Micellar Solution:						
	40.00	1.29	37.20	1.27	51.90	4.30
C- 1AAQ in SDS Microemulsion:						
	36.80	4.13	38.40	7.20	55.20	9.34
D- 1AAQ in SDS Micellar Solution:						
	34.60	3.99(a)	36.9	4.13	66.30	8.45
E- 1AAQ in CTAB Microemulsion:						
	25.40	7.14	29.00	9.45	30.00	8.76
F- 1AAQ in CTAB Micellar Solution:						
	-	-	-	-	5.85	3.77

Table 18: Γ_o Values Obtained from Chronocoulometric Data of 1AAQ in Pure Aqueous, Micelles and Microemulsion Systems at Different Temperatures.

System	15°C Γ_o moles	25°C Γ_o moles	30°C Γ_o moles
(A) Pure Aqueous			
	7.12×10^{-13}	1.93×10^{-12}	1.96×10^{-12}
(B) CTAB Microemulsion			
	7.78×10^{-12}	8.97×10^{-12}	9.26×10^{-12}
(C) CTAB Micelles			
	-	-	2.45×10^{-12}
(D) Triton X-100 Micelles			
	2.91×10^{-12}	3.08×10^{-12}	5.57×10^{-12}
(E) Triton X-100 Microemulsion			
	2.44×10^{-12}	8.22×10^{-12}	8.90×10^{-12}
(F) SDS Micelles			
	2.01×10^{-12}	2.27×10^{-12}	2.39×10^{-12}
(G) SDS Microemulsion			
	1.32×10^{-11}	1.40×10^{-11}	2.22×10^{-11}

3.3.2 Adenine and cytosine (Nucleic Acids)*

The cyclic voltammograms of 0.2 mM of nucleic acids, cytosine and adenine, were recorded in micellar and microemulsion systems of three different types of surfactants and in pure aqueous acetate-buffer solution of pH 4.0. Cationic (cetyltrimethylammonium bromide, CTAB), anionic (sodium dodecyl sulphate, SDS) and nonionic [octylphenoxypoly(oxyethylene), Triton X-100] model surfactants were used in this investigation. Well defined voltammograms were obtained for cytosine and adenine in all systems as represented in Figs.(27-31). The voltammograms obtained at different sweep rates (20-200 mV/sec) in microemulsion media are essentially similar and showed one cathodic peak on the cathodic scan, corresponding to the reduction of cytosine or adenine moiety (Figs. 28&30). The voltammetric behaviour of adenine and cytosine in the corresponding micellar solutions are essentially similar and showing a single reduction step, as represented in Figs. (29&31). No oxidation peaks were observed in the reverse scan which confirms the irreversible nature of the electrode process. Furthermore, the peak potentials ($E_{p,c}$) display a cathodic shift on increasing the sweep rate (υ), revealing the irreversible nature [148] of the electrode reaction pathway.

On comparing the voltammograms of cytosine and adenine in aqueous buffer solution in one hand and in micellar and microemulsions of three different surfactants on the other hand, it becomes apparent that the peak current ($I_{p,c}$) values obtained for cationic CTAB micelles and microemulsion systems is significantly higher than that obtained in Triton X-100, SDS micelles, microemulsions and aqueous buffer solutions, respectively. The change in the peak current can be due to the change in solvation [191] and variation of the effective size of depolarizer species.

An important aspect to be considered in electrochemical investigations in surfactant solutions is the adsorption of surfactant on the electrode surface and its effect on the electrochemical reactions. Our previous results on the electrochemical oxidation of ferrocene in

* This work was initiated by Prof. Y.M. Temerk, Assuit University, Faculty of Science-Chemistry Department.

the microemulsion types did not show any significant effect that could be ascribed to surfactant adsorption on the electrode surface. Previous investigators also did not find any effect attributed to surfactant adsorption [97]. All the results observed in these studies could be explained based on electrostatic and/or hydrophobic interactions of the surfactant with various species (reactant, intermediate and products) of the electrochemical reaction.

On employing the following relationship [192] that correlates the peak potential ($E_{p,c}$) with the sweep rate (υ), the values of (αn_a) parameter for the electrode reaction of the compounds under consideration can be evaluated:

$$E_p = -1.14(RT/\alpha n_a F) + (RT/\alpha n_a F).\ln(k^{\circ}_{f,h}/D^{1/2}) - (RT/2\alpha n_a F).\ln(\alpha n_a \upsilon) \qquad \textbf{(III.11)}$$

Thus, on plotting E_p versus $\ln(\upsilon)$, linear correlations of slope values proportional to (αn_a) are obtained. Values of the transfer coefficient (α) can also be evaluated for the probable values of (n_a) by considering the number of electrons involved in the potential-determining step (n_a) may be one or two. As shown in Tables (19-22), the most probable values of the transfer coefficient (α) in the investigation media revealed that (n_a) is equal to unity. These results reveal that the rate-limiting step of the electrode process may involve one electron.

According to Delahay [148], for the irreversible electron transfer process, the peak current function can be expressed according to the following equation:

$$I_p = 3.01x10^5 n\,(\alpha n_a) A D^{1/2} C_A \upsilon^{1/2} \qquad \textbf{(III.12)}$$

The plots of cathodic peak current ($I_{p,c}$) versus square root of sweep rate ($\upsilon^{1/2}$) as represented in Figs.(32&33) show linear correlations passing through the origin indicating the diffusion nature of

the electrode reaction [148]. The slopes of these plots were used in determining the apparent diffusion coefficients. These results indicate that complications observed in aqueous solutions due to adsorption and catalytic effects on the electrode surface are eliminated in microemulsions. This is because surfactant systems provide a nonaqueous environment for solubilization of the hydrophobic core of cytosine and adenine, thereby preventing their adsorption on the electrode surface. The electrostatic effects of ionic surfactants are generally less in microemulsion droplets compared with micellar solutions due to the additional oil component. The CTAB systems behave ideally because cationic surfactants are known to stabilize anion radicals [190]. Stabilization is also possible in the presence of nonionic surfactant molecules where the anion radical will be present at the interface between the hydrocarbon core and the polar poly(oxyethylene) sheath. Also, anionic SDS is known to kinetically stabilize anion radicals of nitrobenzene [91]. The mechanism of stabilization has been suggeseted to be electrostatic and/or hydrophobic interactions with reactant, intermediate and products.

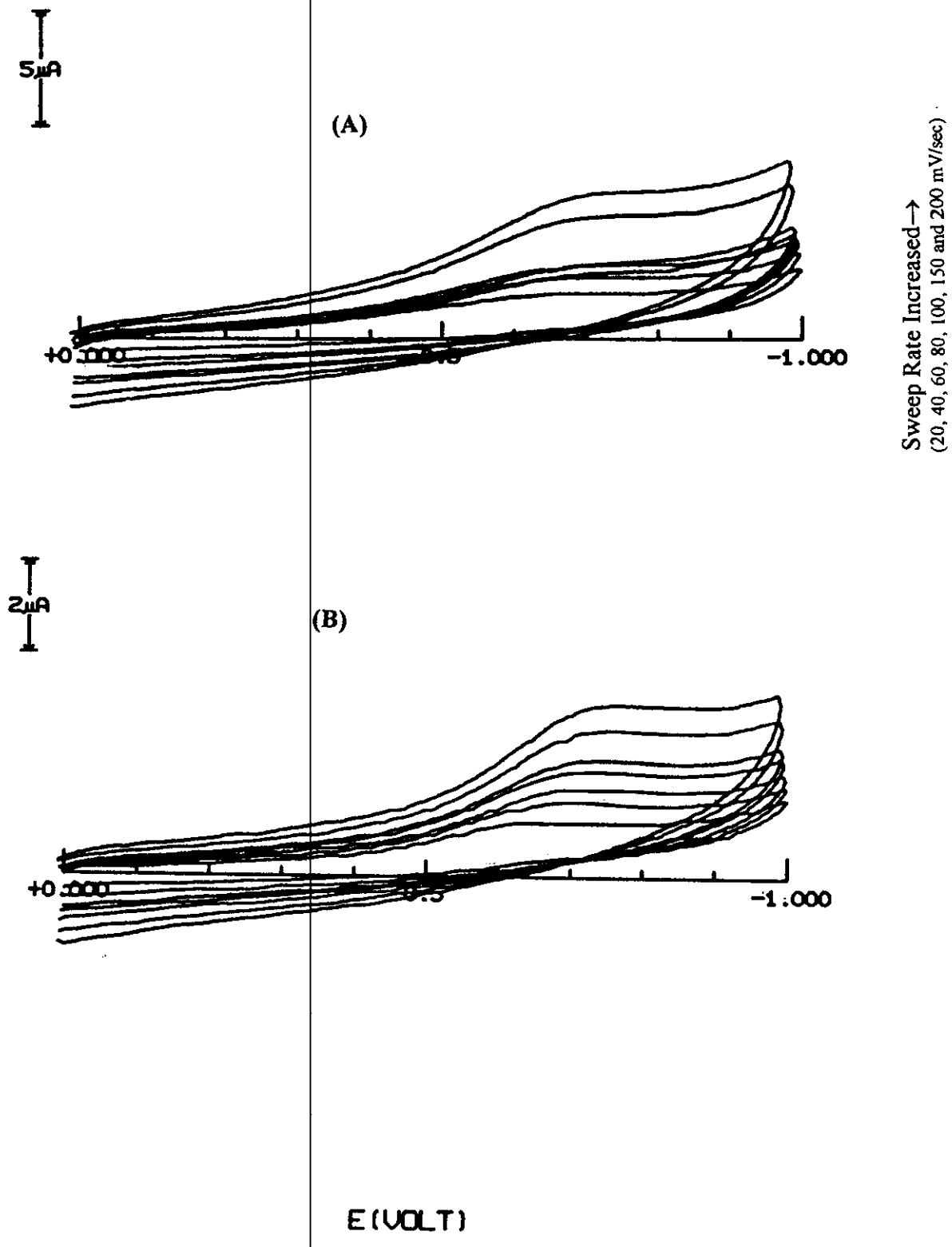

Figure 27: Cyclic voltammgrams recorded in pure aqueous acetate buffer solution of pH 4.0 for (a) Adenine and (b) Cytosine. The sweep rates are 20, 40, 60, 80, 100, 150 and 200 mV/sec.

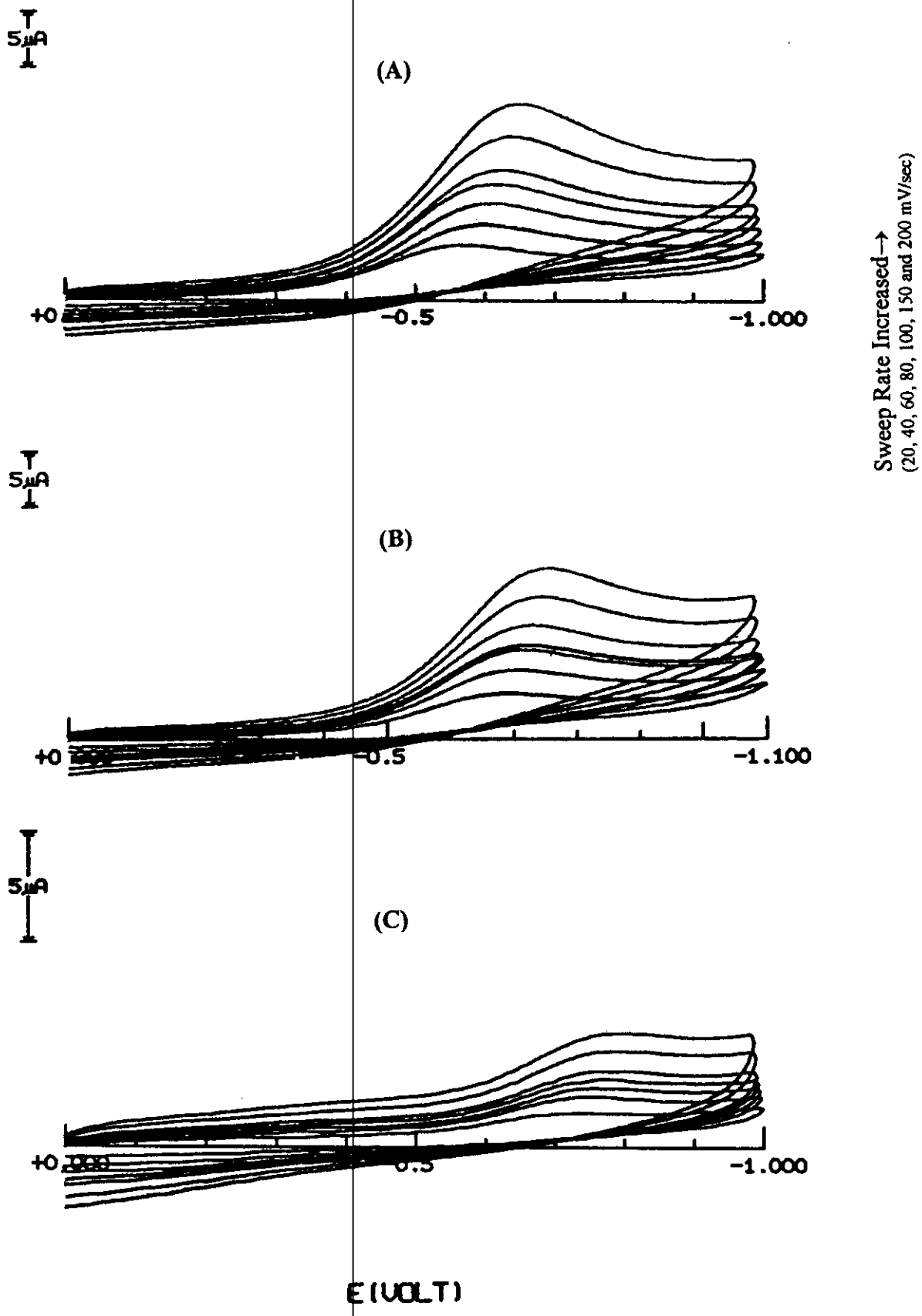

Figure 28: Cyclic voltammograms of adenine obtained in different microemulsion systems at 25°C, (a) CTAB, (b) Triton X-100 and (c) SDS. The sweep rate ares 20, 40, 60, 80, 100, 150 and 200 mV/sec.

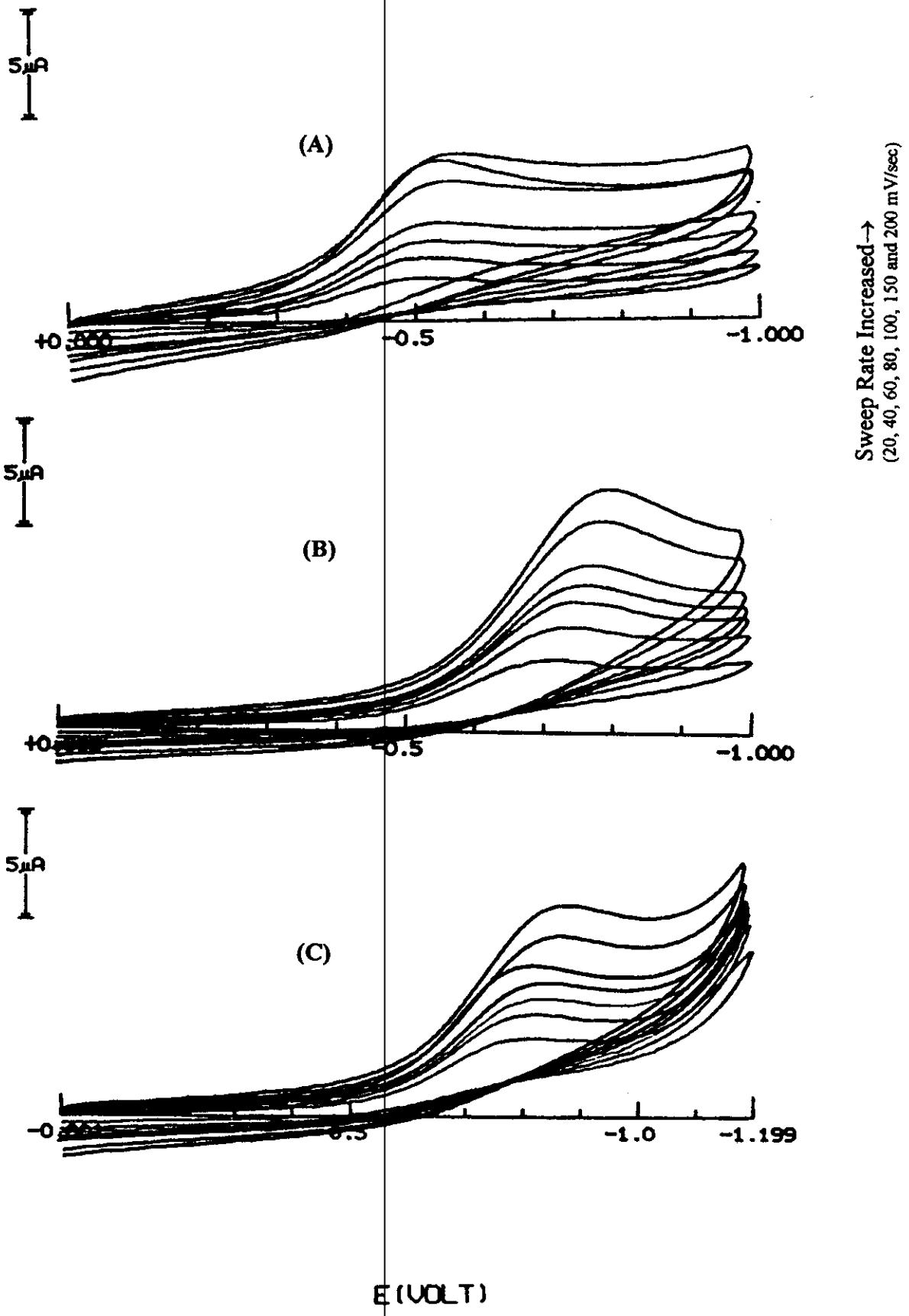

Figure 29: Cyclic voltammograms of adenine obtained in different micellar solutions at 25°C, (a) CTAB, (b) Triton X-100 and (c) SDS. The sweep rate ares 20, 40, 60, 80, 100, 150 and 200 mV/sec.

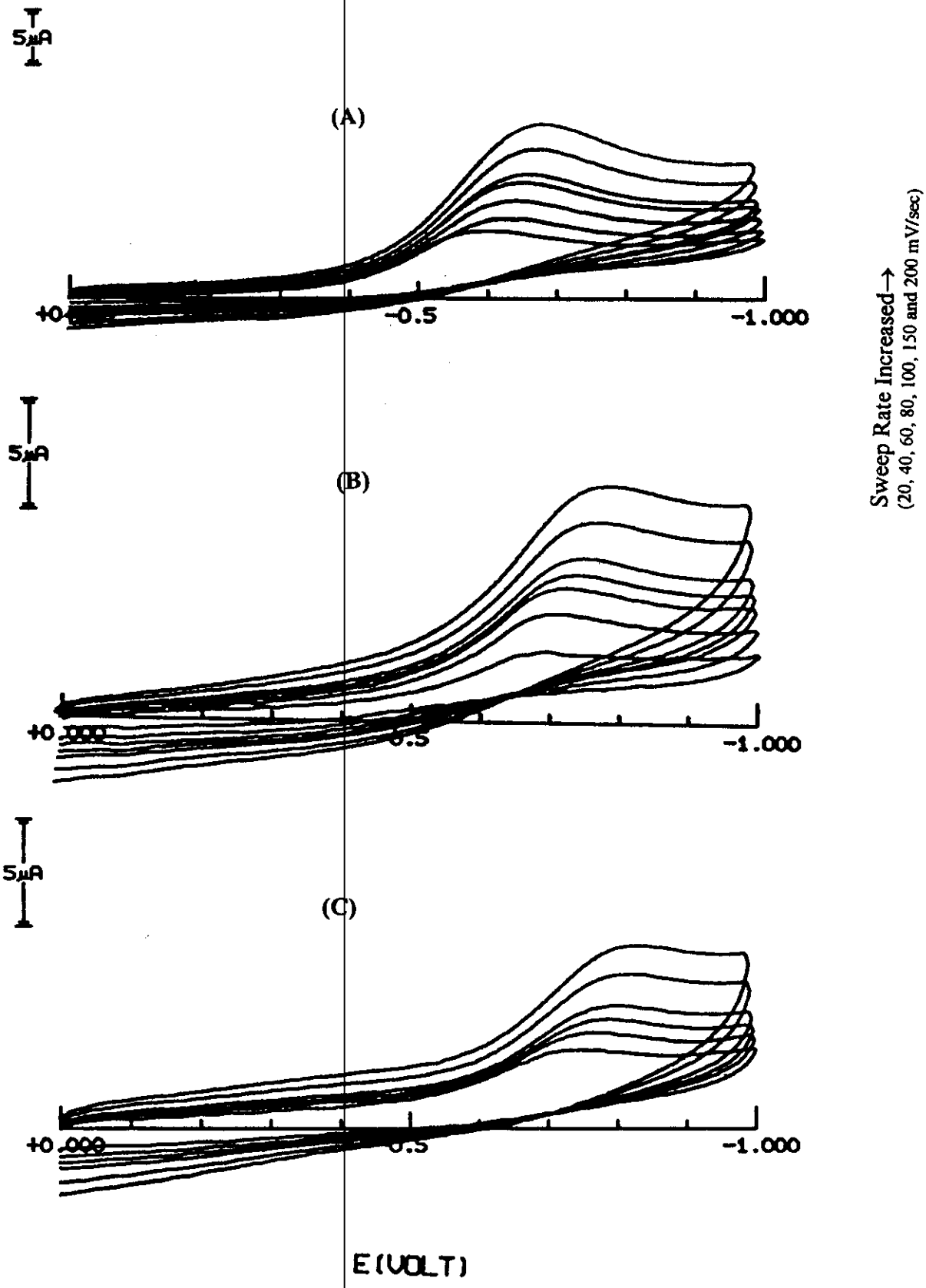

Figure 30: Cyclic voltammograms of cytosine obtained in different microemulsion systems at 25°C, (a) CTAB, (b) Triton X-100 and (c) SDS. The sweep rate ares 20, 40, 60, 80, 100, 150 and 200 mV/sec.

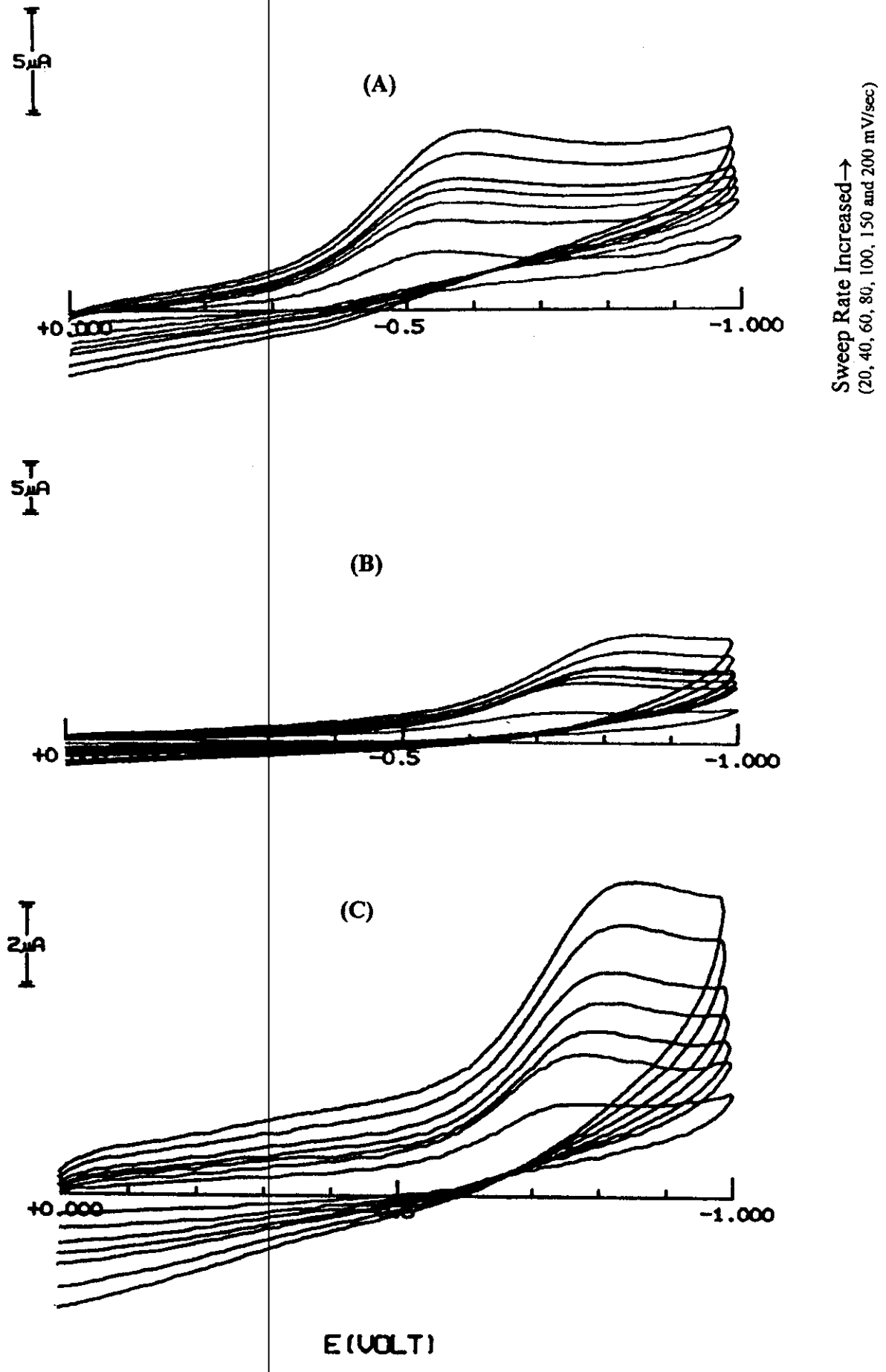

Figure 31: Cyclic voltammograms of cytosine obtained in different micellar solutions at 25°C, (a) CTAB, (b) Triton X-100 and (c) SDS. The sweep rate ares 20, 40, 60, 80, 100, 150 and 200 mV/sec.

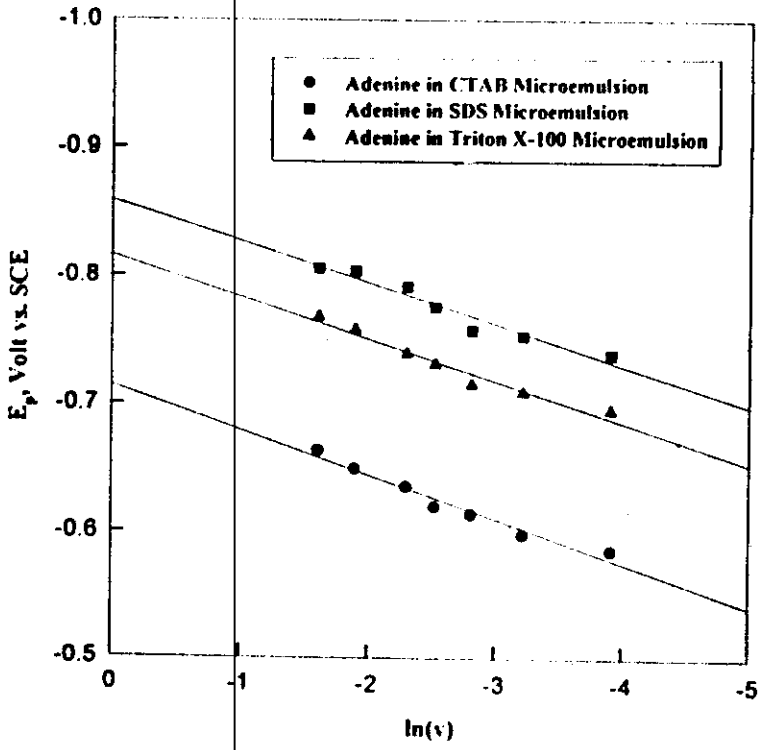
Adenine in CTAB Microemulsion
Adenine in SDS Microemulsion
Adenine in Triton X-100 Microemulsion
E_p, Volt vs. SCE
ln(v)

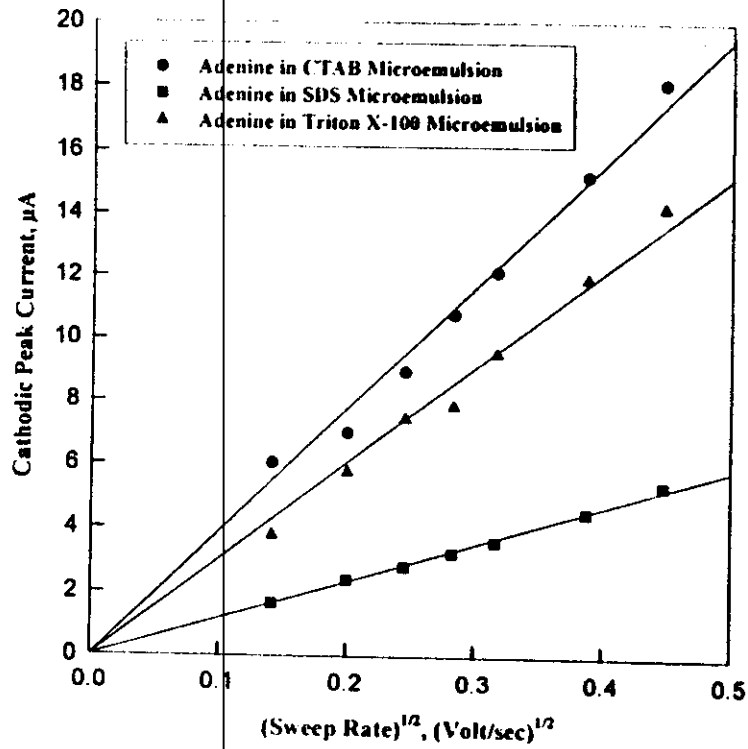
Adenine in CTAB Microemulsion
Adenine in SDS Microemulsion
Adenine in Triton X-100 Microemulsion
Cathodic Peak Current, μA
(Sweep Rate)$^{1/2}$, (Volt/sec)$^{1/2}$

Figure 32:

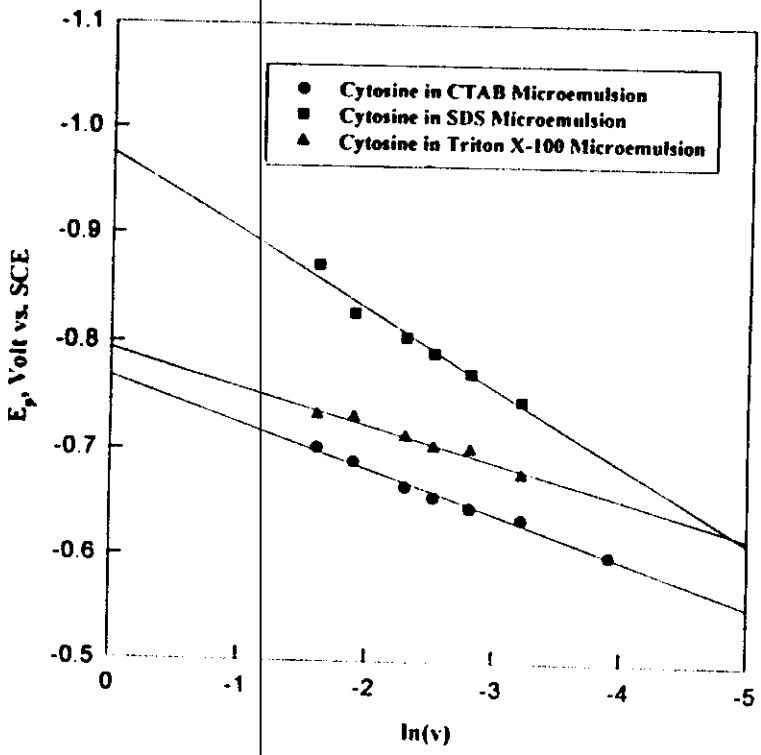
Cytosine in CTAB Microemulsion
Cytosine in SDS Microemulsion
Cytosine in Triton X-100 Microemulsion
E_p, Volt vs. SCE
-1.1
-1.0
-0.9
-0.8
-0.7
-0.6
-0.5
0
-1
-2
-3
-4
-5
ln(v)

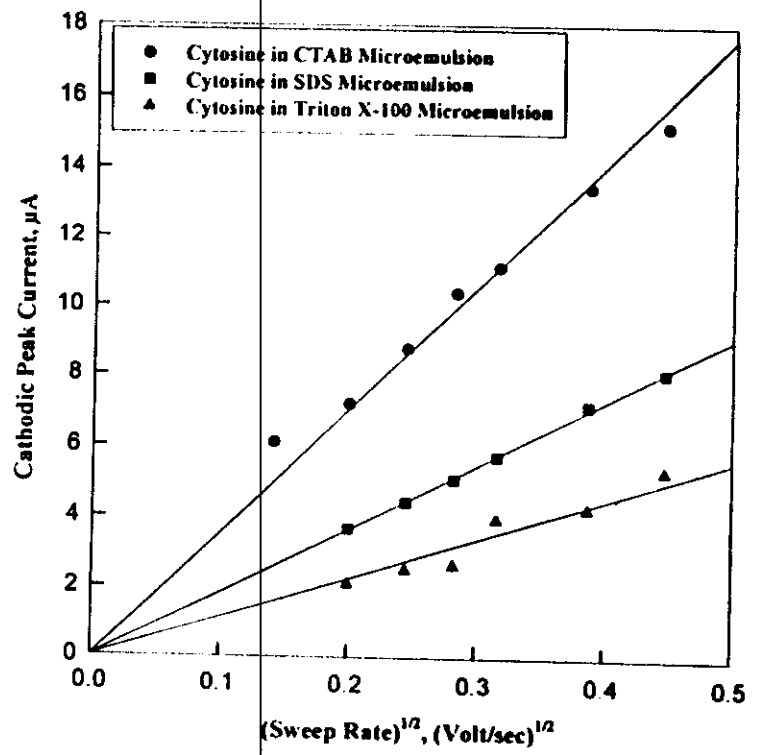
Cytosine in CTAB Microemulsion
Cytosine in SDS Microemulsion
Cytosine in Triton X-100 Microemulsion
Cathodic Peak Current, μA
18
16
14
12
10
8
6
4
2
0
0.0
0.1
0.2
0.3
0.4
0.5
(Sweep Rate)$^{1/2}$, (Volt/sec)$^{1/2}$

Figure 33:

Table 19: Cyclic Voltammetric Data Obtained for 0.20 mM Cytosine in Pure Aqueous and Microemulsion Systems of different Surfactant Types at 25°C.

System	Sweep Rate mV/sec	$I_{p,c}$ μA	$-E_{p,c}$ mV	$dE_p/d\ln\upsilon$ ($x10^2$)	$Dx10^6$ cm^2/sec	α n_a=1.0	α n_a=2.0
(A) Pure Aqueous							
	20	1.23	656				
	40	1.71	714				
	60	2.01	748				
	80	2.41	740	4.60	1.89	0.28	0.14
	100	2.68	744				
	150	3.33	768				
	200	3.90	768				
(B) CTAB							
	20	4.60	602				
	40	5.54	636				
	60	7.08	646				
	80	8.46	656	4.10	2.09	0.31	0.16
	100	9.29	666				
	150	11.25	690				
	200	13.50	703				
(C) SDS							
	40	3.68	748				
	60	4.45	774				
	80	5.11	792	6.10	1.03	0.21	0.11
	100	5.75	806				
	150	7.20	828				
	200	8.12	872				
(D) Triton X-100							
	40	2.11	678				
	60	2.52	702				
	80	2.65	704	3.50	0.33	0.37	0.19
	100	3.97	714				
	150	4.29	732				
	200	5.36	734				

Table 20: Cyclic Voltammetric Data Obtained for 0.20 mM Cytosine in Micellar Solutions of Different Surfactants at 25°C.

System	Sweep Rate mV/sec	I_p μA	$-E_p$ mV	$dE_p/d\ln\upsilon$ ($x10^2$)	$Dx10^6$ cm^2/sec	α n_a=1.0	α n_a=2.0
(A) CTAB	20	6.00	555				
	40	7.76	564				
	60	8.60	569				
	80	9.13	574	2.50	3.96	0.52	0.26
	100	9.97	600				
	150	10.98	590				
	200	12.38	594				
(B) SDS							
	20	2.21	783				
	40	3.43	778				
	60	3.98	794				
	80	4.65	830	3.70	5.96	0.35	0.18
	100	5.39	830				
	150	6.52	846				
	200	7.59	856				
(C) Triton X-100							
	20	2.28	676				
	40	2.79	708				
	60	3.25	720				
	80	3.50	742	4.30	7.40	0.30	0.15
	100	3.86	740				
	150	5.07	764				
	200	5.86	776				

Table 21: Cyclic Voltammetric Data Obtained for 0.20 mM Adenine in Pure Aqueous and Microemulsion Systems of Different Surfactant Types at 25°C.

System	Sweep Rate mV/sec	$I_{p,c}$ μA	$-E_{p,c}$ mV	$dE_p/d\ln\upsilon$ ($x10^2$)	$Dx10^5$ cm^2/sec	α n_a=1.0	α n_a=2.0
(A) Pure Aqueous							
	20	2.01	654				
	40	2.79	672				
	60	2.82	734				
	80	3.20	740	5.20	3.37	0.25	0.13
	100	3.80	748				
	150	5.52	756				
	200	6.47	770				
(B) CTAB	20	6.04	586				
	40	7.67	598				
	60	9.37	614				
	80	10.92	620	4.00	2.21	0.32	0.16
	100	12.46	636				
	150	15.21	650				
	200	17.79	664				
(C) SDS							
	20	1.65	740				
	40	2.40	754				
	60	2.81	758				
	80	3.24	776	3.20	0.14	0.39	0.20
	100	3.60	792				
	150	4.51	804				
	200	5.37	806				
(D) Triton X-100							
	20	3.78	696				
	40	5.76	710				
	60	7.44	716				
	80	7.85	732	3.00	0.96	0.43	0.22
	100	9.54	740				
	150	11.93	758				
	200	14.22	768				

Table 22: Cyclic Voltammetric Data Obtained for 0.20 mM Adenine in Micellar Solutions of Different Surfactants at 25°C.

System	Sweep Rate mV/sec	$I_{p,c}$ μA	$-E_{p,c}$ mV	$dE_p/d\ln\upsilon$ ($x10^2$)	$Dx10^6$ cm^2/sec	α na=1.0	α n_a=2.0
(A) CTAB	20	2.76	508				
	40	3.76	514				
	60	4.52	536				
	80	5.30	544	3.50	16.7	0.38	0.19
	100	6.28	546				
	150	7.26	562				
	200	8.52	576				
(B) SDS							
	20	2.30	799				
	40	4.46	819				
	60	5.90	866				
	80	7.49	871	3.80	6.12	0.33	0.17
	100	8.65	879				
	150	11.04	899				
	200	12.79	914				
(C) Triton X-100							
	20	3.37	720				
	40	4.84	746				
	60	6.06	748				
	80	6.87	764	3.80	7.98	0.33	0.17
	100	9.54	740				
	150	11.93	758				
	200	14.22	768				

3.3.3 Coumarin and Schiffer azo compounds

3.3.3.1 The electrochemical behaviour of 8-(phenylazo)-6,7-dihydroxy-4-methyl-coumarin (Ia) in microemulsion media

3.3.3.1.1 Measurements at glassy carbon electrode (GCE)

Cyclic voltammograms of $2x10^{-3}$ M of 8-(phenylazo)-6,7-dihydroxy-4-methyl-coumarin (Ia) azodye were recorded in three different microemulsion systems containing CTAB, SDS and Triton X-100 as model surfactants at the glassy carbon electrode and in pure aqueous solution. A well defined single cathodic peak was observed in all microemulsion media, as represented in Figs. (34&35a). No oxidation peaks were observed on the reverse scan which indicated the irreversible nature of the reduction process. Since the coumarin azodye which containnig heteroring nucleus is slightly soluble in pure aqueous media and its solubility is not more than $8x10^{-5}$ M in 0.1 M NaBr solution, therefore, the voltammograms of coumarin azodye at that concentration were recorded in pure aqueous containing 0.1 M NaBr supporting electrolyte and showed only a single reduction step (Fig. 35a). The voltammograms recorded at different sweep rates varying from 20 to 500 mV/sec are essentially similar and show one cathodic peak on the cathodic scan. No peaks were observed also in the reverse scan indicating the irreversibility of the electrode process.

On comparing the peak current ($I_{p,c}$) of coumarin azodye in CTAB, SDS and Triton X-100 microemulsions and in pure aqueous solution, it is clear that the peak current is slightly different from one system to another depending on the size and charge of the microemulsion droplet. The peak potential ($E_{p,c}$) displayed a cathodic shift on increasing the sweep rate which confirmed the irreversible nature of the electrode process

[148]. It was found that the reduction process takes place at less negative potentials in CTAB system compared to Triton X-100 and SDS dependig on the electrostatic interactions and stabilization effects of surfactants on different entities formed in solution during the electroreduction process. The plots of the peak potential (E_p) versus ln(υ) of coumarin azodye in different surfactant systems and in pure aqueous solution showed linear correlations, as represented in Fig. (35b&36a). On employing the following relationship [192] that correlates the shift in peak potential with the sweep rate (υ), the kinetic parameters of the electrode process could be obtained. The slopes of the linear plots of E_p-ln(υ) correlations are proportional to αn_a. Therefore, the transfer coefficient (α) in the different media could be evaluated for the propable values of (n_a) by considering the number of electrons involved in the rate-determining step (n_a) may be one or two. As shown from Table (23), the most probable α-values in all media were obtained at $n_a = 1$. These results indicated that the rate-determining step should involves one electron.

According to Delahay [148], using equation (III.12) the plots of the cathodic peak current versus square root of sweep rate ($\upsilon^{1/2}$) give linear correlations as represented in Figs. (35c&36b). The linear correlations obtained mostly passing through the origin revealing that the reduction process of this compound is mainly controlled by diffusion in all microemulsion media. But in pure aqueous solution a deviation from passing through the origin is observed which may be due to adsorption phenomenon.

3.3.3.1.2 Measurements at hanging dropping mercury electrode (HDME)

Due to the low solubility of coumarin azodyes in pure aqueous solutions, the measurements were done in 40% (v/v) ethanol. Three compounds of each series were

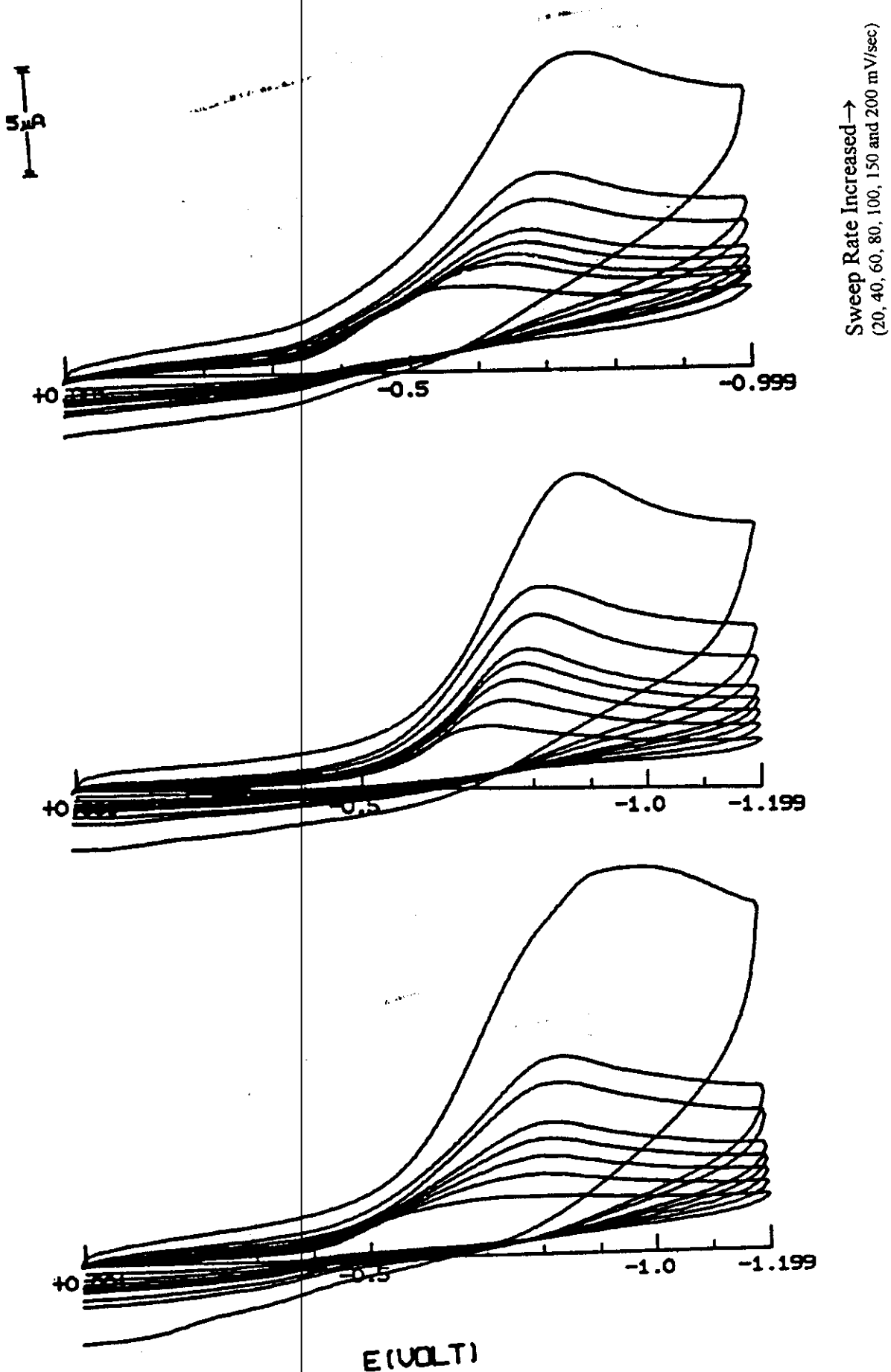

Figure 34: Cyclic voltammograms of 8-phenylazo-(6,7-dihydroxy-4-methyl)-coumarin (I_a) in microemulsion systems containing different surfactants (a)CTAB, (b)Triton X-100 and (c) SDS. The sweep rates are 20, 40, 60, 80, 100, 150, 200 and 500 mV/sec.

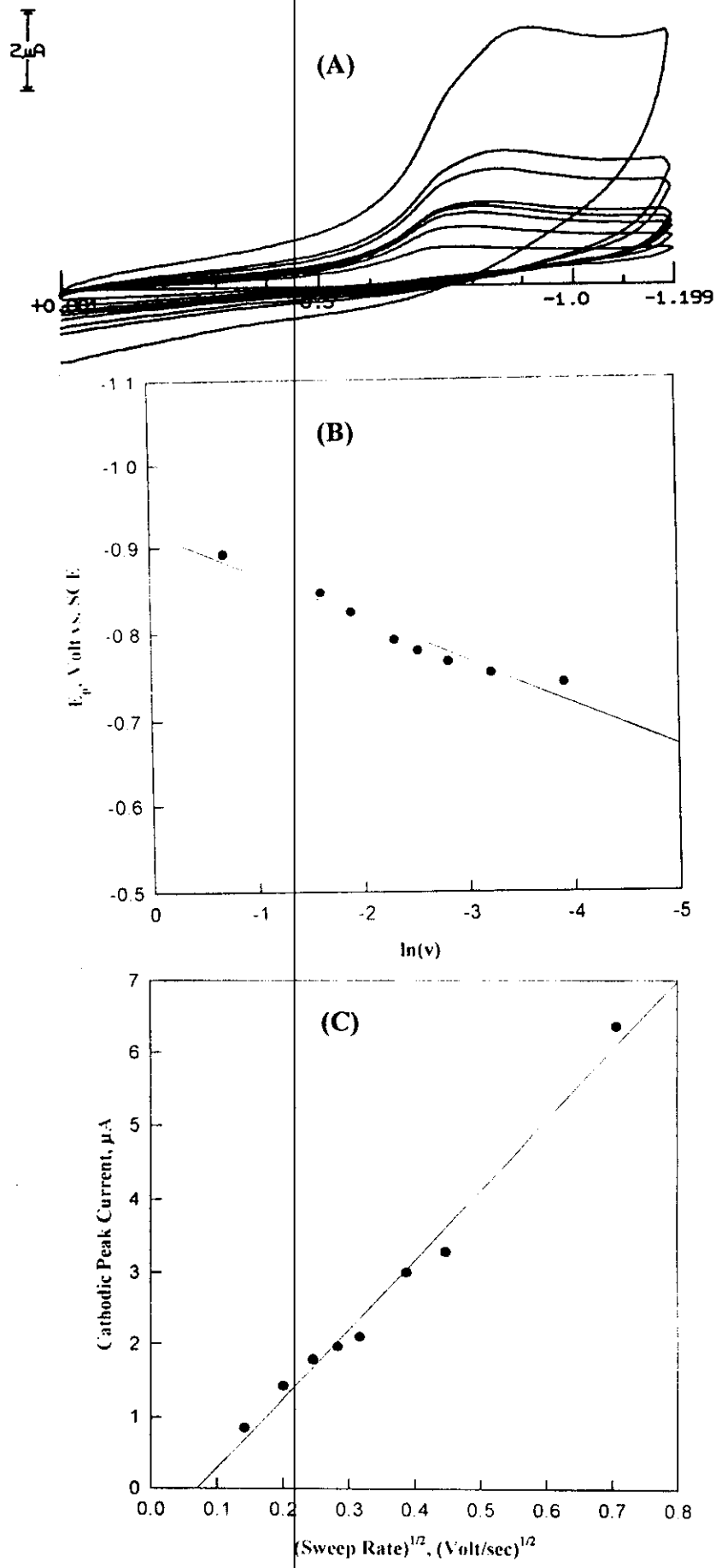

Figure 35: (a) Cyclic voltammograms of compound (Ia) in pure aqueous solution containing only 0.1 M NaBr, (b) its E_p-ln(v) plot and (c) its I_p-$\upsilon^{1/2}$ plot.

Peak Current of Coumarin Azo in different Microemulsion Systems at 25°C

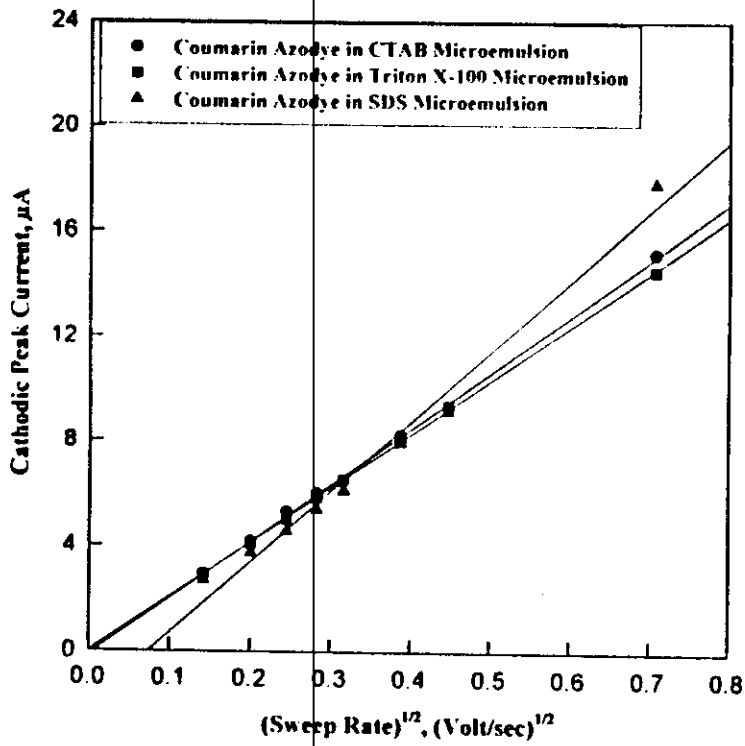

Coumarin Azodye in Different Microemulsion Systems at 25°C.

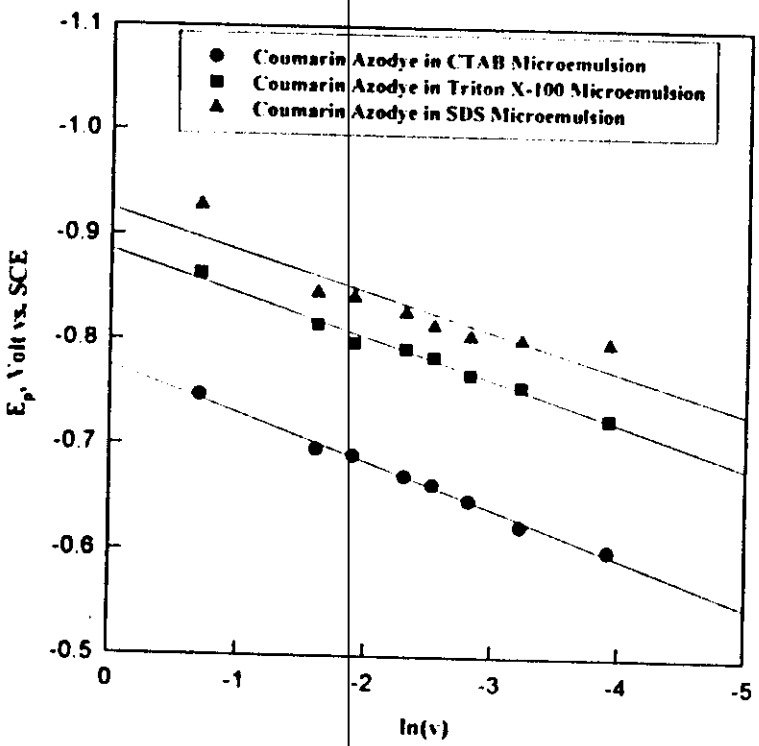

Figure 36:

taken to study the effect of substituents on the electrode process. The cyclic voltammograms and DP-polarograms of $1x10^{-4}$ of each of 8-(phenylazo)-6,7-dihydroxy-4-methyl)-coumarin, (Ia), 8-(4'-chlorophenylazo)-6,7-dihydroxy-4-methyl-coumarin (Ib), 8-(4'-methoxyphenylazo)-6,7-dihydroxy-4-methyl-coumarin, (Ic), (series I) and 1-phenylazo-2-hydroxy-6-naphthalenesulfonic acid (IIa), 1-(2'-carboxyphenylazo)-2-hydroxy-6-naphthalenesulphonic acid (IIb) and 1-(2'-methoxyphenylazo)-2-hydroxy-6-naphthalenesulphonic acid (IIc) (series II) were recorded in Britton-Robinson buffer solutions of pH range 2-12 containing 40% (v/v) ethanol for compounds of series (I), while for compounds of series (II) which are water-soluble, the voltammograms were recorded in pure aqueous buffer solutions. Two techniques were used, cyclic voltammetry (CV) and differential pulse polarography (DPP). The recorded voltammograms and d.p-polarograms showed only a single reduction wave for all the compounds under investigation. In cyclic voltammetry, no oxidation peaks were observed in the reverse scan which indicate the irreversible nature of the reduction process. The cyclic voltammograms that recorded for the compounds of the two series (I&II) at different pH values are shown in Figs. (37-42). Also, the dp-polarograms for the compounds under investigations showed a cathodic shift in peak potentials on increasing the pH of the electrolysis solution, which is further confirmed the irreversible nature of the electrode process, Figs. (43a-48a). The d.p-polarograms showed a splitting in wave in the pH range ($8.0<pH<10$), which indicates the presence of deprotonated forms of the reducible species. The effect of sweep rate on the reduction peaks of coumarin azodyes, series (I) and Schiffer azodyes, series (II) from media of different pH values was recorded, Figs. (37-42). It was found that on increasing the sweep rate the peak potential displayed a cathodic shift to more negative

values which is further indicates the irreversibility of the electrode process. The peak current was slightly decreased on increasing the pH of the electrolysis solution due to the increased viscosity of the medium.

On employing the relationship that correlate the peak potential E_p and the sweep rate (υ), equation (III.11), and on plotting E_p versus ln(υ) for all compounds under investigations, linear relationships are obtained at different pH values, Figs.(49a-54a). The transfer coefficient (α) values were determined from the slopes of these linear plots at the probable values of n_a. The most suitable α-values were obtained at n_a equal to 1.0, Tables (24&25). These results indicate that the rate-determining step should involve one electron.

Using the relation correlate the peak current and the scan rate [148], and on plotting peak current (I_p) versus the square root of scan rate ($\upsilon^{1/2}$) at different pH values, linear correlations intersecting the negative part of the cathodic peak current axis were obtained, which indicate some adsorption contribution to the electrode process was developed, Figs. (49b-54b). The adsorption was found to be slightly increased in alkaline media.

On increasing the pH of the electrolysis solution, the peak potentials obtained from both cyclic voltammetry and differential pulse polarographic techniques were shifted to more negative potentials denoting the irreversibility of the waves and the consumption of protons in the reduction processes. The plots of $E_{p,c}$ (obtained from d.p polarography) versus pH of solution at sweep rate showed linear relationship indicating that only one mechanism is operating the system in acidic, neutral and alkaline media, Figs. (43b-48b). The value of slopes (ranging from 66-86 mV) indicate that the reduction processes involved proton consumption.

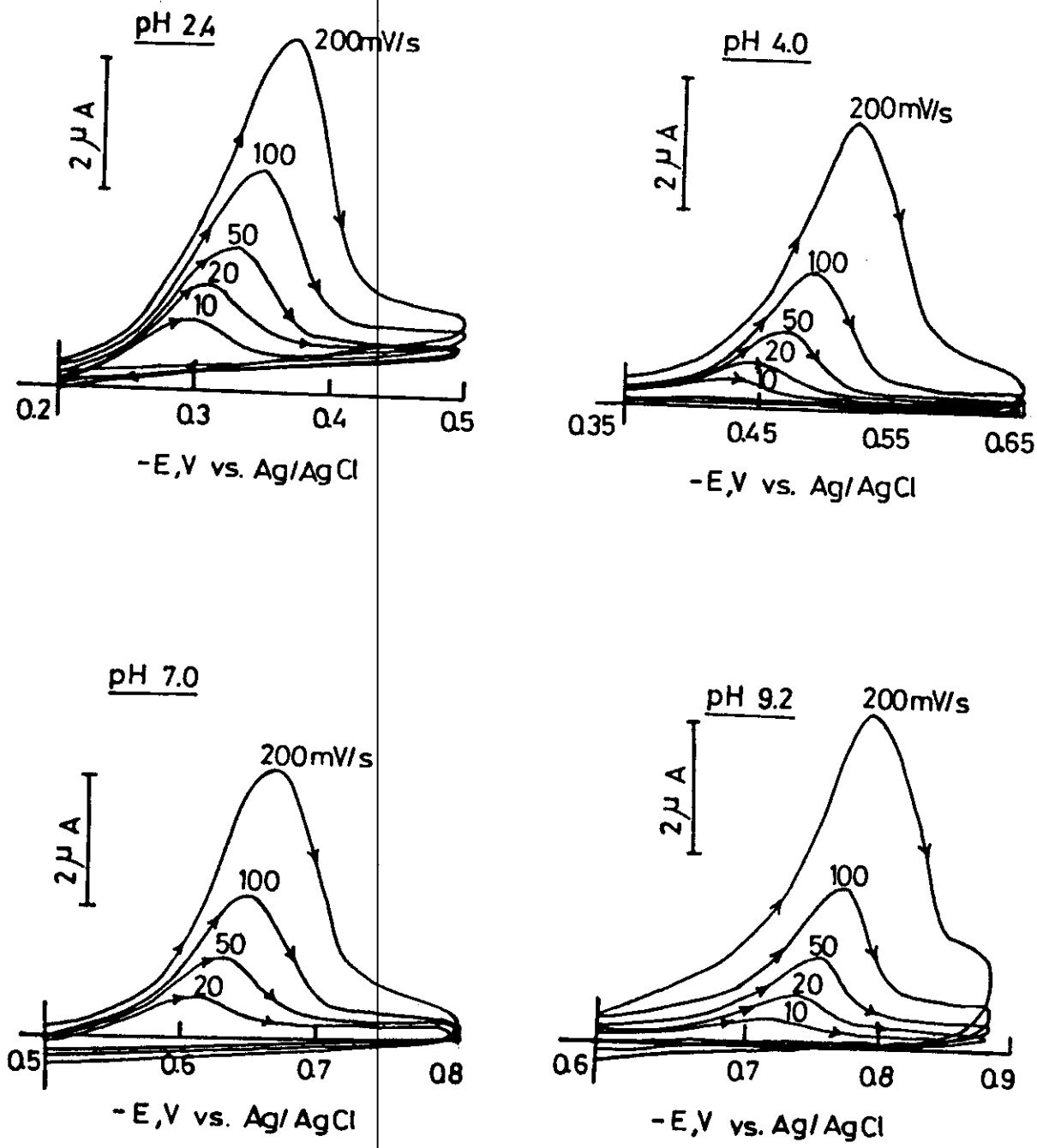

Figure 37: Cyclic voltammograms of coumarin azodye (Ia) in buffer solutions of different pH values at different sweep rates.

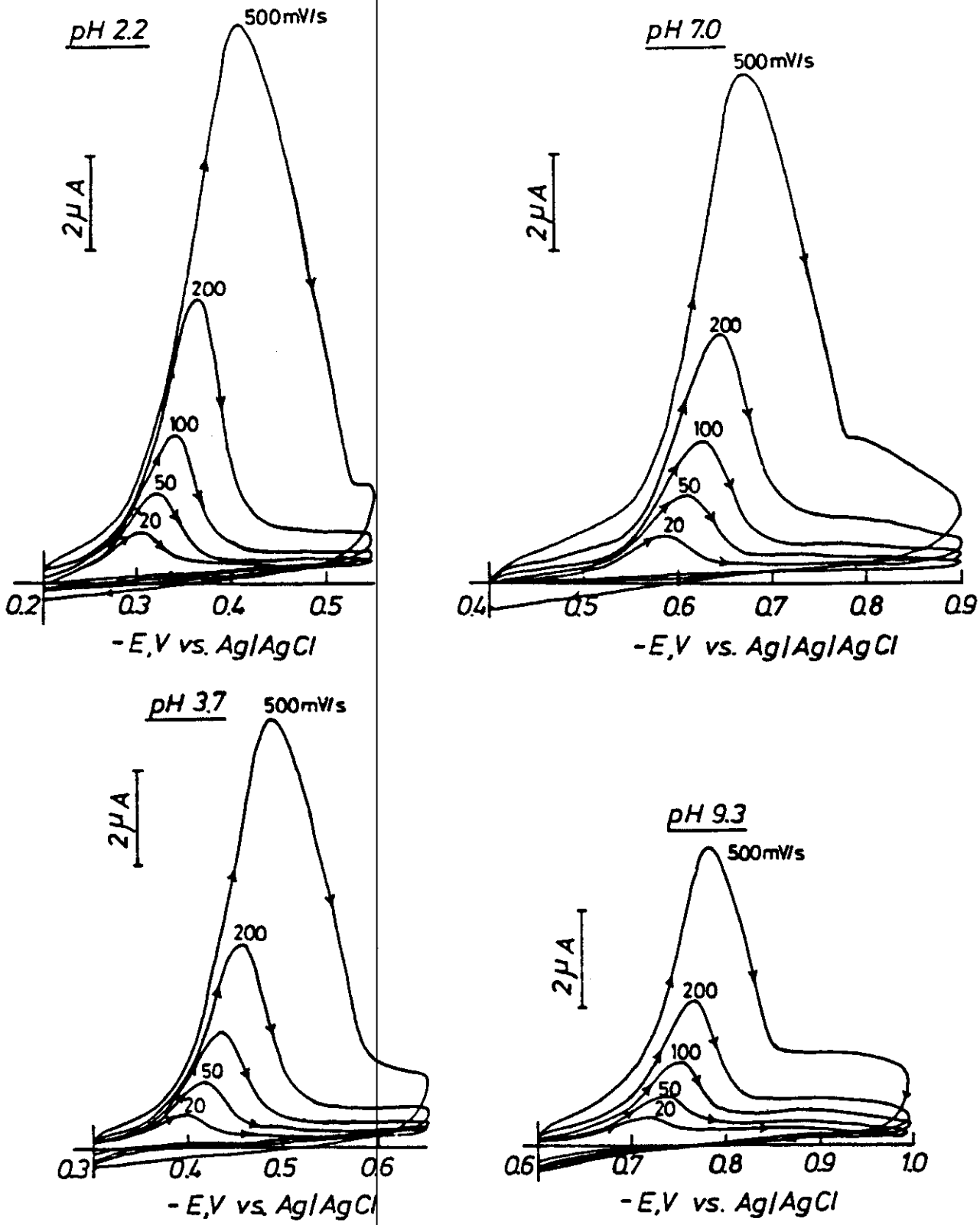

Figure 38: Cyclic voltammograms of coumarin azodye (I_b) in buffer solutions of different pH values at different sweep rates.

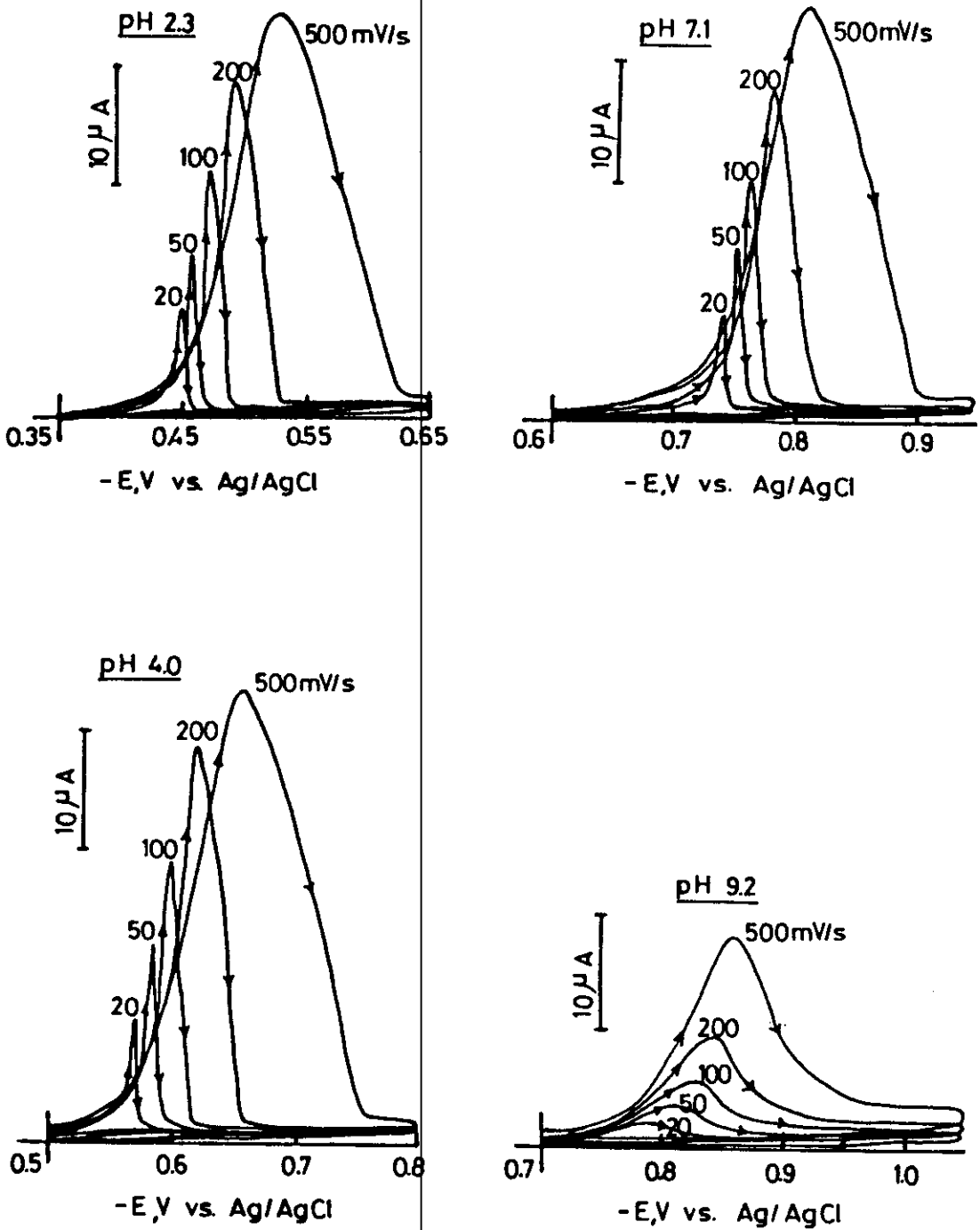

Figure 39: Cyclic voltammograms of coumarin azodye (Ic) in buffer solutions of different pH values at different sweep rates.

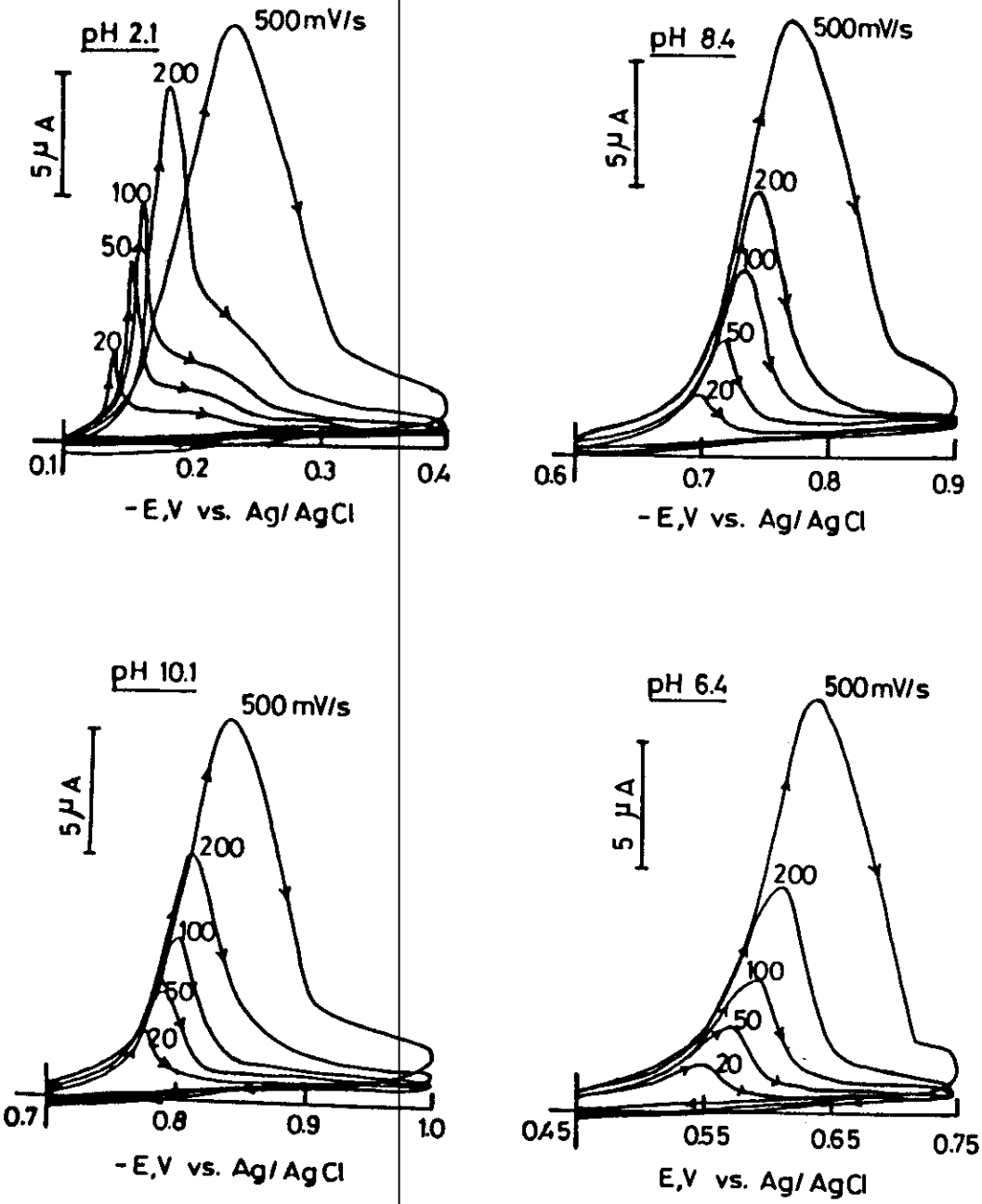

Figure 40: Cyclic voltammograms of Schiffer azodye (IIa) in buffer solutions of different pH values at different sweep rates.

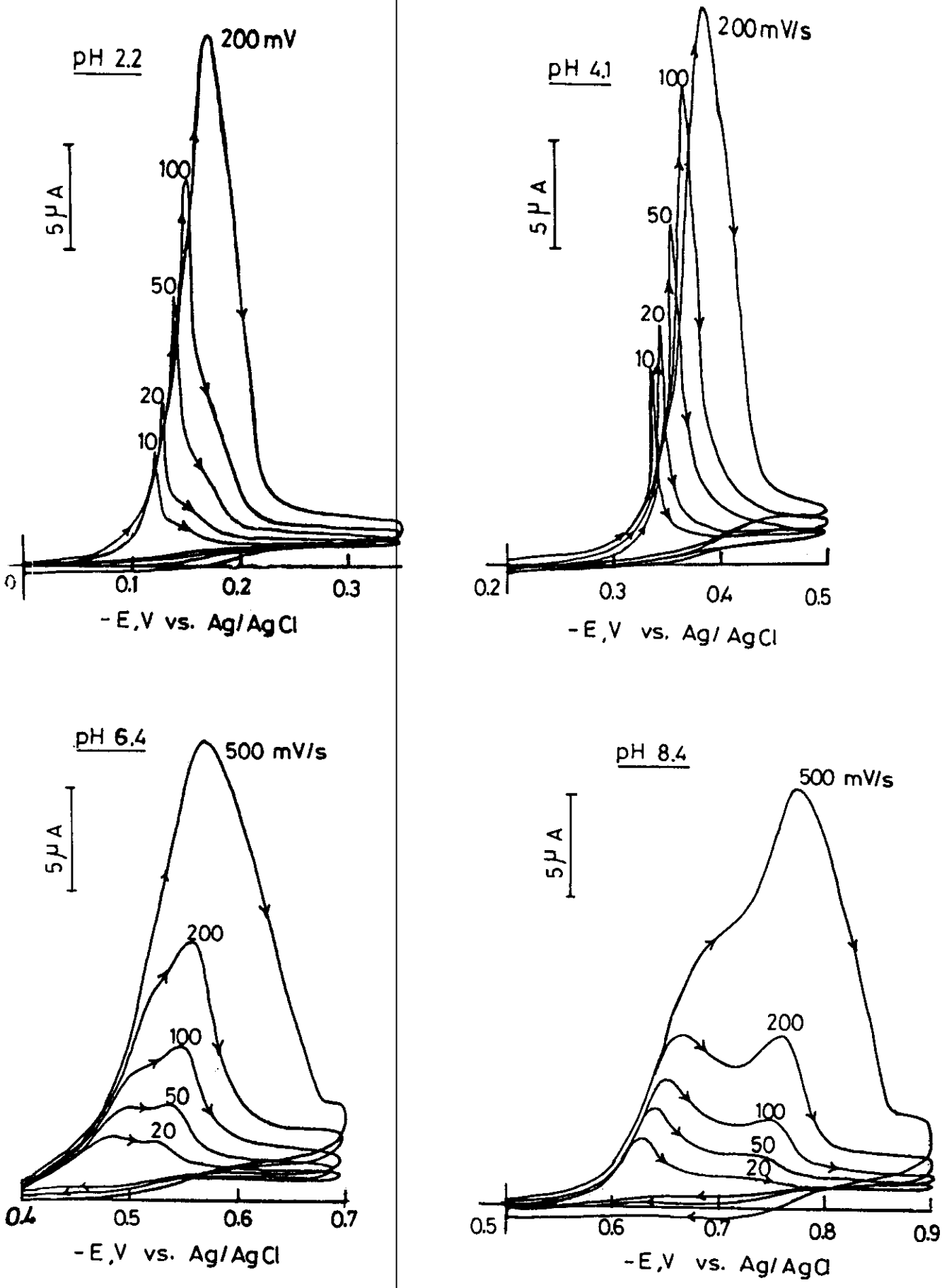

Figure 41: Cyclic voltammograms of Schiffer azodye (IIb) in buffer solutions of different pH values at different sweep rates.

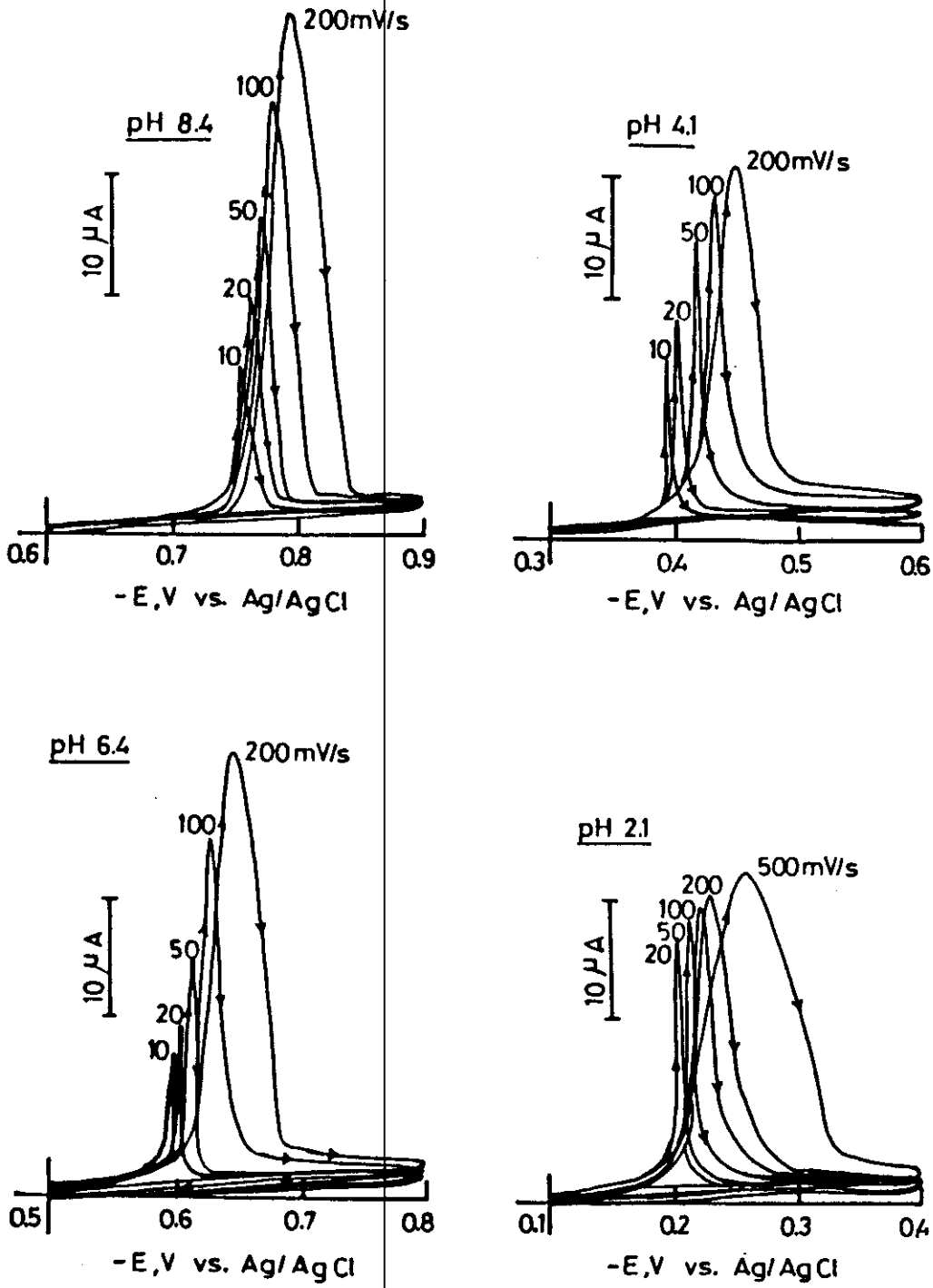

Figure 42: Cyclic voltammograms of Schiffer azodye (IIc) in buffer solutions of different pH values at different sweep rates.

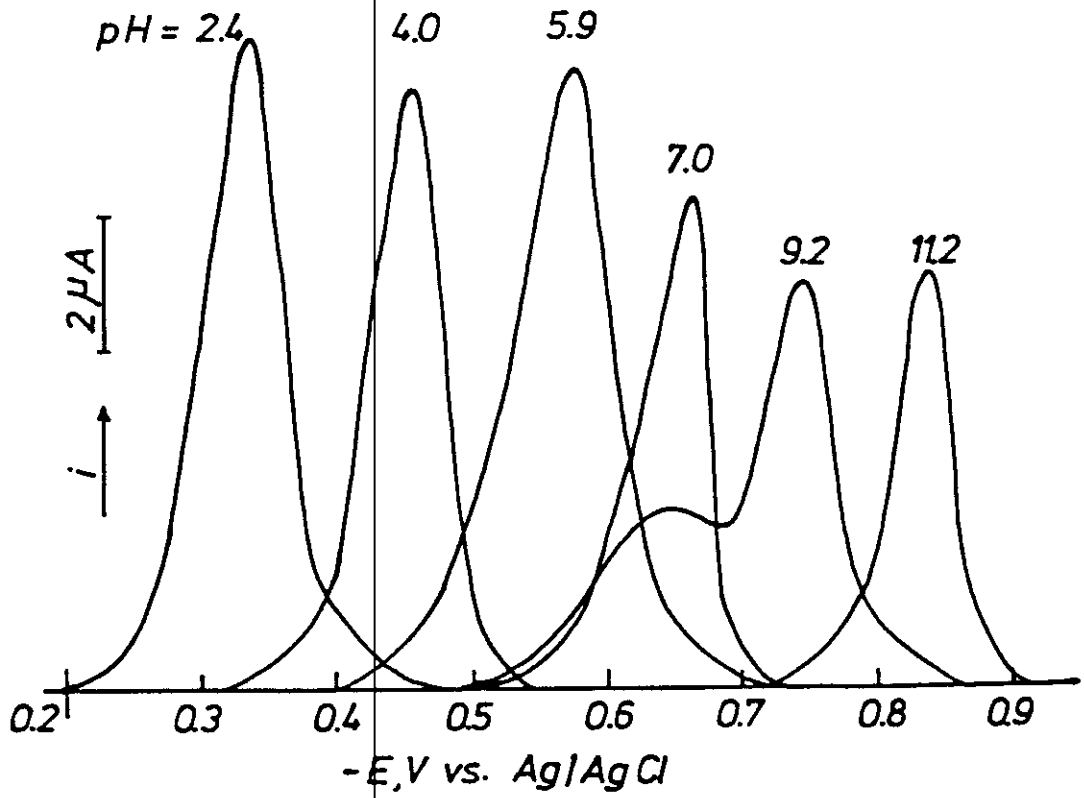

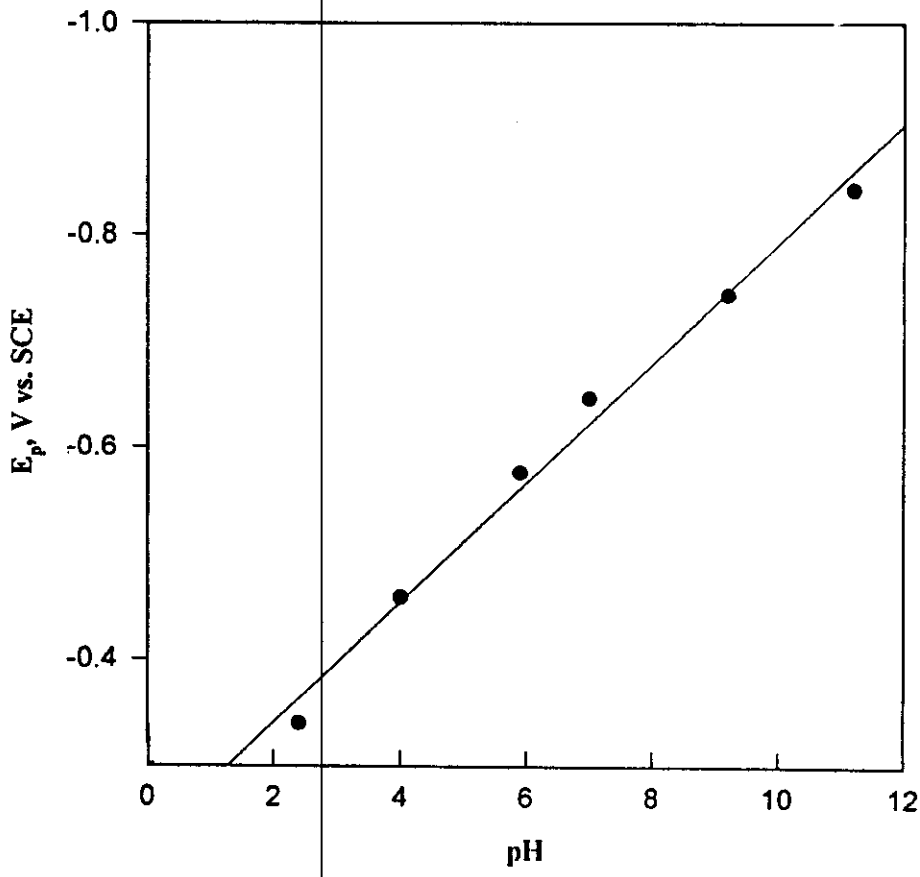

Figure 43: DP-polarograms of coumarin dye (Ia) in buffer solutions of different pH values.

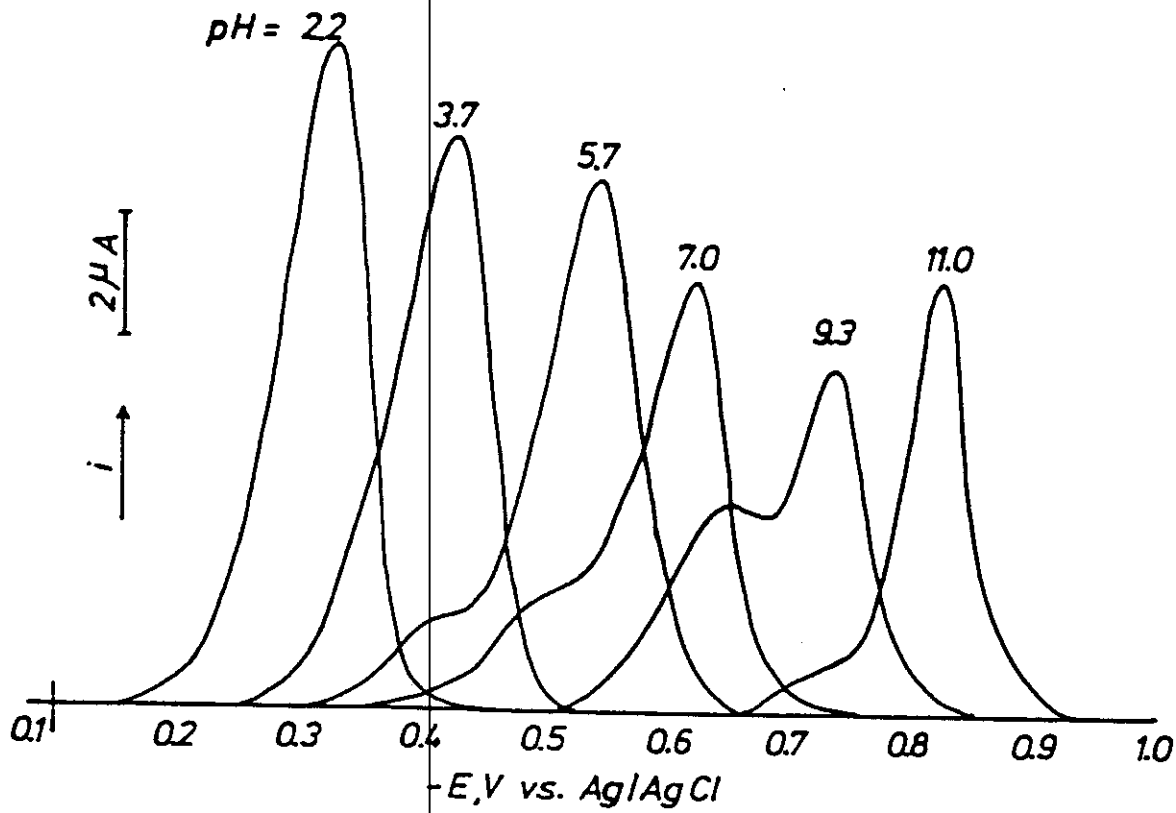

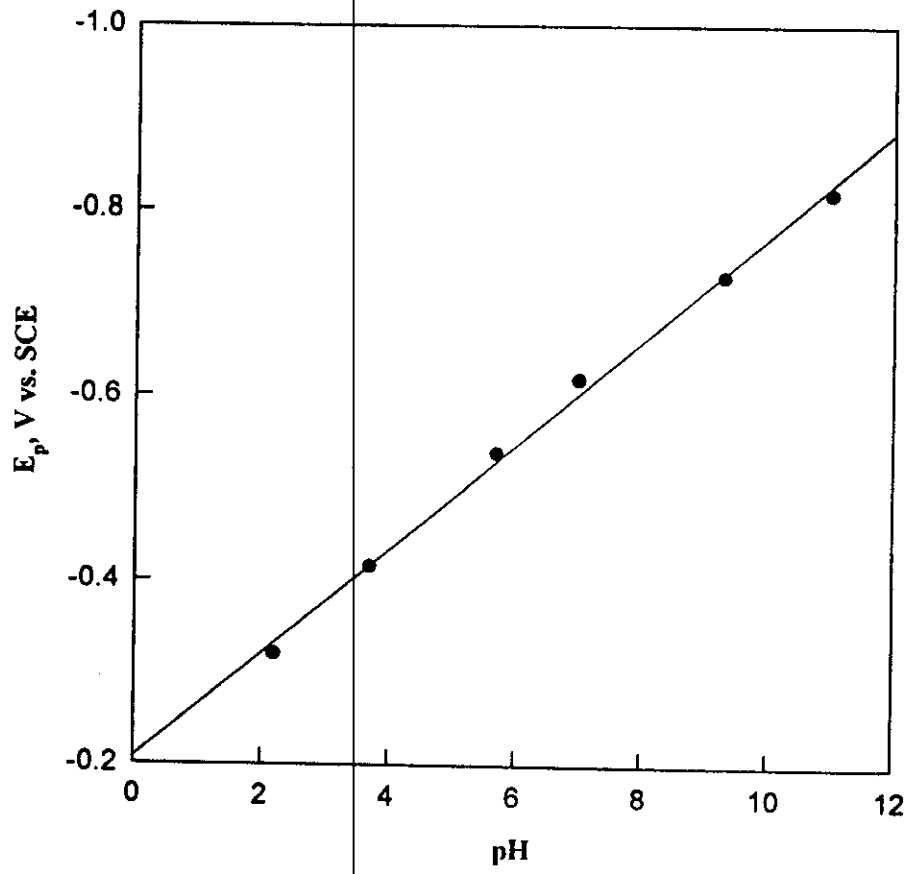

Figure 44: DP-polarograms of coumarin dye (Ib) in buffer solutions of different pH values.

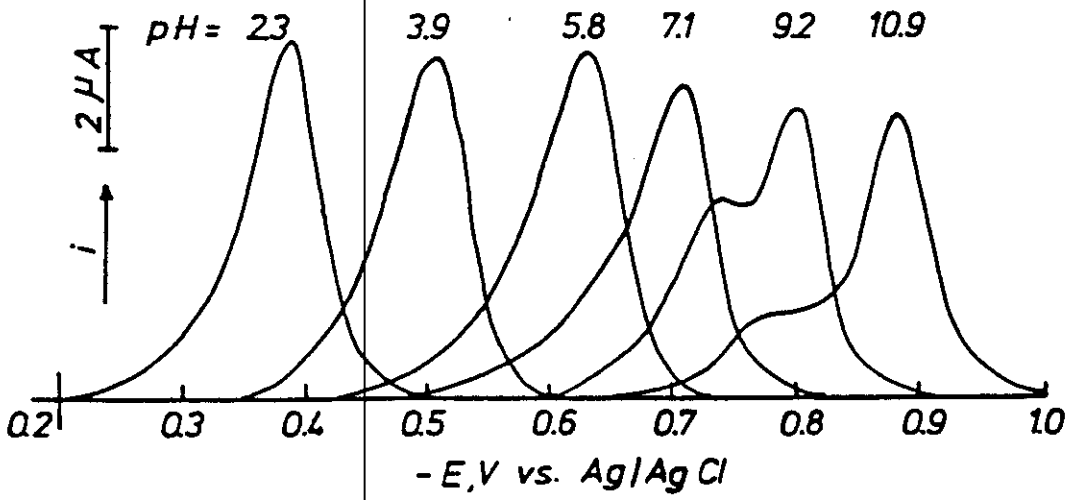

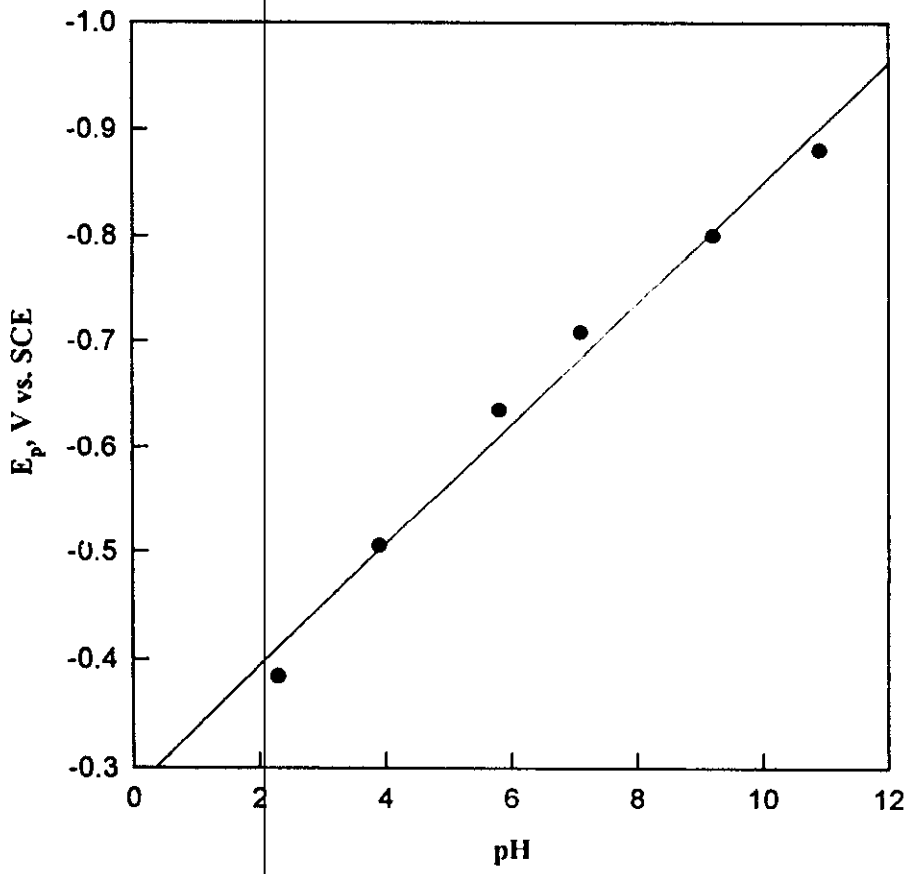

Figure 45: DP-polarograms of coumarin dye (Ic) in buffer solutions of different pH values.

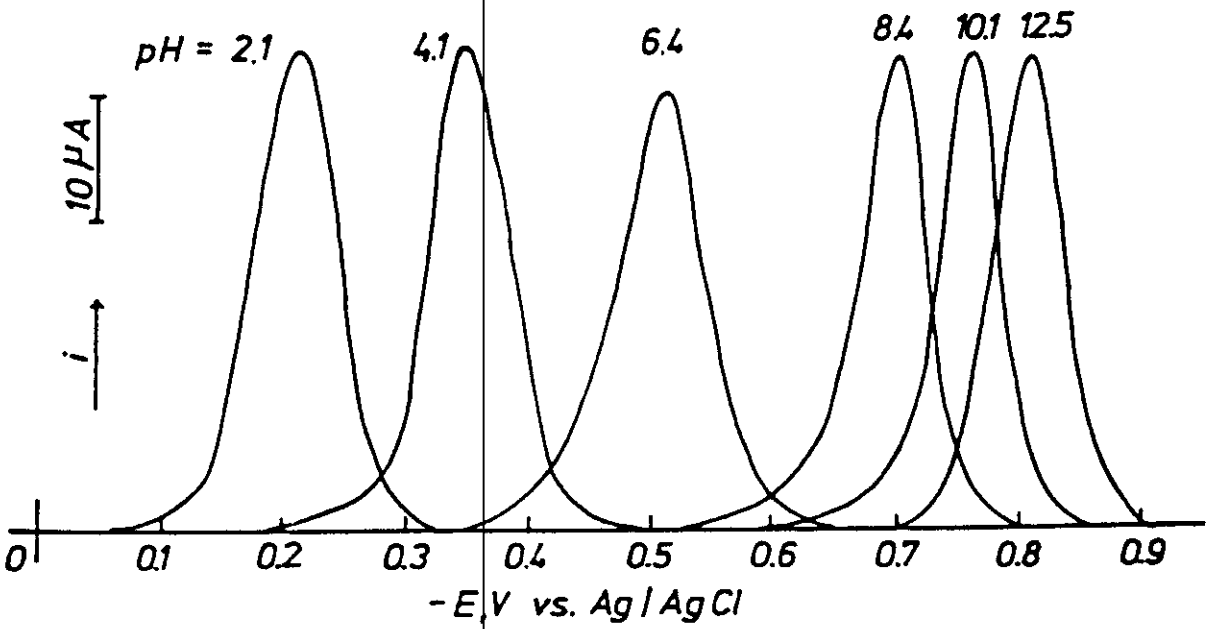

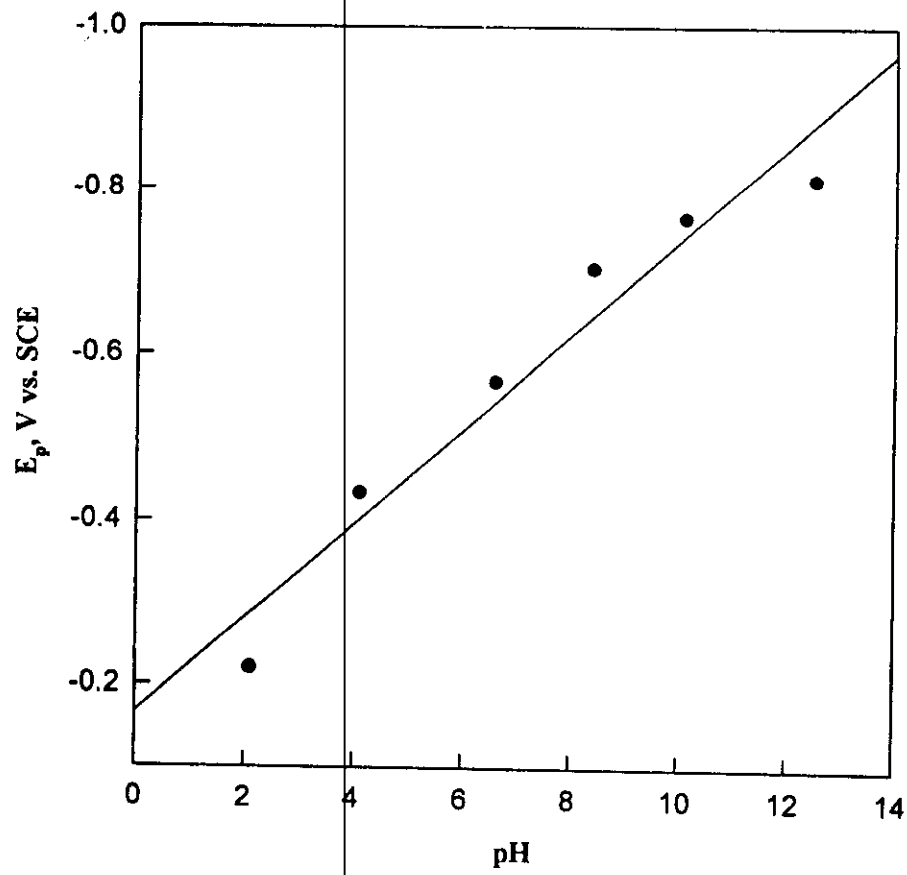

Figure 46: DP-polarograms of Schiffer dye (IIa) in buffer solutions of different pH values.

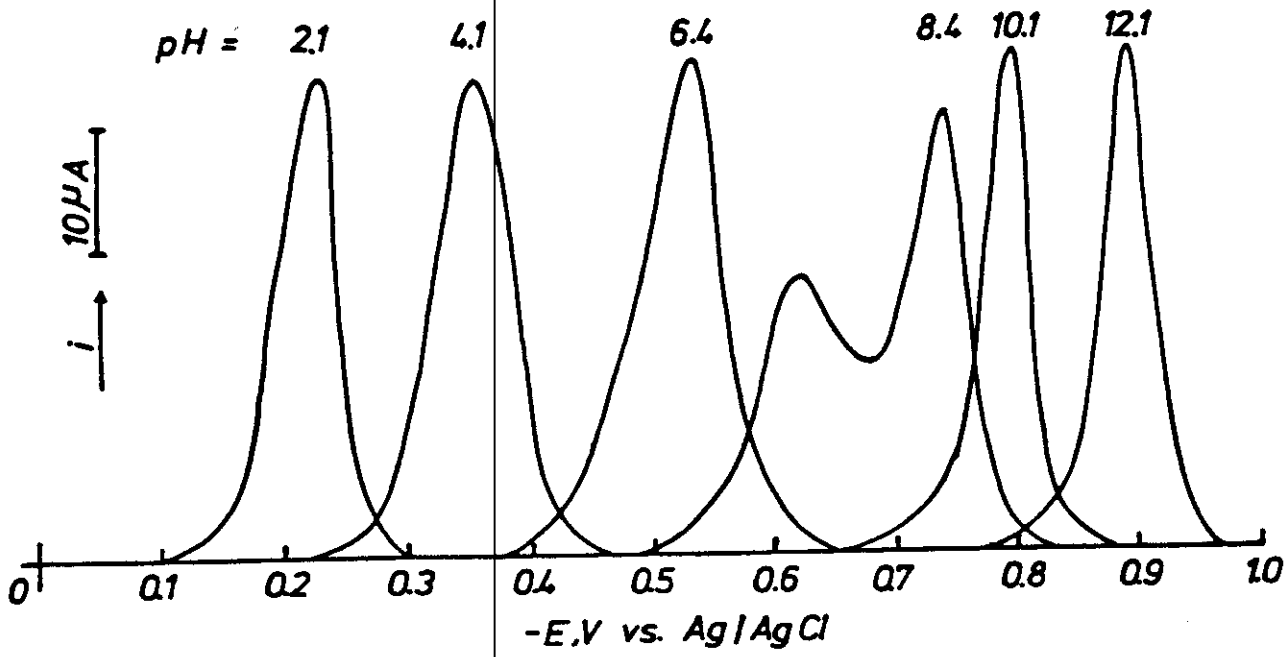

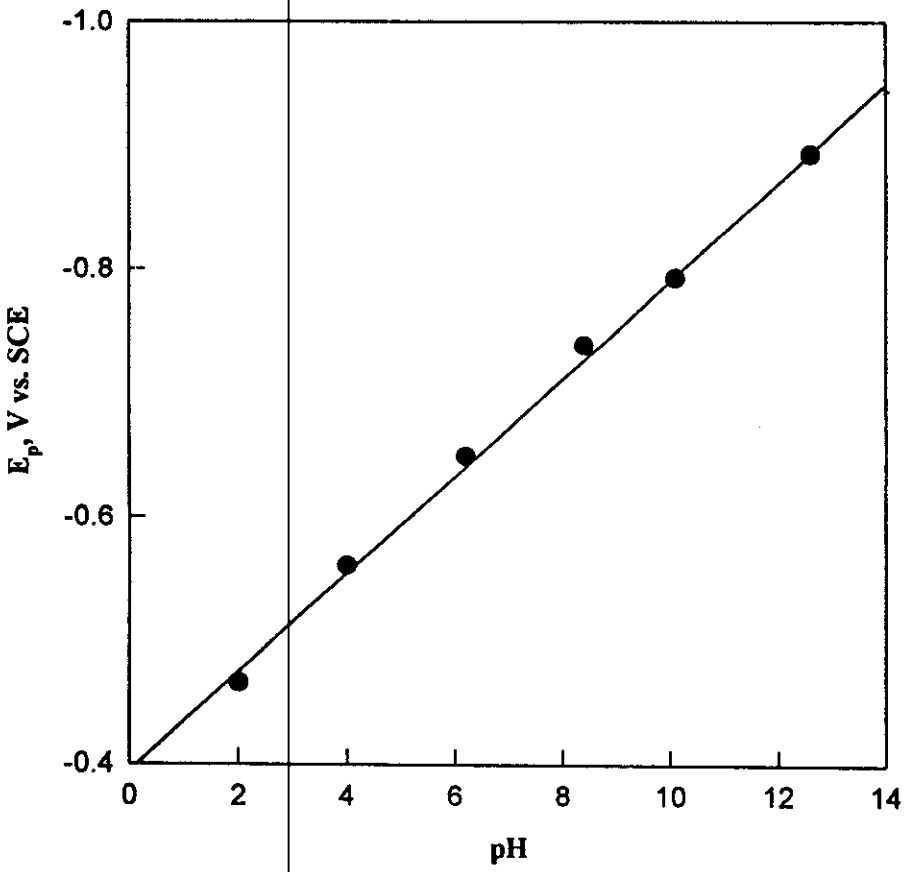

Figure 47: DP-polarograms of Schiffer dye (IIb) in buffer solutions of different pH values.

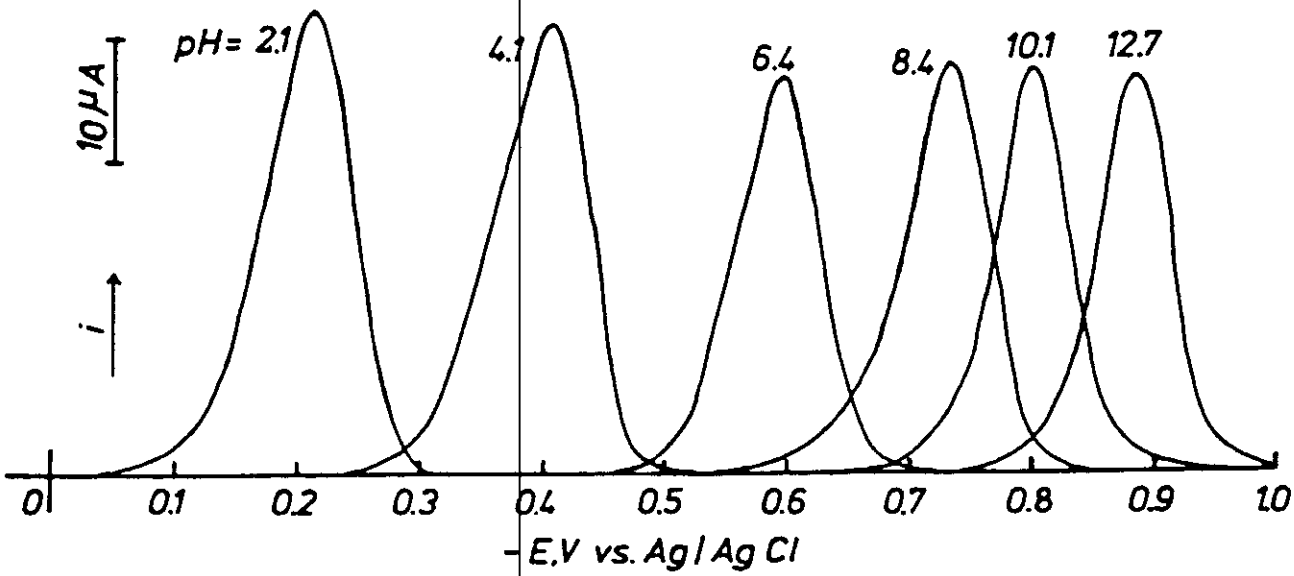

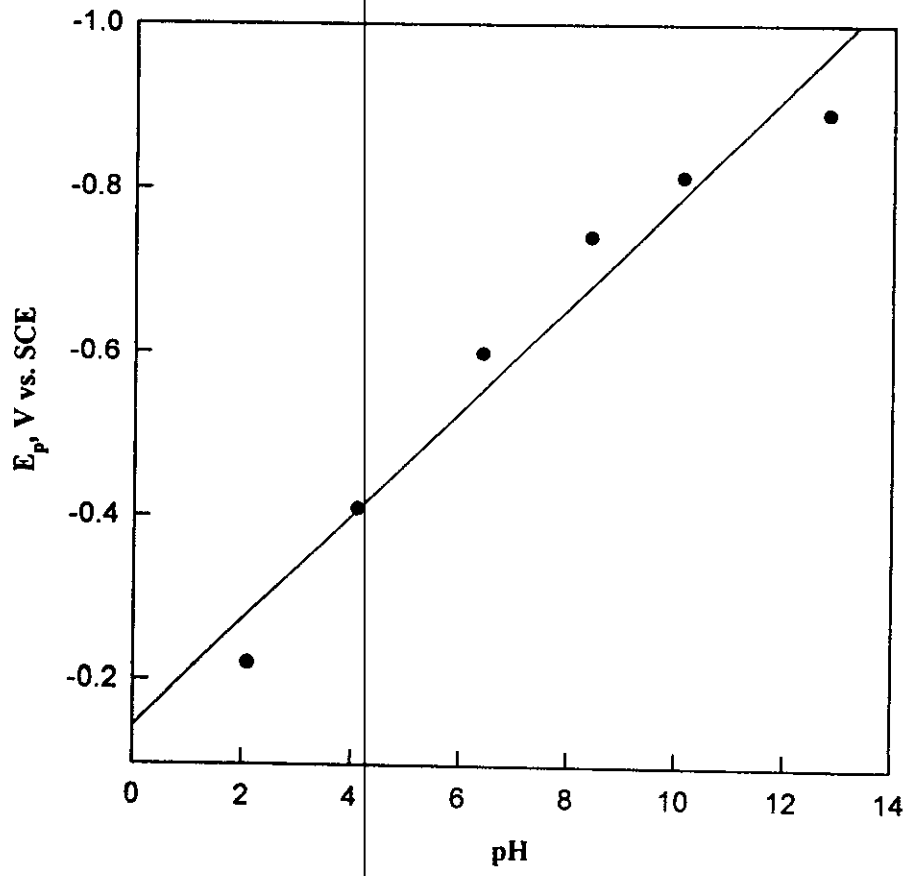

Figure 48: DP-polarograms of Schiffer dye (IIc) in buffer solutions of different pH values.

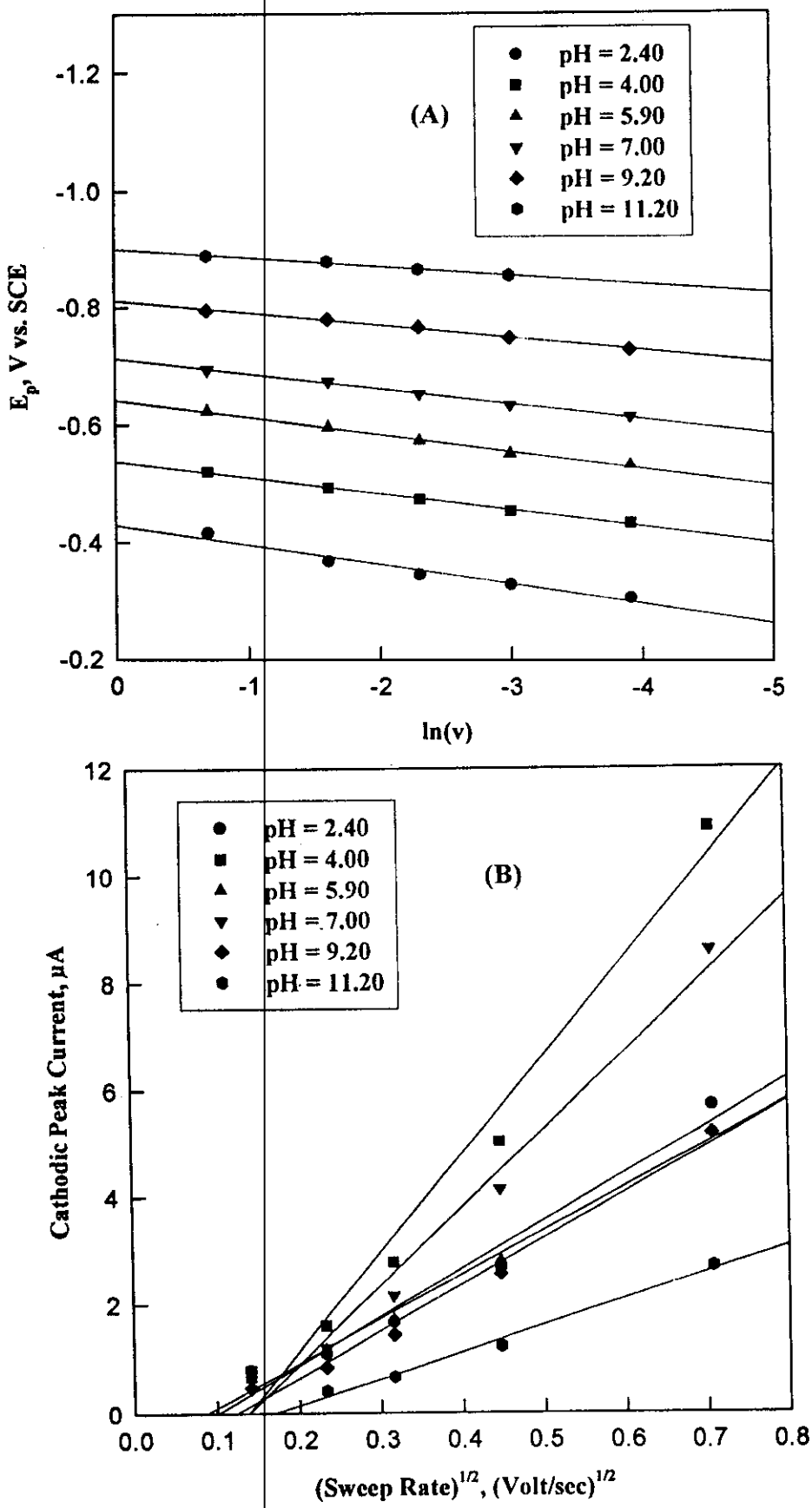

Figure 49: The plots of (a) E_p versus ln(υ) and (b) cathodic peak current versus $\upsilon^{1/2}$ for coumarin azodye (Ia) in aqueous buffer solutions of different pH values.

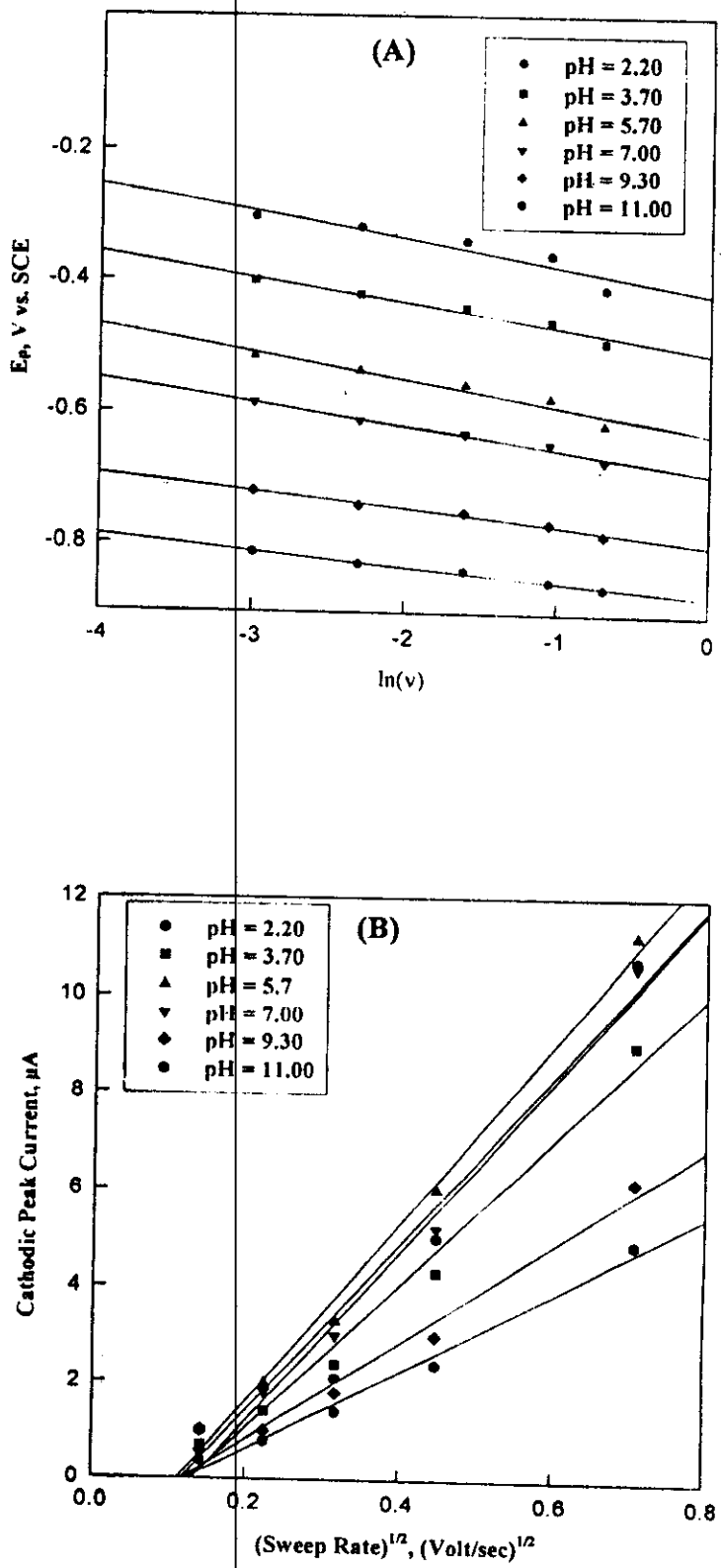

Figure 50: The plots of (a) E_p versus ln(υ) and (b) cathodic peak current versus $\upsilon^{1/2}$ for coumarin azodye (Ib) in aqueous buffer solutions of different pH values.

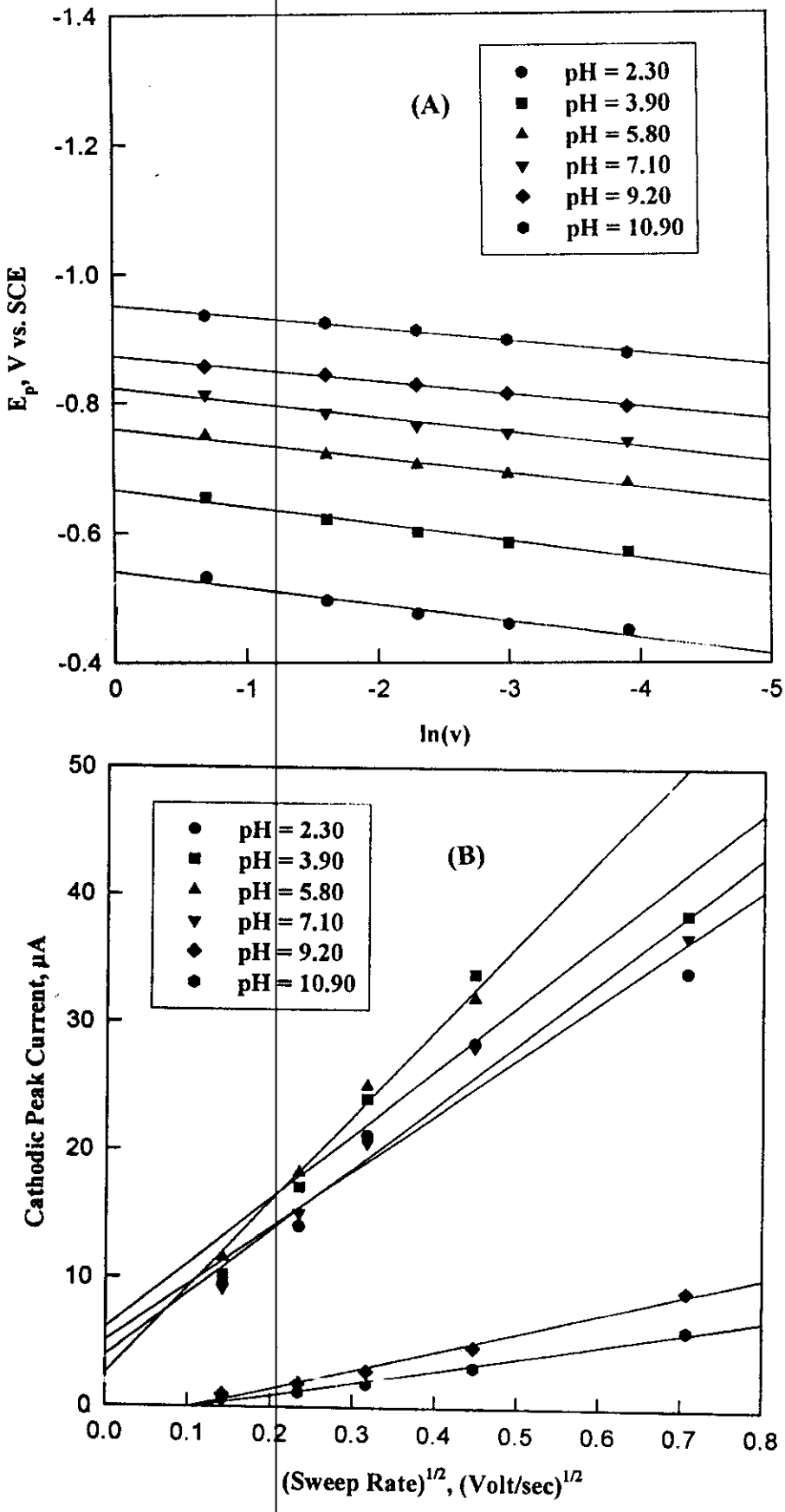

Figure 51: The plots of (a) E_p versus ln(υ) and (b) cathodic peak current versus $\upsilon^{1/2}$ for coumarin azodye (Ic) in aqueous buffer solutions of different pH values.

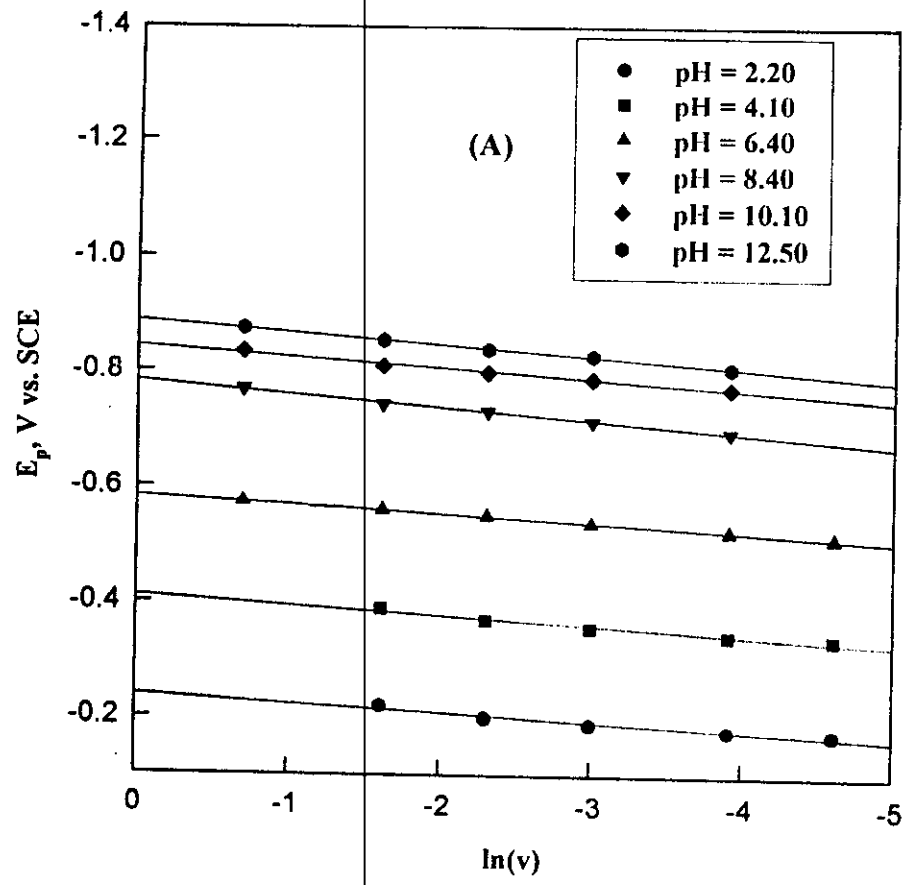

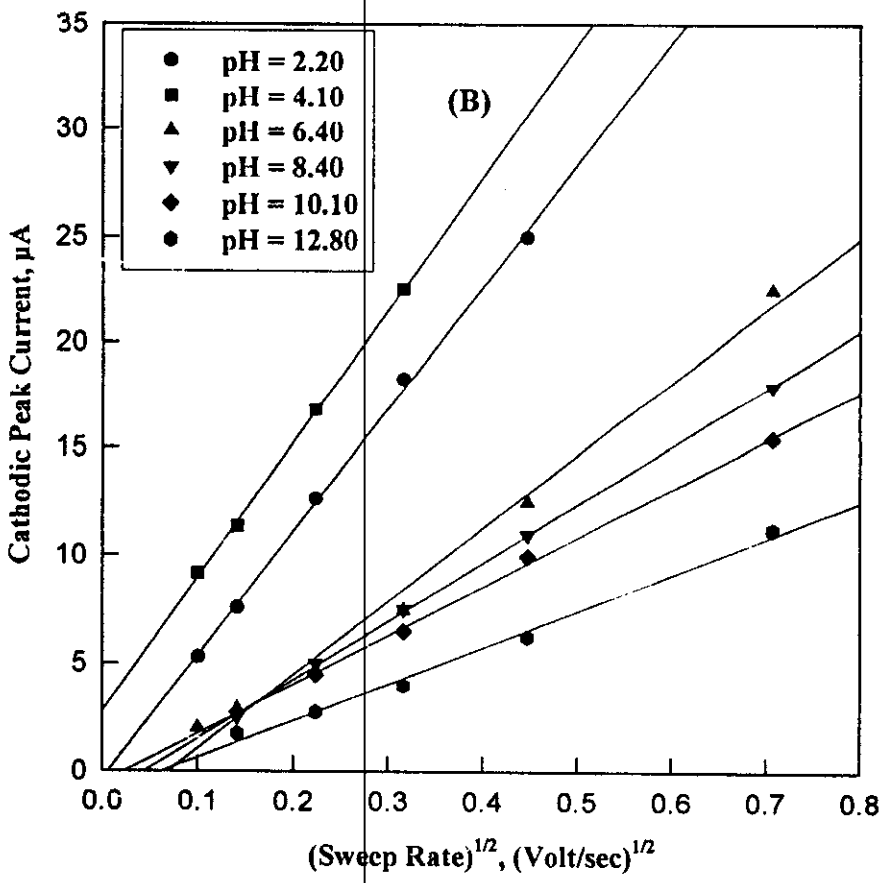

Figure 52: The plots of (a) E_p versus ln(υ) and (b) cathodic peak current versus $\upsilon^{1/2}$ for Schaffer azodye (IIa) in aqueous buffer solutions of different pH values.

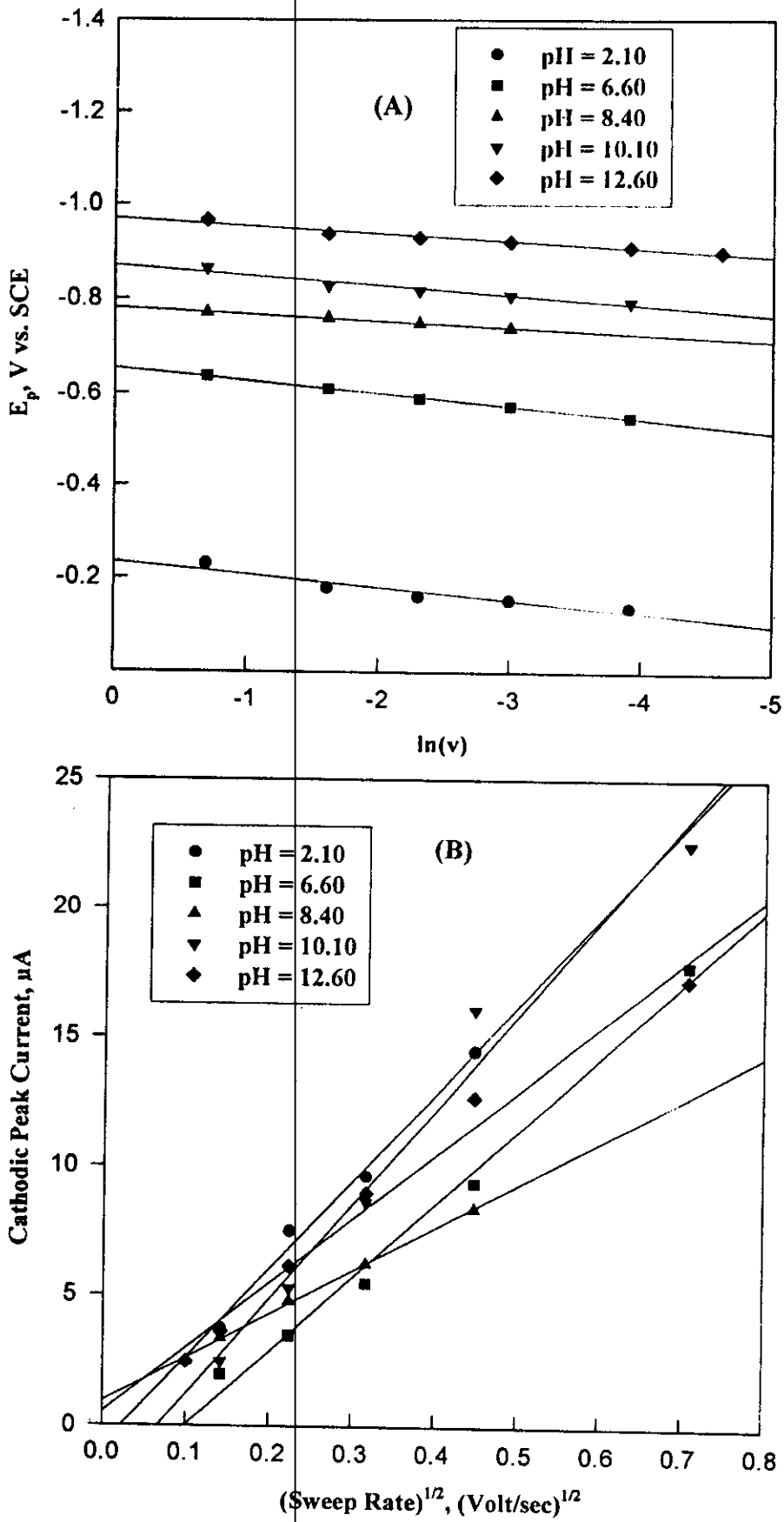

Figure 53: The plots of (a) E_p versus ln(υ) and (b) cathodic peak current versus $\upsilon^{1/2}$ for Schaffer azodye (IIb) in aqueous buffer solutions of different pH values.

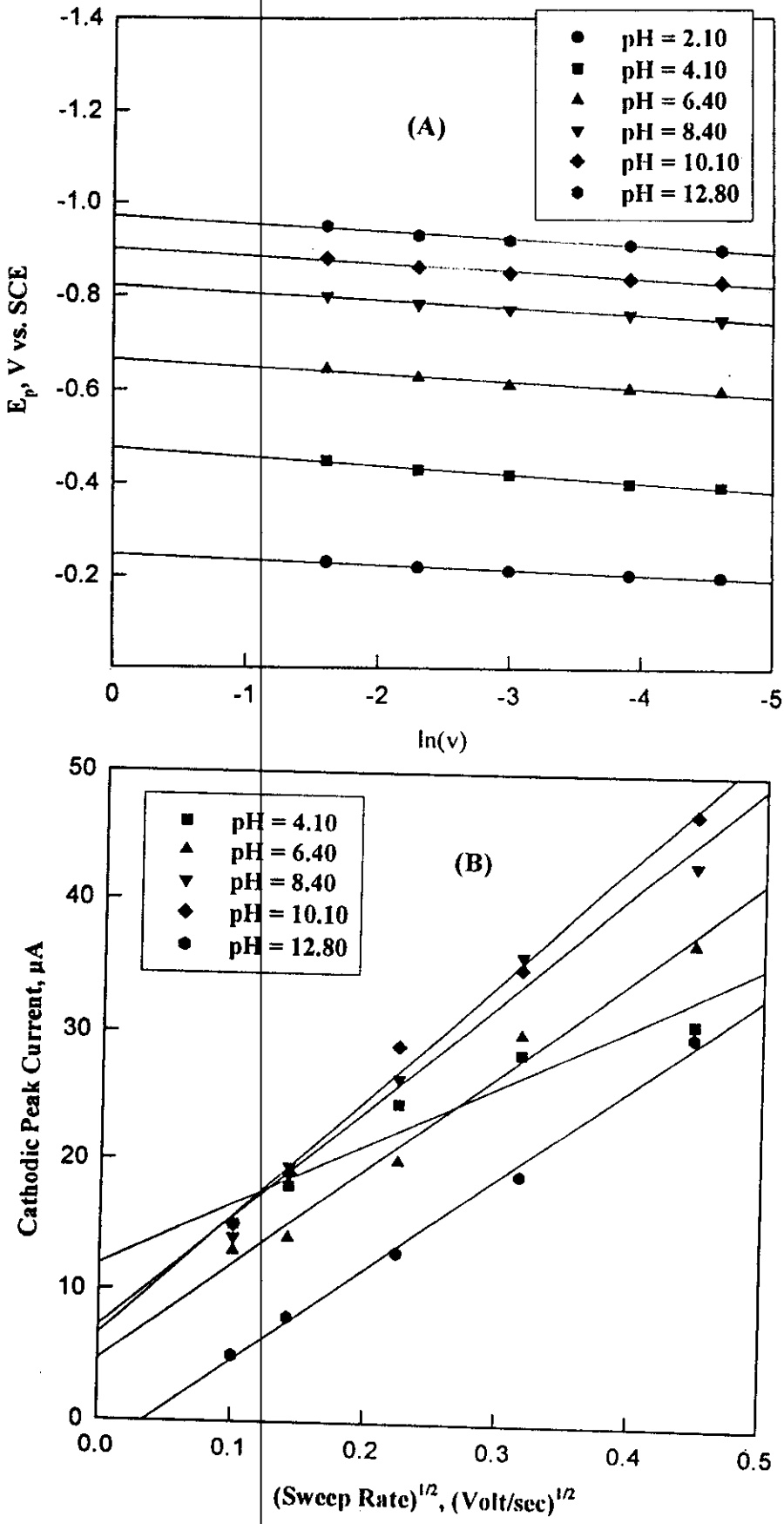

Figure 54: The plots of (a) E_p versus ln(υ) and (b) cathodic peak current versus $\upsilon^{1/2}$ for Schaffer azodye (IIc) in aqueous buffer solutions of different pH values.

The number of protons at the rate-determining step Z_H^+ was determined at different pH values for compounds of series I & II from the differential pulse polarography using the following relationship [193]:

$$Z_H^+ = (\Delta E_p/\Delta pH)/(0.0591/\alpha n) \qquad \textbf{(III.13)}$$

It was found that the number of electrons participating in the rate-determining step to be unity ($Z_H^+ = 1.0$).

3.3.3.1.3 Substituent effects

The peak potential values of a related organic compounds depend mainly on the type of substituent, where structural changes can cause changes in the number of observed peaks, the peak height and in the character of peaks, also it depends on the reversibility of the system. For an irreversible system, which is our case of study, the shift in peak potential is a function of logarithm of the rate constant, or the activation energy of the electrode process. This can be only if the transfer coefficient is not differed in magnitude [194]. Thus, the difference between the half-wave potential of the unsubstituted, $E_{1/2}(H)$, and that of the substituted benzenoid derivatives, $E_{1/2}(X)$ can be related to the rate constant according to the following relationship [194]:

$$\Delta E_{1/2} = (2.303RT/\alpha n_a F)\log (k_X/k_H) \qquad \textbf{(III.14)}$$

or

$$\Delta E_{1/2} = \rho_{(\pi, R)}\, \sigma_X \qquad \textbf{(III.15)}$$

where $\rho_{(\pi, R)}$ is called the reaction constant expressed in volts and σ_X is the total polar substituent constant, (Hammett substituent constant).

In the present investigation, for coumarin azodyes (series I) the substituent was introduced into the para-position of the homocyclic phenyl ring attached to the azo group. The peak potentials of the compounds Ia, Ib and Ic were recorded at different pH values from the plots of E_p (obtained from d.p polarography) versus pH curves at pH's 4.00, 6.00, 8.00 and 10.00. It was found generally that, compound substituted by electron withdrawing groups like, p-Cl, was reduced at less negative potentials compared to the unsubstituted compound. On the reverse, compound possessing electron donating groups like, p-OCH_3, was reduced at higher negative potentials. On plotting the peak potentials (E_p) of compounds Ia, Ib and Ic versus σ_X in solution of different pH values, linear correlations were obtained of slope ranges from 5.84 to 6.34, Fig. (55). The values of σ_X were obtained from the tabulation of Ritchie and Sager [194]. These results indicate that compounds containing electron withdrawing groups accelerate the reduction process due to the decreased basicity of the unprotonated nitrogen atom linked to the phenyl ring and consequently promotes the reduction of the electroactive N=N center. On the other hand, compounds possessing electron donating groups were reduced at more negative potentials which attributed to the increased electron density on the N=N center leading to retardation of the reduction process.

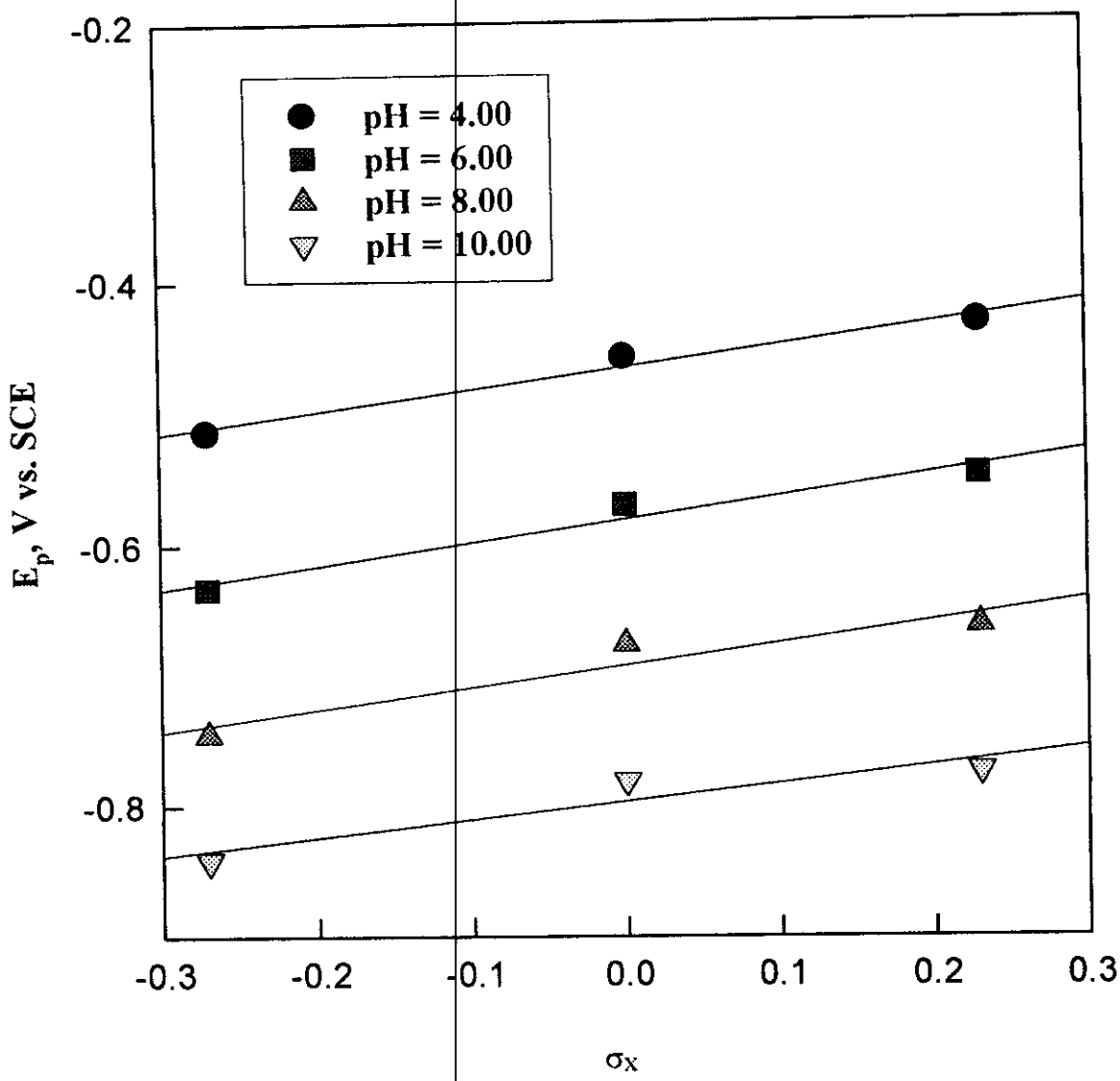

Figure 55: Hammett substituent effect of coumarin dyes (series I).

Table 23: Cyclic Voltammetric Data Obtained for 0.20 mM 8-(phenylazo)-6,7-dihydroxy-4-methylcoumarin (Ia) in Pure Aqueous and Microemulsion Systems at 25°C.

System	Sweep Rate mV/sec	$I_{p,c}$ μA	$-E_{p,c}$ mV	$dE_p/d\ln\upsilon$ ($x10^2$)	$Dx10^6$ cm^2/sec	α n_a=1.0	α n_a=2.0
Pure aqueous							
	20	0.92	744				
	40	1.42	755				
	60	1.79	767				
	80	1.96	779	4.96	8.16	0.26	0.13
	100	2.05	792				
	150	2.87	825				
	200	3.28	847				
	500	6.35	892				
CTAB Microemulsion							
	20	2.93	602				
	40	4.18	624				
	60	5.29	648				
	80	6.00	663	4.51	6.19	0.28	0.14
	100	6.47	671				
	150	8.23	690				
	200	9.31	696				
	500	15.20	747				
SDS Microemulsion							
	20	2.67	799				
	40	3.73	802				
	60	4.56	805				
	80	5.38	815	3.90	7.68	0.33	0.17
	100	6.08	828				
	150	7.92	842				
	200	9.15	846				
	500	17.83	928				
Triton X-100 microemulsion							
	20	2.91	726				
	40	4.08	757				
	60	5.02	768				
	80	5.82	785	4.11	5.23	0.31	0.16
	100	6.52	793				
	150	8.08	798				
	200	9.37	816				
	500	14.58	864				

Table 24: Cyclic voltammetric Data Obtained for Coumarin Azo-Compounds (Ia-Ic) at Different pH Values and at 25°C.

Compound	pH	$dE_p/d\ln(\upsilon)$ ($x10^2$)	αn_a	
			$n_a = 1.0$	$n_a = 2.0$
(Ia)	2.40	3.30	0.39	0.20
	4.00	2.76	0.47	0.24
	5.90	2.86	0.45	0.23
	7.00	2.52	0.51	0.26
	9.20	2.04	0.63	0.32
	11.20	1.47	0.88	0.44
(Ib)	2.20	3.20	0.40	0.20
	3.70	2.81	0.46	0.23
	5.70	3.18	0.40	0.20
	7.00	2.62	0.49	0.25
	9.30	1.85	0.69	0.35
	11.00	1.59	0.81	0.41
(Ic)	2.30	2.57	0.50	0.25
	3.90	2.63	0.49	0.25
	5.80	2.25	0.76	0.38
	7.10	2.26	0.57	0.28
	9.20	1.93	0.67	0.34
	10.90	1.85	0.69	0.35

Table 25: Cyclic voltammetric Data Obtained for Schiffer Azo-Compounds (IIa-IIc) at Different pH Values and at 25°C.

Compound	pH	$dE_p/dln(\upsilon)$ ($x10^{-2}$)	αn_a	
			$n_a = 1.0$	$n_a = 2.0$
(IIa)	2.20	1.44	0.89	0.45
	4.10	1.63	0.79	0.40
	6.40	1.50	0.86	0.43
	8.40	2.14	0.60	0.30
	10.10	1.80	0.71	0.36
	12.50	1.98	0.65	0.33
(IIb)	2.10	2.64	0.49	0.25
	6.60	2.72	0.47	0.24
	8.40	1.31	0.98	0.49
	10.1	2.09	0.62	0.31
	12.60	1.58	0.81	0.41
(IIc)	2.10	1.42	0.90	0.45
	4.10	1.87	0.48	0.24
	6.40	1.55	0.83	0.42
	8.40	1.44	0.89	0.45
	10.10	1.57	0.83	0.42
	12.80	1.57	0.83	0.42

3.3.3.1.4 Complex formation of Schiffer azodyes with Cu^{+2} and Zn^{+2} ions using differential pulse polarography

The reduction of metal ions complexes and evaluation of their stability constants by differential pulse polarographic method depends mainly on the changes undergone by the reduction waves of the metal cations when their coordination spheres are occupied by molecules other than water. The reduction potential of complexed metal ions is almost shifted toward more negative values compared with the simple metal ions and the diffusion current changes usually becoming smaller. This behaviour could be attributed to the formation of bulky complexed ion which required more energy for the reduction at the dropping mercury electrode.

The polarographic reduction of the simple metal ions of Cu^{+2} and Zn^{+2} of $1x10^{-4}$ M concentrations in 0.1 M $NaNO_3$ solutions were recorded using differential pulse polarography. The d.p polarograms of these simple metal ions showed a reversible behaviour as observed from the half-peak width ($W_{1/2}$). The half-peak width was found to be 60 mV and 59 mV for Cu^{+2} and Zn^{+2}, respectively. The effect of ligand concentration of 1-phenylazo-2-hydroxy-6-naphthalenesulfonic acid (IIa), 1-(2-carboxyphenylazo)-2-hydroxy-6-naphthalenesulphonic acid (IIb) and 1-(2-methoxyphenylazo)-2-hydroxy-6-naphthalenesulphonic acid (IIc) on the reduction peaks of Cu^{+2} and Zn^{+2} ions were recorded in 0.1 M $NaNO_3$. The addition of ligand is applied within the concentration range from $1x10^{-5}$ to $1x10^{-3}$ M. The d.p polarograms were recorded at 25 mV pulse amplitude and of pulse height 5 mV/sec. The gradual addition of the ligand to the simple metal ions of each of Cu^{+2} and Zn^{+2} ions was found to affect peak currents (I_p) as well as the peak

potential (E_p). Generally, as the ligand concentration is increased the peak currents is decreased and this behaviour is attributed to the increased bulk of the comlexed metal ions. Also, the peak potentials (E_p) of the simple metal ion showed a cathodic shift on increasing the ligand concentration. These results confirmed the complex formation of the metal ion with the free lone-pair of electrons localized on the nitrogen atom in the azo-centre and o-OH group in the phenyl ring.

It is of importance to test the reversibility of the system after the complex formation. The reversibity of each system was tested in terms of half-peak widths ($W_{1/2}$) of the differential pulse polarograms and it was found to lies between 58 and 76 mV which confirmed that the reduction of complexed metal ions takes place quasi-reversible, Table (26). These results were further confirmed by cyclic voltammetry technique where the peak separation was found to in the range of 40 mV.

The shift in the peak potential ($\Delta E_p = E_p(c) - E_p(s)$) measured from differential pulse polarograms due to complex formation of azo compound IIa was found to be 47 and 113 mV, for Zn^{+2} and Cu^{+2}, respectively, Table (26). This shift in peak potentials was used in the determination of the overall stability constants of the metal complexes and their stoichiometry.

Since the systems under investigations are still behaves reversibly, the overall stability constants of the metal complexes and their coordination numbers were determined by using the following equation [195]:

$$\mathbf{E_p(c) = E_p(s) - (0.0591/n) \log \beta_{Mxj} - j(0.0591/n) \log C_X} \qquad \textbf{(III.16)}$$

or $\Delta E_p = -(0.0591/n) \log \beta_{Mxj} - j(0.0591/n) \log C_X$ (III.17)

where $E_p(c)$ and $E_p(s)$ are the peak potentials of the complexed and free metal ions, respectively, j is the coordination number and C_X is the molar concentration of the ligand. This equation shows that the shift in peak potential of the reduction process to the negative direction increases with increasing stability of the complex. The plots of ΔE_p versus log C_X showed linear correlations for both Cu^{+2} and Zn^{+2} complexes, Fig. 56(a&b). The slopes of these linear plots were used in the estimation of the stoichiometry (j) of the formed complexes. The coordination number (j) was determined from the values of slopes and found to equal to 1 and 2 for Cu^{+2} and 2 for Zn^{+2} (Table 26), indicating the presence of 1:1 and 1 : 2 [metal : ligand] complexes in solution. From the values of the intercept of the relation [III.17] which is equal to (0.0591/n) log β_{Mxj}, the values of the overall stability constant of different complexes were determined. The values of log β_{Mxj} were found to be 7.85 and 6.13 in case of Cu^{+2} and Zn^{+2} complexes, respectively. Inspection of these values indicate that the formation constant of Cu^{+2} complex is higher than that of Zn^{+2} which could be attributed to the smaller ionic size of copper, therefore higher positive charge density was located and available for the interaction with ligand to form more stable complexes.

The effect of substituents in the phenyl ring of the Shiffer azodyes on the stability of complexes of Cu^{+2} and Zn^{+2} ions in solution was also studied. The compounds used were , 1-(2'-carboxyphenylazo)-2-hydroxy-6-naphthalenesulphonic acid (IIb) and 1-(2'-methoxyphenylazo)-2-hydroxy-6-naphthalenesulphonic acid (IIc). It was found that on

increasing the ligands concentration, the peak current decreases, also the peak potentials of both Cu^{+2} and Zn^{+2} shifted in the cathodic direction, confirming the complexes formation.The magnitude of the shift due to addition of ligand was expressed in terms of ΔE_p, Tables (27&28). ΔE_p values indicate that the total shift on adding $1x10^{-3}$ M of ligand IIb to each of Cu^{+2} and Zn^{+2} solutions were 120 and 75 mV, respectively, whereas, that in case of adding $1x10^{-3}$ M of ligand IIc 130 and 48 mV, respectively, Tables (27&28).

On employing the relationship [III.15], the plots of ΔEp versus log C_X showed linear correlations, Figs. (57&58). The slopes of these plots is equal to j(0.0591/n), from which the coordination number (j) was determined and found to be 2 for Cu^{+2} with the ligands IIb and IIc, while it was found to be 1 in case of Zn^{+2} with the same ligands. These results were indicative of 1 : 2 [metal : ligand] complexes with of Cu^{+2} with compounds II & III, while it forms 1 : 1 complexes with Zn^{+2}. From the intercepts of the plots the overall stability constants were determined. Values of log β_{Mxj} of Cu^{+2} and Zn^{+2} complexes were determined and represented in Tables (27&28). Inspection of these values indicate that the complexes of Cu^{+2} with compounds IIa, IIb and IIc showed that the stability constant was increased and this is because the o-COOH substituted was a center for chelation by loosing proton. While in case of Cu^{+2} complex with compound IIc (o-OCH_3 substituted) it has to affect the azo ligand in two ways, sterric effect and as mesomeric effect, the mesomeric effect localized the lone-pair of electrons on the nitrogen of azo group therefore its basisity is increased favouring of complex formation. Whereas, Zn^{+2} complexes with o-OCH_3 substituted, compound III, showed lower stability constants and this behaviour may be attributed to steric factor of OCH_3 and the bulky Zn^{+2} ions.

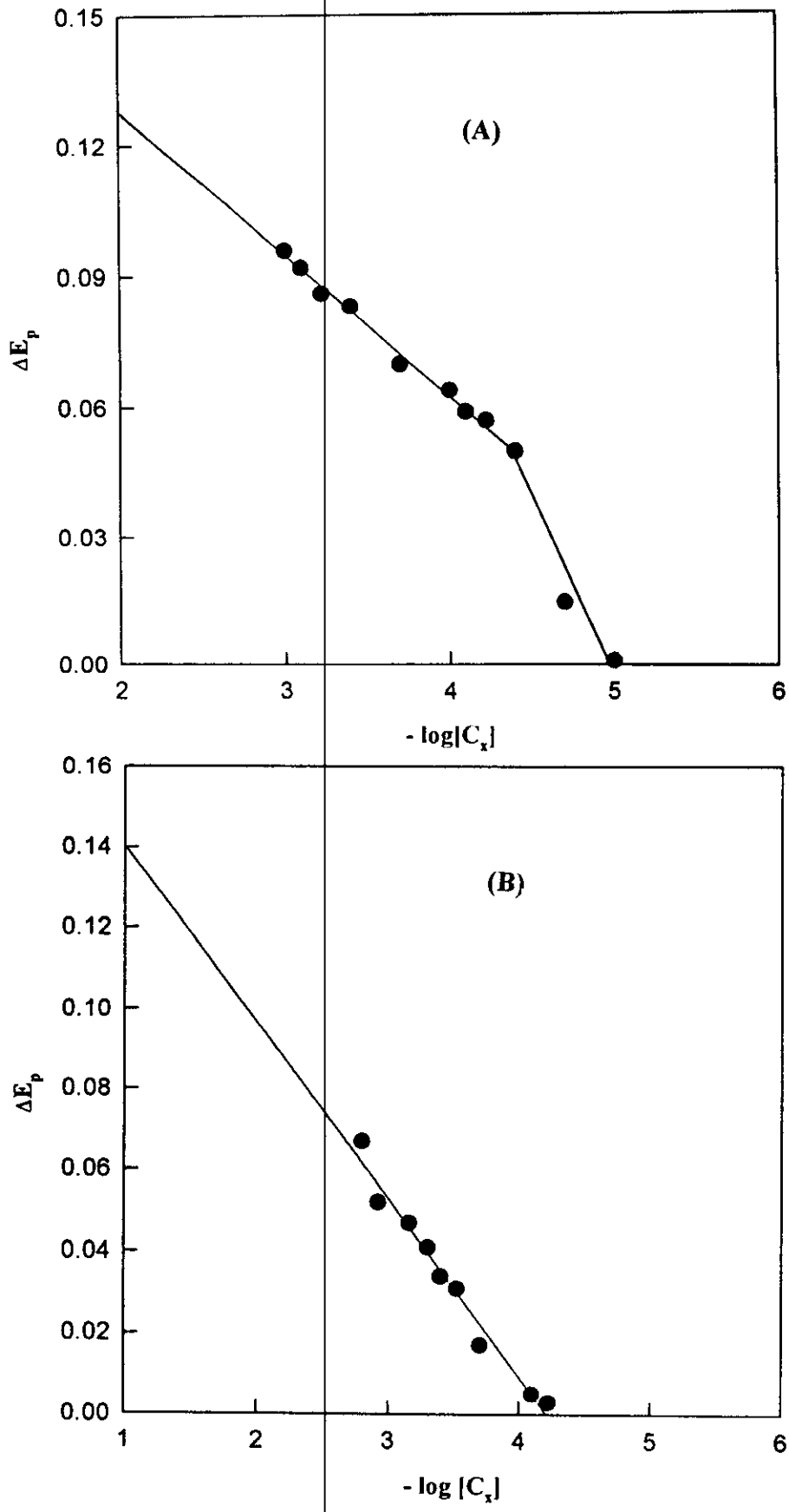

Figure 56: The plots of ΔE_p versus log[C_X] for the complex formation of compound (IIa) with (a) Cu^{+2} ions and (b) Zn^{+2} ions.

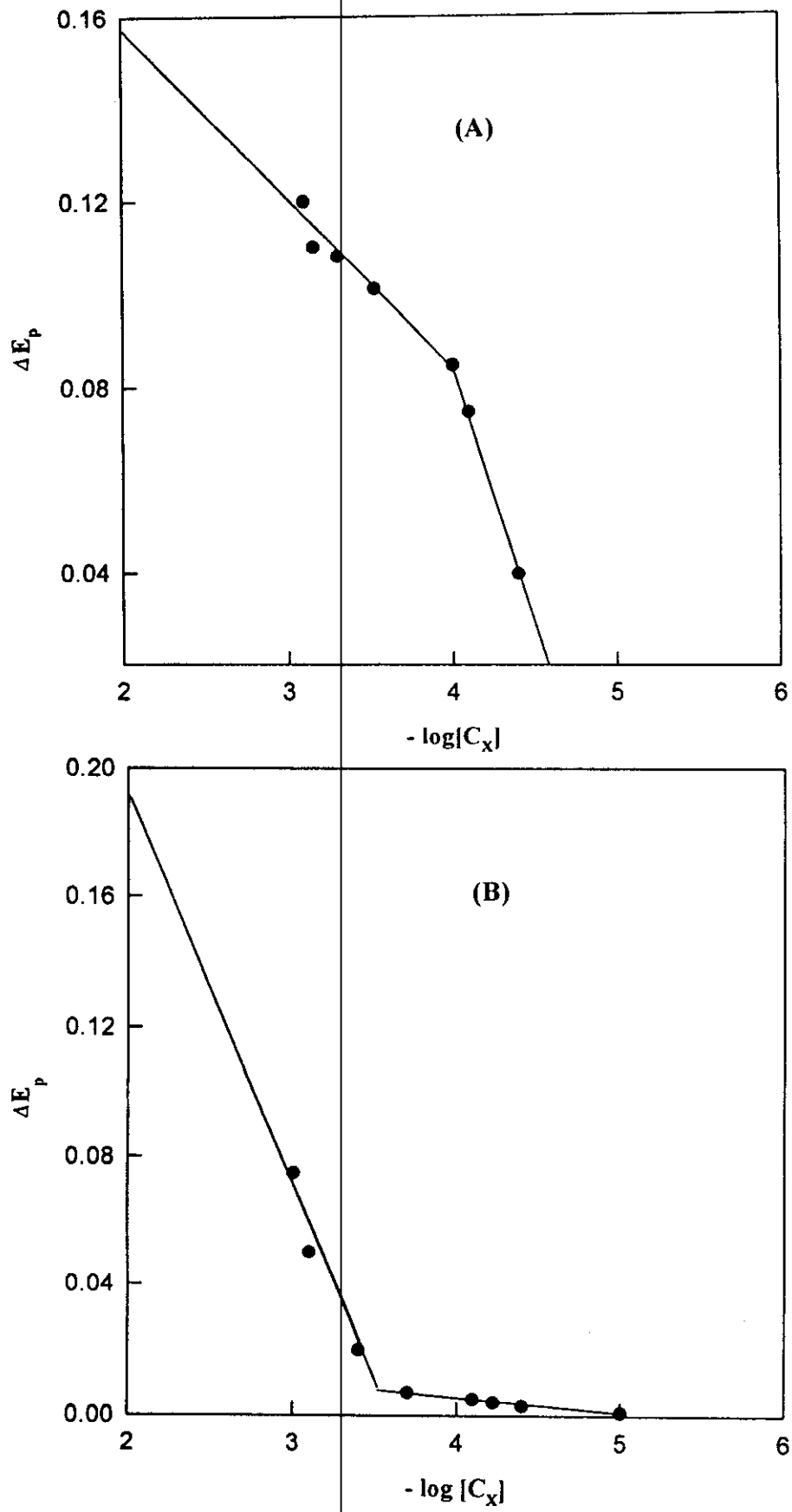

Figure 57: The plots of ΔE_p versus $\log[C_X]$ for the complex formation of compound (IIb) with (a) Cu^{+2} ions and (b) Zn^{+2} ions.

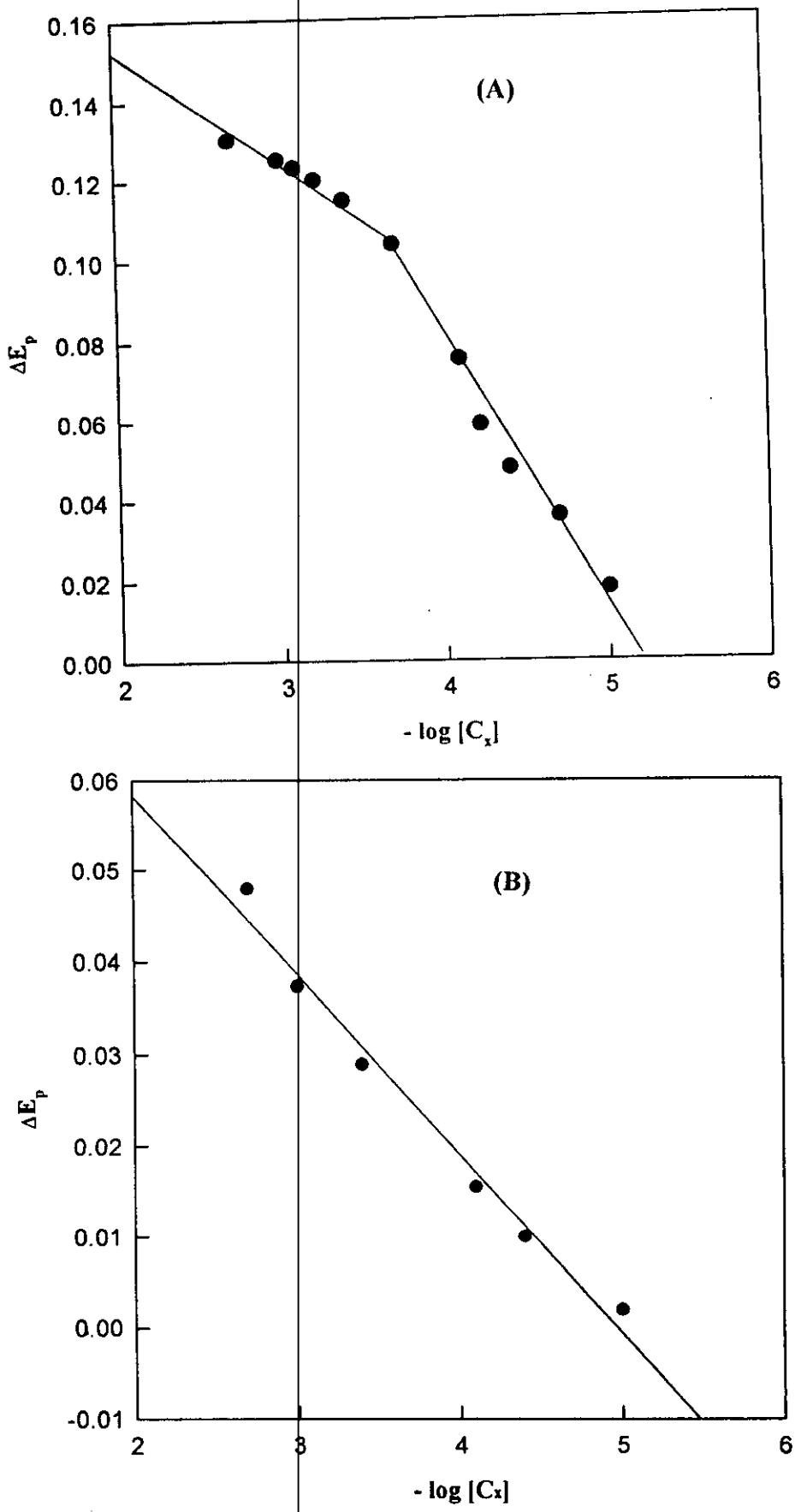

Figure 58: The plots of ΔE_p versus log[C_X] for the complex formation of compound (IIc) with (a) Cu^{+2} ions and (b) Zn^{+2} ions.

Table 26: Differential Pulse Polarograghic Data Obtained for Cu(II) and Zn(II) Complexes with 1-Phenylazo-2-hydroxy-6-naphthalenesulfonic acid (IIa) in 0.1 M $NaNO_3$ Solutions.

[Ligand] (M)	E_p mV	ΔE_p mV	$W_{1/2}$ mV	Stoichiometry	log β_{MXj}
(A) Cu(II) Complexes					
0.0	- 0.151	0.000	70		
$1x10^{-5}$	- 0.165	0.015	72		
$4x10^{-5}$	- 0.200	0.050	92		
$6x10^{-5}$	- 0.207	0.057	74		
$8x10^{-5}$	- 0.209	0.059	62	1 : 1	6.57
$1x10^{-4}$	- 0.214	0.064	74		
$2x10^{-4}$	- 0.220	0.070	69	1 : 2	13.94
$4x10^{-4}$	- 0.233	0.083	76		
$6x10^{-4}$	- 0.236	0.086	72		
$8x10^{-4}$	- 0.242	0.092	69		
$1x10^{-3}$	- 0.246	0.096	73		
(B) Zn(II) Complexes					
0.0	- 1.093	0.000	60		
$6x10^{-5}$	- 1.096	0.003	64		
$8x10^{-5}$	- 1.098	0.005	66		
$2x10^{-4}$	- 1.110	0.017	65		
$3x10^{-4}$	- 1.124	0.031	63	1 : 2	6.13
$4x10^{-4}$	- 1.127	0.034	73		
$5x10^{-4}$	- 1.134	0.041	74		
$7x10^{-4}$	- 1.140	0.047	70		
$1x10^{-3}$	- 1.145	0.052	59		
$1.6x10^{-3}$	- 1.160	0.067	68		

Table 27: Differential Pulse Polarograghic Data Obtained for Cu(II) and Zn(II) Complexes with 1-(2'-Carboxyphenylazo)-2-hydroxy-6-naphthalenesulfonic acid (IIb) in 0.1 M $NaNO_3$ Solutions.

[Ligand] (M)	E_p mV	ΔE_p mV	$W_{1/2}$ mV	Stoichiometry	log β_{MXj}
(A) Cu(II) Complexes					
0.0	- 0.151	0.000	70		
$1x10^{-5}$	- 0.176	0.025	77		
$2x10^{-5}$	- 0.187	0.036	65		
$4x10^{-5}$	- 0.196	0.045	60		
$6x10^{-5}$	- 0.210	0.059	60		
$8x10^{-5}$	- 0.226	0.075	69		
$2x10^{-4}$	- 0.255	0.104	74	1 : 2	9.57
$4x10^{-4}$	- 0.266	0.115	79		
$6x10^{-4}$	- 0.271	0.120	78		
$8x10^{-4}$	- 0.274	0.123	80		
$1x10^{-3}$	- 0.276	0.125	80		
$2x10^{-3}$	- 0.281	0.130	82		
(B) Zn(II) Complexes					
0.0	- 1.093	0.000	60		
$1x10^{-5}$	- 1.098	0.005	66		
$4x10^{-5}$	- 1.103	0.010	72		
$8x10^{-5}$	- 1.109	0.016	70	1 : 1	5.72
$4x10^{-4}$	- 1.117	0.024	70		
$1x10^{-3}$	- 1.130	0.037	62		
$2x10^{-3}$	- 1.141	0.048	59		

3.3.4 Kinetic parameters of the electrode reactions

3.3.4.1 Reversible reactions

The standard rate constant of electron transfer (k_o) of reversible or quasi-reversible reactions like, ferrocene or 1AAQ, respectively is determined and discussed. As reported earlier the electrochemical oxidation of ferrocene in CTAB, SDS and Triton X-100 microemulsion systems showed a reversible one electron charge transfer since the peak separation ΔE_p is around 60 mV at sweep rates varying from 20 to 200 mV/sec. Nicholson [196] has developed the theory of absolute rate equation to include electron transfer reactions in reversible systems. The results of theoretical calculations made it possible to use cyclic voltammetry for measuring the standard rate constant for electron transfer reversible systems. Since a system which appears to behave reversible at one frequency may be made to exhibit kinetic behaviour at higher frequencies as indicated by the increase of anodic and cathodic peak separation. This can be achieved by increasing the triangular wave frequency untill the peak potential separation becomes greater than 60/n mV. Under these conditions by applying fast scan cyclic voltammetry, it may be possible to study the kinetics of the electrode reaction and the peak potential separation should be taken as a measure of the standard rate constant of electron transfer. By using the final form of the equation that derived by Nicholson which was given in the form [196]:

$$\Psi = \gamma^{\alpha} k_o / [\pi n F \upsilon D_o / RT]^{1/2} \qquad \textbf{(III.18)}$$

where γ is defined by the ratio of $(D_O/D_R)^{1/2}$, α is the charge transfer coefficient and it is taken to equal 0.5, while the term γ^{α} is neglected assuming equal diffusion coefficients or very small differences, but if there is considerable differences, it can not be neglected like in case of 1AAQ. An important notice is that at higher sweep rates the ohmic resistence is may seriously contribute

to the peak potential separation, and Ψ value when there is ohmic potential effect has to be given as following:

$$\Psi = 1/(nF/RT).nFA \times (\pi a D_o)^{1/2} C_o R_u \qquad \text{(III.19)}$$

In our work the ohmic resistence is automatically componsated by BAS-100 Electrochemical Analyzer. The practical peak potential separation ΔE_p was obtained from the electrochemical oxidation of ferrocene in different microemulsion systems. After its multiplication by the number of electrons involved in the electrode process (n), the value of Ψ corresponding to $(n.\Delta E_p)$ was taken directly from Nicholson tabulation. The rate constant (k_o) of the electrode process of ferrocene in different microemulsion systems as well as in pure aqueous solution was determined at 25°C. At sweep rate 20 mV/sec, the rate constant of ferrocene in SDS microemulsion was found to equal 0.0287 cm/sec. While it was found to equal 0.0723 cm/sec in CTAB microemulsion at 200 mV/sec and 25°C.

By using the same method of Nicholson [196], the rate constant of the electrode process of 1AAQ was determined from microemulsion systems. It was found that reduction of 1AAQ takes place quasi-reversible, as observed from the increase of peak separations (ΔE_p) on increasing sweep rate and the deviation of the anodic to cathodic peak current ratios ($I_{p,a}/I_{p,c}$) from unity. The values of k_o was determined at 200 mV/sec and found to equal 0.008, 0.0032 and 0.0056 cm/sec at 25°C in CTAB, SDS and Triton X-100 microemulsions, respectively, Table (29). Inspection of these values confirmed our previous results on 1AAQ reduction that the electrode process takes place faster in CTAB than Triton X-100 and SDS microemulsion systems due to the elecrostatic effect excerted by the surfactant molecules at the negatively charged electrodes.

3.3.4.2 Irreversible reactions

The heterogeneous rate constant of the electrode reaction ($k^{\circ}_{f,h}$) for adenine, cytosine and 8-(phenylazo)-6,7-dihydroxy-4-methyl-coumarin (Ia) reductions in micelles and microemulsion systems containing cationic CTAB, anionic SDS and nonionic Triton X-100 surfactants and in pure aqueous media can be determined using equation (III.11). Values of the heterogeneous rate constant ($k^{\circ}_{f,h}$) for the compounds under investigations were determined and found to be higher in CTAB systems than in aqueous buffer solution, SDS or Triton X-100, Tables (29). These results indicate that the electrostatic effect of CTAB increases the electron affinity in the vicinity of the cathodic electrode. Also, it indicated that the complications of pure aqueous system such as adsorption and catalytic activity was disappeared in microemulsion systems.

Values of the heterogeneous rate constant ($k^{\circ}_{f,h}$) of the electrode reactions of azo-compounds derived from 6,7-dihydroxycoumarin (series I) and Schiffer azodyes (series II) were determined in aqueous buffer solutions of different pH values, Tables (30&31). Generally, the data listed in Tables (30&31) indicate that the rate constant ($k^{\circ}_{f,h}$) decreases with increasing the pH value. This behaviour revealed that the electrode reaction becomes more difficult (i.e more difficult electron transfer) and more irreversible on increasing the pH of the electrolysis medium.

3.3.4.3 Calculation of the free energy of activation from the experimental data

The free energy of activation characterizing the electrode process could be determined by applying the results of the absolute rate theory [197,198]. For a totally irreversible wave, the energy of activation ($\Delta G^{\#}$) can be related to the formal rate constant ($k_{f,h}$) at a potential E by the following relationship [197,198]:

$$\Delta G^{\#} = (RT/0.434)\log(K_1T/h) + \log\delta + (\alpha n_a F/2.303)E - \log(k_{f,h}) \qquad \textbf{(III.20)}$$

where K_1 is the Boltzman constant, h is the Plank's constant and δ is a factor which can be taken equal to 2×10^{-8} cm. By substituting the numerical values for the different constants K_1, h and δ at 300°K, the above equation becomes [199,200]:

$$\Delta G^{\#} = 5778.8[5.097 + (\alpha n_a/0.05909)E - \log k_{f,h}] \qquad \textbf{(III.21)}$$

from which the value of $\Delta G^{\#}$ at the selected potential E can be readily evaluated. At E = 0 V (vs. NHE) the equation becomes [199,200]:

$$\Delta G^{\#} = 5778.8(5.097 - \log k^{\circ}_{f,h}) \qquad \textbf{(III.22)}$$

Values of the energy of activation ($\Delta G^{\#}$) of the electrode process for 1AAQ, adenine, cytosine and 8-(phenylazo)-6,7-dihydroxy-4-methyl-coumarin (Ia) recorded in CTAB systems were found to be less than that obtained in pure aqueous, Triton X-100 and SDS systems, Table (29). These results indicate that the electrode reaction is more difficult in anionic SDS due to the electrostatic repulsion effect and subsequently required high energy of activation compared to CTAB. These facts showed the effect of surfactant as local environment on the kinetics and electron transfer reactions at the vicinity of elctrode.

Values of the energy of activation ($\Delta G^{\#}$) characterizing the electrode reaction of azo compounds of series I&II recorded in aqueous buffer solutions of different pH values were calculated and listed in Tables (30&31). It was found that, the $\Delta G^{\#}$ values increases with

increasing the pH of the electrolysis solutions. This behaviour could be attributed to the fact that, protonated or neutral molecules existing at lower pH values can be readily diffused to the electrode surface which in turn reduces the values of energy of activation. On the other hand, at higher pH values the non-protonated forms are present at the electrode surface leading to the requirements of higher values of energy of activation, Tables (30&31).

Table (29): Kinetic Parametrs Obtained from Cyclic Voltammetric Behaviour of 1AAQ, Adenine, Cytosine and 8-(Phenylazo)-6,7-dihydroxy-4-methyl-coumarin (Ia) in Micelles and Microemulsion Systems Containing Different Surfactant Types at 25°C.

System	$k^{\circ}_{f,h}$ cm/sec	$\Delta G^{\#}$ KJ/mol
1-Amino-9,10-anthraquinone		
(A) CTAB Microemulsion	0.0084	11.9
(B) Triton X-100 Microemulsion	0.0056	12.9
(C) SDS Microemulsion	0.0032	14.2
Adenine		
(A) CTAB Micelles (a)	4.92×10^{-6}	251.3
(B) CTAB Microemulsion	1.90×10^{-5}	237.2
(C) Triton X-100 Micelles	1.54×10^{-6}	263.5
(D) Triton X-100 Microemulsion	9.00×10^{-7}	269.2
(E) SDS Micelles	2.24×10^{-7}	283.7
(F) SDS Microemulsion	1.48×10^{-7}	288.1
Cytosine		
(A) Pure Aqueous	3.09×10^{-6}	256.2
(B) CTAB Micelles (a)	3.67×10^{-6}	254.4
(C) CTAB Microemulsion	1.46×10^{-5}	239.9
(D) Triton X-100 Micelles	4.19×10^{-6}	253.0
(E) Triton X-100 Microemulsion	1.21×10^{-6}	266.1
(F) SDS Micelles	5.15×10^{-7}	275.0
(G) SDS Microemulsion	1.17×10^{-5}	242.3
8-(Phenylazo)-6,7-dihydroxy-coumarin (Ia)		
(A) Pure Aqueous	3.10×10^{-6}	256.2
(B) CTAB Microemulsion	1.14×10^{-5}	242.5
(C) Triton X-100 Microemulsion	1.59×10^{-6}	263.2
(D) SDS Microemulsion	9.26×10^{-7}	268.9

a- measured at 30°C.

Table 30: Kinetic Data Obtained from Cyclic Voltammetric Measurements of the compounds of series (I) in Aqueous Buffer Solutions of Different pH Vaules Containing 40% (v/v) Ethanol, at 25°C.

Compound	pH	$k^{\circ}_{f,h}$ cm/sec	$\Delta G^{\#}$ KJ/mol
(Ia)	2.40	1.85×10^{-4}	213.3
	4.00	8.20×10^{-6}	246.0
	5.90	1.72×10^{-6}	262.4
	7.00	1.58×10^{-7}	287.3
	9.20	1.00×10^{-9}	336.7
	11.20	2.11×10^{-13}	429.3
(Ib)	2.20	1.05×10^{-4}	219.3
	3.70	1.43×10^{-5}	240.2
	5.70	3.86×10^{-6}	253.9
	7.00	3.24×10^{-7}	279.8
	9.30	4.93×10^{-10}	347.9
	11.00	2.70×10^{-12}	402.6
(Ic)	2.30	6.06×10^{-6}	249.2
	3.90	6.37×10^{-7}	272.8
	5.80	1.90×10^{-8}	309.2
	7.10	4.00×10^{-9}	323.8
	9.20	1.36×10^{-10}	361.4
	10.90	9.61×10^{-12}	389.2

Table 31: Kinetic Data Obtained from Cyclic Voltammetric Measurements of the compounds of series (II) in Pure Aqueous Buffer solutions of Different pH Vaules at 25°C.

Compound	pH	$k^{\circ}_{f,h}$ cm/sec	$\Delta G^{\#}$ KJ/mol
(IIa)	2.20	1.65×10^{-3}	190.3
	4.10	8.62×10^{-6}	245.5
	6.40	1.50×10^{-8}	311.9
	8.40	6.00×10^{-9}	321.3
	10.10	1.04×10^{-10}	364.3
	12.50	1.45×10^{-10}	360.8
(IIb)	2.10	2.71×10^{-3}	185.1
	6.60	1.23×10^{-6}	265.8
	8.40	1.71×10^{-12}(b)	407.4
	10.10	5.03×10^{-10}	347.7
	12.60	1.84×10^{-13}	430.8
(IIC)	2.10	8.92×10^{-4}	196.8
	4.10	3.69×10^{-6}	254.4
	6.40	1.00×10^{-9}	340.5
	8.40	3.18×10^{-12}	400.8
	10.10	1.30×10^{-12}	410.2
	12.80	1.39×10^{-13}	433.7

(b) = Second peak

3.3.5 Thermodynamic parameters

To determine the thermodynamic parameters of the electrochemical reduction of 1AAQ, adenine, cytosine and 8-(phenylazo)-6,7-dihydroxy-4-methyl-coumarin (Ia) from micelles and microemulsions of three different surfactant types. The effect of temperature on the cyclic voltammetric behaviour of adenine and cytosine were recorded in cationic CTAB, anionic SDS and nonionic Triton X-100 micelles and microemulsion systems. On comparing the voltammograms obtained at 288.15 and 308.15 °K with those obtained at 298.15 °K, it can be concluded that similar voltammetric responses were obtained displaying only a single irreversible reduction step. The voltammetric features of the compounds under investigation recorded at different temperatures showed a slight shift of the peak potential to less negative values on increasing the temperature, on the other hand, the peak current ($I_{p,c}$) is increased. The change of temperature influences peak currents by its effect on the viscosity of the electrolysis solution as well as the diffusion coefficient which is related to viscosity [201]. Therefore, on increasing the temperature it was found that the diffusion coefficients were increased by 1.29 to 4.55% per degree, Table (32).

On plotting the peak current ($I_{p,c}$) versus $\upsilon^{1/2}$ at temperatures 288.15 and 303 °K, linear correlations were obtained. The slopes of these linear plots in addition to the slopes obtained at 298.15 °K were used to estimate the apparent diffusion coefficients. Values shown in Table (32), revealed the increase in the diffusion coefficient on increasing temperature of the electrolysis solution.

The peak potential displayed a slight shift toward less negative values on increasing the temperature from 288.15 to 303.15 °K. These results indicates that the electrode reaction becomes less irreversible at higher temperatures. On employing the relationship (III.11), and on plotting E_p versus $\ln(\upsilon)$ at 288.15 and 303.15°K linear correlations were obtained. The slopes of

these linear plots were used to estimate the transfer coefficient α at the probable n_a values which is either one or two. The heterogeneous rate constant ($k^{\circ}_{f,h}$) of the electron transfer process was determined utilizing values of slopes and intercepts of the E_p-ln(υ) plots. Inspection of the values of $k^{\circ}_{f,h}$ obtained at different temperatures revealed that the rate constant increases with increasing the temperature from 288.15 to 303.15 °K.

On employing the Arrhenius type equation [202], which relates the rate constant to the temperature changes and has given as following:

$$k^{\circ}_{f,h} = A.\exp[-E_a/RT] \qquad \textbf{(III.23)}$$

where E_a is the activation energy in calories, R is the gas constant in cal./deg., $k^{\circ}_{f,h}$ is the rate constant of electron transfer process in cm/sec and A is a collision factor. The plots of log($k^{\circ}_{f,h}$) versus 1/T showed linear correlation for 1AAQ, adenine, cytosine and 8-(phenylazo)-6,7-dihydroxy-4-methyl-coumarin, (Ia), in all micellar and microemulsion media. The slopes of the linear plots were used to estimate the apparent activation energies (E_a) in different systems. The enthalpy change of activation, $\Delta H^{\#}$, for adenine, cytosine, 1AAQ and coumarin azodye (Ia) reductions in micelles and microemulsion media can be deduced from the slopes of the log($k^{\circ}_{f,h}$)-1/T plots and utilizing the following relationship:

$$\Delta H^{\#} = E_a - RT \qquad \textbf{(III.24)}$$

The corresponding energy of activation $\Delta G^{\#}$ of the electrode process was determined using the equation (III.22). The accompanied entropy change of the system ($\Delta S^{\#}$) was calculated using the well known relationship:

$$\Delta G^{\#} = \Delta H^{\#} - T\Delta S^{\#} \qquad \text{(III.25)}$$

The thermodynamic parameters of the electrode reaction of 1AAQ, adenine and cytosine moieties and compound (Ia) in micellar solutions and microemulsion systems are calculated and listed in Tables (33-35). Inspection of these values generally showed positive enthalpy change accompanied the reduction processes, which indicate the endergonic nature of the electrode process. Negative entropy change was observed in case of adenine, cytosine and coumarin azodye (Ia) reductions which indicates an ordered electrode reaction process becomes less ordered on increasing temperature, Tables (33-35). The quasi-reversible reduction of 1AAQ in microemulsion systems showed a positive entropy change. In general, it was found that the electrode process takes place faster in CTAB than SDS and Triton X-100 systems due to the increased electron affinity. The presence of surfactant as local environment of the depolarizer molecule has to affect the electrode kinetics in different ways.

Table 32: diffusion coefficients and data obtained at different temperatures from cyclic voltammetry of adenine and cytosine.

System	288.15°K D_O (cm^2/sec)	298.15°K D_O (cm^2/sec)	303.15°K D_O (cm^2/sec)	Temperature Coefficient
(A) Adenine in CTAB Micelles				
	-	-	1.67×10^{-5}	- 1.29 1.38
(B) Adenine in Triton X-100 Micelles				
	4.56×10^{-6}	7.98×10^{-6}	9.86×10^{-6}	- 1.75 2.16
(C) Cytosine in CTAB Micelles				
	-	-	3.46×10^{-6}	- 1.99 3.48
(D) Cytosine in Triton X-100 Micelles				
	2.92×10^{-6}	7.40×10^{-6}	1.33×10^{-5}	- 2.53 4.55
(E) Cytosine in SDS Micelles				
	4.17×10^{-6}	5.96×10^{-6}	7.10×10^{-6}	- 1.43 1.70

Table 33: Thermodynamic parameters Obtained from Voltammetric Behavior of Adenine in Different Surfactant Systems.

System	15°C			25°C			30°C		
	$\Delta G^{\#}$ KJ/mol	$\Delta H^{\#}$ KJ/mol	$-\Delta S^{\#}$ J/mol	$\Delta G^{\#}$ KJ/mol	$\Delta H^{\#}$ KJ/mol	$-\Delta S^{\#}$ J/mol	$\Delta G^{\#}$ KJ/mol	$\Delta H^{\#}$ KJ/mol	$-\Delta S^{\#}$ J/mol
A- CTAB Micellar Solution:									
	251.3	77.92	572.2(a)	235.5	77.83	503.7	230.7	77.75	473.6
B- CTAB Microemulsion:									
	250.9	82.47	584.8	237.2	82.39	519.2	232.7	82.35	496.2
C- SDS Micellar Solution:									
	285.3	35.66	851.9	283.7	35.62	832.7	274.5	35.58	785.8
D- SDS Microemulsion:									
	293.5	17.82	957.2	288.1	17.74	907.1	284.6	17.69	881.0
E- Triton X-100 Micellar Solution:									
	264.8	22.55	841.0	263.5	22.46	808.8	258.7	22.43	780.0
F- Triton X-100 Microemulsion:									
	277.2	55.41	769.9	269.2	55.33	717.5	264.4	55.29	690.2

Measurements at: a- 30

Table 34:Thermodynamic Parameters Obtained Volammetric Behavior of Cytosine in Different Surfactant Systems.

System	15°C			25°C			30°C		
	$\Delta G^{\#}$ KJ/mol	$\Delta H^{\#}$ KJ/mol	$-\Delta S^{\#}$ J/mol	$\Delta G^{\#}$ KJ/mol	$\Delta H^{\#}$ KJ/mol	$-\Delta S^{\#}$ J/mol	$\Delta G^{\#}$ KJ/mol	$\Delta H^{\#}$ KJ/mol	$-\Delta S^{\#}$ J/mol
A- CTAB Micellar Solution:									
	252.6	101.40	498.9(a)	232.9	101.32	420.1	225.9	101.24	386.2
B- CTAB Microemulsion:									
	254.4	106.98	511.6	239.9	106.89	446.4	230.1	106.85	406.8
C- SDS Micellar Solution:									
	284.1	198.94	290.5	275.0	198.90	255.4	255.4	198.86	186.4
D- SDS Microemulsion:									
	258.6	115.19	498.1	242.3	115.10	426.8	232.8	115.06	388.5
E- Triton X-100 Micellar Solution:									
	268.9	44.77	778.3	253.0	44.69	698.9	249.1	44.65	674.7
F- Triton X-100 Microemulsion:									
	297.0	86.05	732.2	266.1	85.96	604.0	235.8	85.92	494.6

Measurements at: a-30

Table 35: Thermodynamic Parameters Obtained from theVolammetric Behaviour of 1AAQ and 8-(Phenylazo)-6,7-dihydroxy-4-methyl-coumarin in Different Surfactant Systems.

System	15°C			25°C			30°C		
	$\Delta G^{\#}$ KJ/mol	$\Delta H^{\#}$ KJ/mol	$\Delta S^{\#}$ J/mol	$\Delta G^{\#}$ KJ/mol	$\Delta H^{\#}$ KJ/mol	$\Delta S^{\#}$ J/mol	$\Delta G^{\#}$ KJ/mol	$\Delta H^{\#}$ KJ/mol	$\Delta S^{\#}$ J/mol
1-Amino-9,10-anthraquinone (1AAQ)									
(A) CTAB Microemulsion									
	11.75	8.76	-10.38	11.94	8.68	-10.96	11.73	8.63	-10.22
(B) Triton X-100 Microemulsion									
	14.08	37.83	82.42	12.86	37.75	83.49	12.80	37.71	82.16
(C) SDS Microemulsion									
	15.31	57.52	146.48	14.25	57.44	144.80	12.85	57.39	146.93
8-(Phenylazo)-6,7-dihydroxy-4-methyl-coumarin (Ia)									
(A) Pure Aqueous									
	258.9	14.71	-847.4	256.2	14.63	-810.2	255.2	14.58	-793.8
(B) CTAB Microemulsion									
	244.3	15.63	-793.7	242.5	15.55	-761.1	240.2	15.51	-741.3
(C) Triton X-100 Microemulsion									
	266.2	16.55	-866.2	263.2	16.47	-827.5	262.1	16.43	-810.5
(D) SDS Microemulsion									
	276.5	43.01	-810.3	268.9	42.93	-757.8	266.9	42.88	-739.1

3.3.6 The electrode reaction mechanisms

3.3.6.1 1-Amino-9,10-anthraquinone (1AAQ)

The electrochemical investigation of 1-amino-9,10-anthraquinone (1AAQ) was performed in micelles and microemulsion of three different surfactant types as well as in pure aqueous solution. Cationic (cetyltrimethylammonium bromide, CTAB), anionic (sodium dodecyl sulphate, SDS) and nonioinic {octylphenoxypoly(oxyethylene), Triton X-100} model surfactants were used in this investigation. The electrochemical techniques that used are cyclic voltammetry, chronocoulometry and rotating disc voltammetry. From cyclic voltammetry, only a single redox pair of peaks were observed on both the cathodic and anodic branches of sweep in micelles and microemulsion media. Except in CTAB micelles a shoulder was developed and appears as a cathodic peak at higher sweep rates. The cathodic and anodic peak currents on the branches of sweep are not equal. The peak current ratio ($I_{p,a}/I_{p,c}$) is less than unity in microemulsion systems and much less in micellar solutions.

The voltammograms of 1AAQ recorded at different sweep rates are essentially similar and no more peaks were observed. At very small sweep rates, the peak potential separation ΔE_p (= $E_{p,c} - E_{p,a}$) is very close to 29 mV. While on increasing the sweep rate, the peak potential separation is increased from 29 to 53 mV. ΔE_p is increased from 29 to 53 in SDS and Triton X-100 microemulsion systems, whereas, in CTAB microemulsion ΔE_p is increased up to 40 mV on increasing the sweep rate from 20 to 200 mV/sec. These facts lead generally to the electrochemical-chemical-electrochemical (ECE) reaction nature, and the reduction process of 1AAQ is chemically quasi-reversible. The protonation of the anion free radical generally leads to a disproportionation reaction [186,187].

Therefore the disproportionation reaction of the anionic free radical $1AAQ^{\cdot -}$ is favored by the decrease of the energy difference between $1AAQ^{\cdot -}$ and $1AAQ^{\cdot\cdot -}$ due to hydrogen bond solvation of the carbonyl group by water molecules [188,189].

The plots of the cathodic and anodic peak currents ($I_{p,c}$ & $I_{p,a}$) of 1AAQ versus square root of sweep rate ($\upsilon^{1/2}$) in micelles and microemulsion media showed linear correlations almost passing through the origin confirming that the electrode reaction is controlled by diffusion.

There is an increase in solubility of 1AAQ in micelles and microemulsion media compared to aqueous solution ($9x10^{-5}$ M). The solubilization of 1AAQ in the presence of surfactant can be due to different effects. Electrostatic attraction of the oppositely charged ends of the dipoles by ionic micelles, association with micelles via surface adsorption on the surfactant film, and solubilization by the hydrophobic effect of micelles or microemulsion, where the hydrophobic domain of microemulsion is larger than that of micelles due to the additional hydrocarbon chains. In the present investigation the deviation of the anodic to cathodic peak current ratio from unity suggests the presence of adsorption. Only most probably the adsorption of 1AAQ takes place in case of cationic CTAB at the negatively charged electrode. But this is not the case since the peak current ratio reaches its maximum and approaching unity in CTAB micelles and microemulsion systems. These results were confirmed from chronocoulometric measurements which indicate that the amount of 1AAQ adsorbed on the electrode surface is about 10^{-12} M. This amount could be considered as negligible effects compared to the original solute concentration ($3x10^{-4}$ M), and the only case is the stabilization mechanisms of the anionic free radical $1AAQ^{\cdot -}$ excerted by the different surfactant types and the observed results

could be explained in terms of stabilization. The stabilization mechanism could be electrostatic and/or hydrophobic. Therefore, the stabilization of $1AAQ^{\cdot-}$ by CTAB seems to hinders the disproportionation reaction (ii)' to a large extent.

In order to evaluate the electrode reaction pathway of 1AAQ at the glassy carbon electrode, it is necessary to calculate the number of electrons consumed in the reduction process. From cyclic voltammetry, the peak potential separation ΔE_p is very close to 30 mV at small sweep rates, which corresponding to 2.0 electrons consumed per reactant molecule; where $\Delta E_p = 0.0591/n$. These results were confirmed by controlled potential electrolysis of 10^{-4} M of 1AAQ from different media. The controlled potential electrolysis was performed on a large indium-tin oxide (ITO) electrode. The cathodic potenial applied during electrolysis is corresponding to the cathodic peak current. The amount of charge collected after complete electrolysis was measured by means of BAS-100 instrument and corrected from the background electrolyte. By applying the Faraday equation which states that:

$$Q = nFW/M \qquad \textbf{(III.26)}$$

where W is the weight of the dissolved sample of 1AAQ in grams, M is its molecular weight and F is the Faraday's constant. The average number of electrons consumed in the reduction process in different microemulsion systems was found to be 2.0. The electrode mechanism can be represented as follows:

$$1AAQ + \bar{e} \Leftrightarrow 1AA\dot{\bar{Q}} \quad (1)$$

$$1AA\dot{\bar{Q}} + H^+ \Leftrightarrow 1AAQ\dot{\bar{H}} \quad (2)$$

$$2(1AA\dot{\bar{Q}}) + 2H^+ \Leftrightarrow 1AAQ + 1AAQH_2 \quad (2.1)$$

$$1AAQ\dot{\bar{H}} + \bar{e} \Leftrightarrow 1AAQ\bar{H} \quad (3)$$

$$1AAQH^- + H^+ \Leftrightarrow 1AAQH_2 \quad (4)$$

3.3.6.2 Nucleic acids

From the controlled potential electrolysis the total number of electrons consumed in the reductions of adenine and cytosine was found to be 4 and 3 electrons, respectively. The voltammetric behaviour of both compounds in micelles and microemulsion media as well as pure aqueous solution, it was found that single reduction step was observed for both adenine and cytosine in all media. The absence of any peak in the anodic scan and the cathodic shift displayed in peak potentials on increasing the sweep rate indicate the irreversibility of the electrode processes. Also, values of the transfer coefficient (α) was found to confirm the irreversible nature of the electrode process. In the light of the data obtained from the electrochemical experiments, structure genesis and published results [203,204], the electrode mechanisms of both adenine and cytosine can be represented by scheme (I) as follows:

3.3.6.3 Coumarin and Schiffer azodyes

Cyclic voltammograms of the reduction of azo compounds derived from 6,7-dihydroxy-4-methylcoumarin (series I) in microemulsion systems and aqueous buffered

The electrode mechanism of adenine

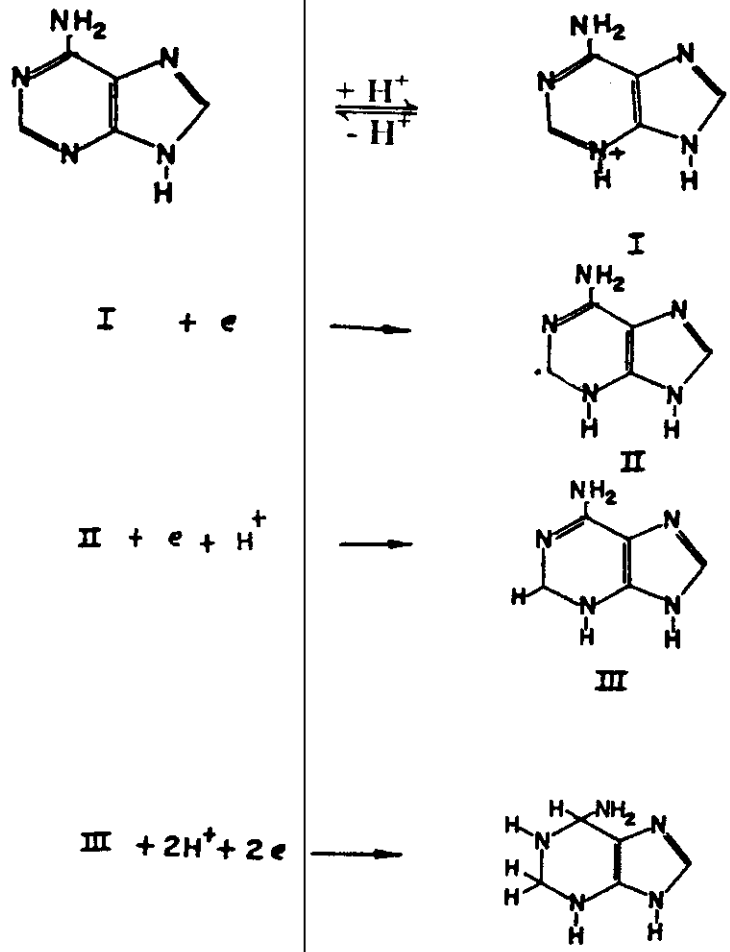

The electrode mechanism of cytosine

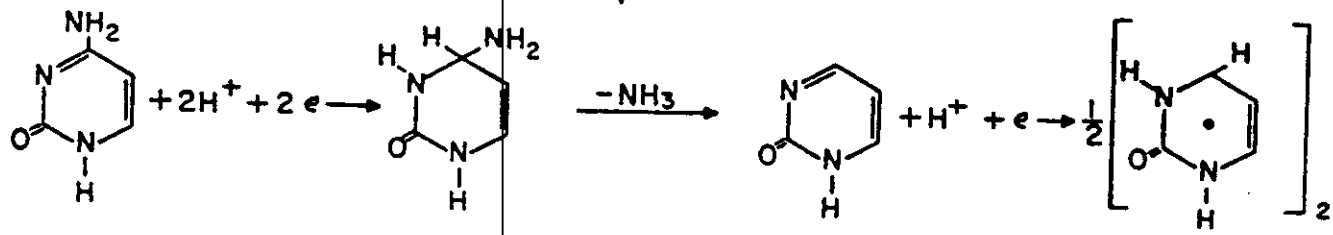

Scheme (I)

solutions of different pH values containing 40% (v/v) ethanol were recorded. Also, the voltammograms of Schiffer azo compounds (series II) were recorded from pure aqueous solutions of different pH values, where these compounds are completely soluble in pure aqueous media under the used concentration ranges. The results obtained revealed that the electrode process takes place irreversibly and controlled by diffusion in microemulsion media, while in aqueous buffered solutions the electrode process showed some adsorption contributions especially in alkaline solutions. Generally, a single reduction peak was shown representing the electroreduction of the only N=N active center within the depolarizer molecules. The peak potentials get shifted to more negative values on increasing the pH of the electrolysis medium, which confirmed the consumption of protons in the reduction processes. The number of protons (Z_H^+) participating in the rate-determining step of all compounds was found to be unity. On the other hand, the most probable α-values for all compounds (series I&II) are obtained at $n_a = 1.0$, indicating that the number of electrons involved in the rate-determining step (n_a) was found to be one. These data suggesting that the rate determining step should involve one electron and one proton.

In order to give the exact mechanism of the electrode process for the reduction of coumarin and Shiffer azodyes, the total number of electrons consumed in the reduction process should be obtained. The total number of electrons (n) was obtained by controlled potential electrolysis (CPE) of $1x10^{-4}$ M of each compound from acidic and basic media at a large mercury pool anode. The negative potential applied during electrolysis is corresponding to the reduction peak value. By using the relationship (III.26), the total number of electrons consumed in the reduction process was found to be 4.0 for coumarin

and Schiffer azodyes in both media. This number of electrons corresponding to the cleavage of the double bond of the N=N center to the amine stage.

The sequences of proton and electron additions were proposed to be either, H^+, e, H^+, e or H^+, e, e, H^+ [205]. In the light of structural genesis of the two series under investigation and based on the obtained results the latter sequence is most probable. Thus, the operating mechanisms of the electrode reaction of coumarin and Schiffer azo compounds is represented by scheme II.

The generalized electrode mechanism:

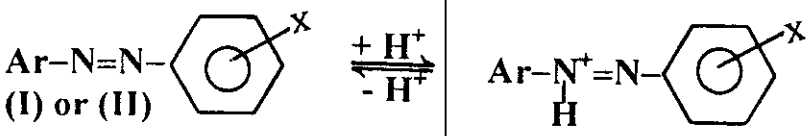

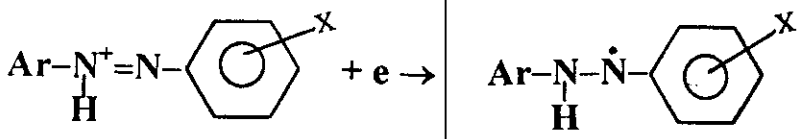

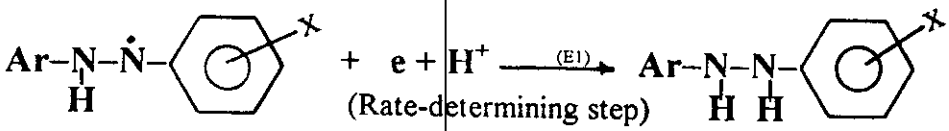

(Rate-determining step)

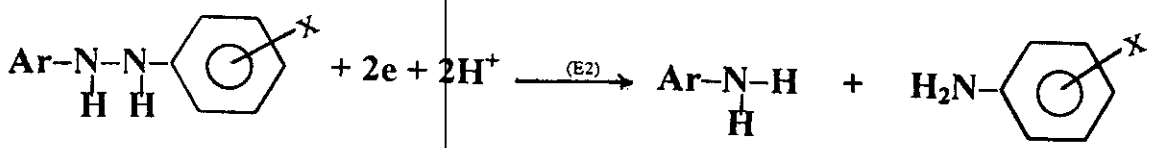

$$(E_1 = E_2 = E_p)$$

For coumarin azo compounds the aryl group (Ar) has the following structure:

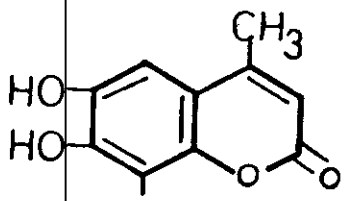

where X = H (Ia), p-Cl (Ib) and p-OCH_3 (Ic).

The aryl group (Ar') of Schiffer azo compounds has the following structure:

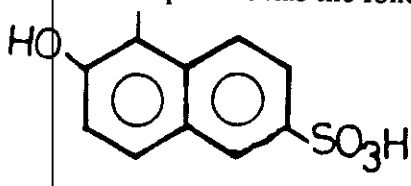

where X = H (IIa), o-COOH (IIb) and o-OCH_3 (IIc)

Scheme (II)